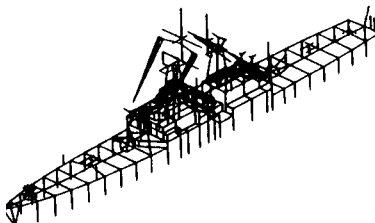
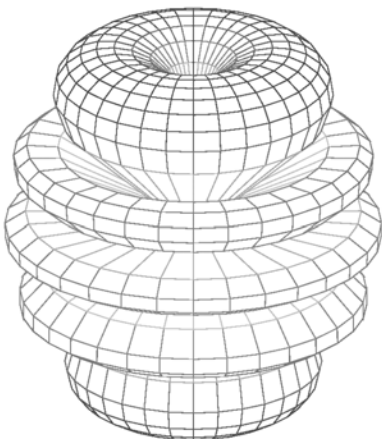
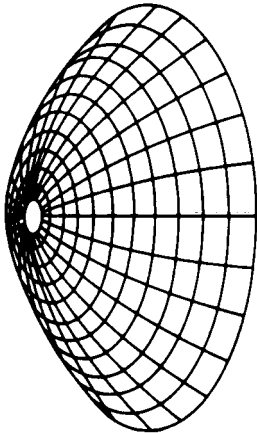
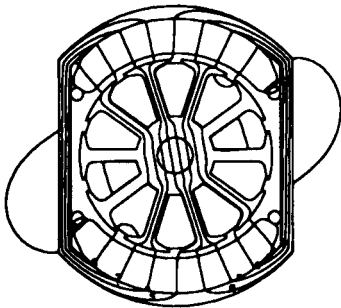
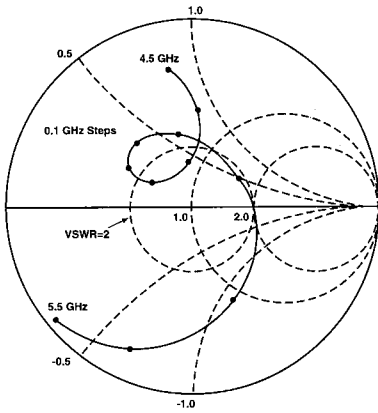
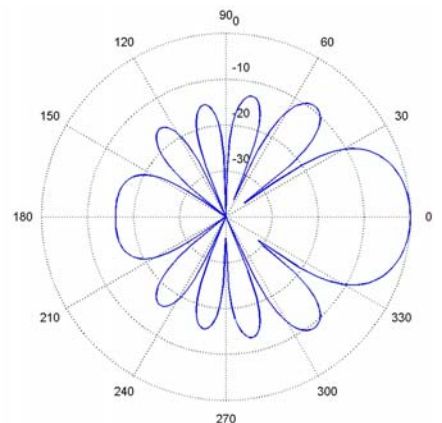


Applied Computational Electromagnetics Society Journal



Editor-in-Chief
Atef Z. Elsherbeni

July 2004
Vol. 19 No. 2
ISSN 1054-4887



GENERAL PURPOSE AND SCOPE: The Applied Computational Electromagnetics Society (*ACES*) Journal hereinafter known as the *ACES Journal* is devoted to the exchange of information in computational electromagnetics, to the advancement of the state-of-the art, and the promotion of related technical activities. A primary objective of the information exchange is the elimination of the need to “re-invent the wheel” to solve a previously-solved computational problem in electrical engineering, physics, or related fields of study. The technical activities promoted by this publication include code validation, performance analysis, and input/output standardization; code or technique optimization and error minimization; innovations in solution technique or in data input/output; identification of new applications for electromagnetics modeling codes and techniques; integration of computational electromagnetics techniques with new computer architectures; and correlation of computational parameters with physical mechanisms.

SUBMISSIONS: The *ACES Journal* welcomes original, previously unpublished papers, relating to applied computational electromagnetics. Typical papers will represent the computational electromagnetics aspects of research in electrical engineering, physics, or related disciplines. However, papers which represent research in applied computational electromagnetics itself are equally acceptable.

Manuscripts are to be submitted through the upload system of *ACES* web site <http://aces.ee.olemiss.edu> See “Information for Authors” on inside of back cover and at *ACES* web site. For additional information contact the Editor-in-Chief:

Dr. Atef Elsherbeni

Department of Electrical Engineering
The University of Mississippi
University, MS 386377 USA
Phone: 662-915-5382 Fax: 662-915-7231
Email: atef@olemiss.edu

SUBSCRIPTIONS: All members of the Applied Computational Electromagnetics Society who have paid their subscription fees are entitled to receive the *ACES Journal* with a minimum of three issues per calendar year and are entitled to download any published journal article available at <http://aces.ee.olemiss.edu>.

Back issues, when available, are \$15 each. Subscriptions to *ACES* is through the web site. Orders for back issues of the *ACES Journal* and changes of addresses should be sent directly to *ACES* Executive Officer:

Dr. Richard W. Adler

ECE Department, Code ECAB
Naval Postgraduate School
833 Dyer Road, Room 437
Monterey, CA 93943-5121 USA
Fax: 831-649-0300
Email: rwa@attglobal.net

Allow four week’s advance notice for change of address. Claims for missing issues will not be honored because of insufficient notice or address change or loss in mail unless the Executive Officer is notified within 60 days for USA and Canadian subscribers or 90 days for subscribers in other countries, from the last day of the month of publication. For information regarding reprints of individual papers or other materials, see “Information for Authors”.

LIABILITY. Neither *ACES*, nor the *ACES Journal* editors, are responsible for any consequence of misinformation or claims, express or implied, in any published material in an *ACES Journal* issue. This also applies to advertising, for which only camera-ready copies are accepted. Authors are responsible for information contained in their papers. If any material submitted for publication includes material which has already been published elsewhere, it is the author’s responsibility to obtain written permission to reproduce such material.

APPLIED COMPUTATIONAL ELECTROMAGNETICS SOCIETY JOURNAL

Editor-in-Chief
Atef Z. Elsherbeni

July 2004
Vol. 19 No. 2
ISSN 1054-4887

The ACES Journal is abstracted in INSPEC, in Engineering Index, DTIC, Science Citation Index Expanded, the Research Alert, and to Current Contents/Engineering, Computing & Technology.

The first, fourth, and sixth illustrations on the front cover have been obtained from the Department of Electrical Engineering at the University of Mississippi.

The third and fifth illustrations on the front cover have been obtained from Lawrence Livermore National Laboratory.

The second illustration on the front cover has been obtained from FLUX2D software, CEDRAT S.S. France, MAGSOFT Corporation, New York.

THE APPLIED COMPUTATIONAL ELECTROMAGNETICS SOCIETY

<http://aces.ee.olemiss.edu>

ACES JOURNAL EDITORS

EDITOR-IN-CHIEF/ACES/JOURNAL

Atef Elsherbeni

University of Mississippi, EE Dept.
University, MS 38677, USA

EDITORIAL ASSISTANT

Matthew J. Inman

University of Mississippi, EE Dept.
University, MS 38677, USA

EDITOR-IN-CHIEF, EMERITUS

David E. Stein

USAF Scientific Advisory Board
Washington, DC 20330, USA

ASSOCIATE EDITOR-IN-CHIEF

Alexander Yakovlev

University of Mississippi, EE Dept.
University, MS 38677, USA

EDITOR-IN-CHIEF, EMERITUS

Ducan C. Baker

EE Dept. U. of Pretoria
0002 Pretoria, South Africa

EDITOR-IN-CHIEF, EMERITUS

Allen Glisson

University of Mississippi, EE Dept.
University, MS 38677, USA

MANAGING EDITOR

Richard W. Adler

833 Dyer Rd, Rm 437 EC/AB
NPS, Monterey, CA 93943-5121, USA

EDITOR-IN-CHIEF, EMERITUS

Robert M. Bevensee

Box 812
Alamo, CA 94507-0516, USA

EDITOR-IN-CHIEF, EMERITUS

Ahmed Kishk

University of Mississippi, EE Dept.
University, MS 38677, USA

ACES JOURNAL ASSOCIATE EDITORS

Giandomenico Amendola

Universita' della Calabria
Rende , Italy

John Beggs

NASA Langley Research Center
Hampton, VA, USA

John Brauer

Ansoft Corporation
Milwaukee, WI, USA

Magda El-Shenawee

University of Arkansas
Fayetteville AR, USA

Pat Foster

Microwave & Antenna Systems
Gt. Malvern, Worc. UK

Cynthia M. Furse

Utah State University
Logan UT, USA

Christian Hafner

Swiss Federal Inst. of Technology
Zurich, Switzerland

Michael Hamid

University of South Alabama,
Mobile, AL, USA

Andy Harrison

Radiance
Huntsville, AL

Chun-Wen Paul Huang

Anadigics, Inc.
Warren, NJ, USA

Todd H. Hubing

University of Missouri-Rolla
Rolla, MO, USA

Nathan Ida

The University of Akron
Akron, OH, USA

Yasushi Kanai

Niigata Institute of Technology
Kashiwazaki, Japan

Leo C. Kempel

Michigan State University
East Lansing MI, USA

Andrzej Krawczyk

Institute of Electrical Engineering
Warszawa, Poland

Stanley Kubina

Concordia University
Montreal, Quebec, Canada

Samir F. Mahmoud

Kuwait University
Safat, Kuwait

Ronald Marhefka

Ohio State University
Columbus, OH, USA

Edmund K. Miller

LASL
Santa Fe, NM, USA

Krishna Naishadham

Wright State University
Dayton, OH, USA

Giuseppe Pelosi

University of Florence
Florence, Italy

Vicente Rodriguez

ETS-Lindgren
Cedar Park, TX, USA

Harold A. Sabbagh

Sabbagh Associates
Bloomington, IN, USA

John B. Schneider

Washington State University
Pullman, WA, USA

Abdel Razek Sebak

University of Manitoba
Winnipeg, MB, Canada

Amr M. Sharawee

American University
Cairo, Egypt

Norio Takahashi

Okayama University
Tsushima, Japan

THE APPLIED COMPUTATIONAL ELECTROMAGNETICS SOCIETY
JOURNAL

July 2004

TABLE OF CONTENTS

“A Rationale for ρ -refinement with the Vector Helmholtz Equation and Two Dimensional Vector Finite Elements” R. S. Preissig and A. F. Peterson.....	65
“The Use of Surface Impedance Boundary Conditions In Time Domain Problems: Numerical And Experimental Validation” S. Barmada, L. Di Rienzo, N. Ida, and S. Yuferev.....	76
“Analysis of Transient Scattering From Conductors Using Laguerre Polynomials as Temporal Basis Functions” B. H. Jung, Y. Chung, M. Yuan and T. K. Sarkar.....	84
“Fast Converging Graded Mesh for Bodies of Revolution with Tip Singularities” K. Hill and T. Van.....	93
“TM Electromagnetic Scattering from 2D Multilayered Dielectric Bodies – Numerical Solution” F. Seydou, R. Duraiswami, N.A. Gumerov, and T. Seppanen	100
“New Compact 3 dB $0^\circ/180^\circ$ Microstrip Coupler Configurations” A. Mohra, A. F. Sheta, and S. F. Mahmoud.....	108
“Advances in Field Theoretical Investigations on Dielectric Image Line Isolators in I-Line Technique” D. Koether, P. Waldow, B. Neuhaus, D. Schreurs, and A. Beyer.....	113
“A LU Decomposition Useful for Antenna Optimization” K. Jamil and E. H. Newman.....	122

A Rationale for p -refinement with the Vector Helmholtz Equation and Two Dimensional Vector Finite Elements

R. Stephen Preissig
Texas Instruments Incorporated
5707 Peachtree Parkway
Norcross, GA 30092

Andrew F. Peterson
School of ECE
Georgia Institute of Technology
Atlanta, GA 30332-0250
peterson@ee.gatech.edu

Abstract: A preliminary study of p -refinement with vector finite elements is reported. Results suggest that improved accuracy can be obtained from representations employing a mixture of polynomial orders instead of a uniform polynomial order. Results also suggest that it might be possible to jump directly from the local error in a $p=0$ expansion to a final representation employing 5 or more polynomial orders. In addition, a new set of hierarchical curl-conforming vector basis functions is proposed.

Introduction

Over the years, there have been many extensions and variations on the classical scalar finite element method. The recent introduction of vector finite elements (edge elements) has created the opportunity for an analogous development of the vector finite element method. One aspect of finite elements is the possibility of adaptive refinement of the finite element mesh, such as the h -refinement process where portions of the mesh are refined to achieve smaller cells and higher accuracy where required, and the p -refinement strategy, where the polynomial order of the representation is selectively increased throughout portions of the mesh [1-3]. Based on work in scalar finite element analysis, it is generally thought that improved convergence can be obtained with one of these refinement schemes or a mixture of h -refinement and p -refinement strategies.

This article considers the benefits of a p -refinement approach for vector finite elements. Texts such as those by Akin [1] and Zienkiewicz

and Taylor [2] discuss p -refinement for scalar finite element applications. The use of vector finite elements, however, is relatively new, and very little has been done to study adaptive methods. Salazar-Palma et al. have explored h -refinement with vector finite elements [3], and several commercial packages (Ansoft's High Frequency Structure Simulator, for one [4]) employ h -refinement with vector elements. Although p -refinement has not been widely considered for the vector case, most aspects of p -refinement for the vector formulation are similar to the scalar formulation. One major difference between the scalar and vector formulations is the basis set, which is correspondingly scalar or vector.

Basis functions

The present investigation considers two-dimensional formulations based on the curl-curl form of the vector Helmholtz equation. A space of vector basis functions suitable for use with the vector Helmholtz equation was introduced by Nedelec in 1980 [5]. These functions maintain tangential cell-to-cell continuity and are known as *curl conforming*. Nedelec's mixed-order basis reduces the number of null valued eigensolutions of the curl-curl operator, which are physically meaningless in a source-free region, and therefore improves computational efficiency [6]. Vector basis functions consistent with Nedelec's spaces have been developed [3, 7]. A goal of the present study was to investigate p -refinement approaches using functions from Nedelec's curl-conforming space.

In practice, p -refinement techniques often incorporate hierarchical basis sets, where the functions comprising order p contain all functions of lower polynomial order. In this manner, p -refinement can be carried out by simply adding a few additional functions during each pass rather than changing the entire set. Several hierarchical vector basis sets have been proposed. Webb and Forghani [8] proposed vector functions for tetrahedral cells that can easily be adapted to triangular cells. They actually only presented functions for the lowest two orders ($p=0$ and $p=1$ in our notation). Wang [9] proposed different vector basis functions based on orthogonal polynomials which may offer improved linear independence. Carrie and Webb [10] proposed a third variety of vector functions for triangles based on Jacobi polynomials. The preceding functions do not appear consistent with Nedelec's spaces. More recently, several authors proposed alternative sets for tetrahedral cells that do appear to be consistent with Nedelec's spaces [11-14]. For completeness, Appendix A summarizes a set of hierarchical functions for triangular cells ranging up to polynomial order 4.5.

Although a practical p -refinement implementation would employ hierarchical bases, for the present investigation we used the interpolatory vector bases of [7] rather than a hierarchical set. The triangular-cell curl-conforming bases of [7], at a given order, provide a representation that is equivalent to that of the hierarchical functions of Appendix A. (In infinite precision arithmetic, the results would be identical.) It is also apparent that a useful implementation of p -refinement would necessarily employ a large dynamic range of basis orders. In the following, results are presented based on a mixture of up to 5 different polynomial orders within the same finite element mesh.

An additional feature of a p -refinement technique is the definition of transition elements, to smooth transition between two regions of different polynomial order. The basis functions employed in this study [7] are each associated with an edge or a patch within the mesh. The patch functions are entirely local to one triangular cell, and contribute no tangential component to any of the cell edges. The tangential continuity of the expansion is ensured by using the same order basis for those functions interpolatory on both sides of a given edge and assigning the same

coefficients to these functions. Thus, these two edge functions may be considered a single edge function which spans both patches common to that edge. Consequently, a transition element is formed when the polynomial order of the functions associated with different edges of the same triangular patch differ. To transition from order p to order q , the basis functions associated with one edge of a triangle may be of order p , while those of another edge are of order q . (We generally constrain the method to no more than two different orders per patch.)

At any stage of the refinement process, a polynomial order is assigned to each edge within the mesh. (A patch order may also be defined as the average of the orders of each of the three edges associated with that patch, rounded up to the next integer.) The goal of the optimization scheme is therefore to determine the order of each edge for the optimal distribution of unknowns throughout the mesh. A more detailed presentation and derivation of the formulation used in this study is presented in reference [15].

Formulation

To investigate the potential advantages of p -refinement, we first wish to determine whether it is possible to obtain a better accuracy/efficiency trade-off using a mixture of basis orders throughout a mesh than it is with a single order. As a canonical problem of interest, we consider the two-dimensional resonant cavity application for the transverse electric (TE) polarization. The vector Helmholtz equation for this situation is

$$\nabla \times \nabla \times \mathbf{E} = k^2 \mathbf{E} \quad (1)$$

For a cavity with perfect electric (PEC) walls, the tangential component of the electric field must vanish on the walls. A weak formulation of the problem is constructed as delineated in Chapter 9 of [6], and we refer the readers to that text for the details. In the following, we consider two specific cavities to illustrate our investigation. The first geometry is a square cavity partially loaded with a dielectric slab with $\epsilon_r=10$. The second structure is a circular cavity with a septum to the center. These examples both possess an exact analytical solution against which to measure the error in a numerical result for the dominant resonant frequency. In addition, the modal

solutions of both of these problems have regions of high variation as well as regions of low variation (Figure 1). The modes of the dielectric-loaded square cavity have relatively high variation within the dielectric, while the circular cavity has a singularity at the tip of the septum, and therefore has a large variation in the vicinity of the tip.

The dielectric-loaded square cavity was studied with three meshes, labeled A, B, and C, having 37, 74 and 158 patches, respectively. The circular cavity was studied with three meshes, labeled D, E and F, having 36, 66 and 128 patches, respectively. In each case, the patch size was relatively uniform throughout the mesh, but the meshes are unstructured. Meshes A and D are shown in Figure 2. For the circular cavity, parabolic curvilinear cells were used along the boundary.

First phase of the study

In the first part of our investigation, we attempted to determine whether a mixture of polynomial orders throughout the mesh offered better accuracy for a given number of unknowns than a representation with a uniform polynomial order. To study this issue, we developed an iterative optimization algorithm that locally adjusted the polynomial order (both up and down) while holding the total number of unknowns fixed. The iterative optimization method used in this study was based on three assumptions:

- (1) The normal discontinuity in the \mathbf{D} -field at cell edges is proportional to the local error. (The normal discontinuity is zero in the true solution.)
- (2) It is optimal for the error to be uniformly distributed throughout the mesh as opposed to localized.
- (3) A localized increase in the number of unknowns will improve the localized solution, decreasing the localized error.

The optimization routine attempts to minimize the standard deviation of the normal discontinuities throughout the mesh for a given number of unknowns. The program first calculates the statistical quantities of interest for the initial distribution of unknowns and attempts to improve the uniformity by increasing the number of

unknowns in highly discontinuous regions and decreasing the number of unknowns in regions with relatively low discontinuities. It was found that the actual limits by which the “high” and “low” discontinuities are defined affect the convergence rate of the optimized solution but not the final solution (if they are picked within reason, of course). These quantities were picked somewhat arbitrarily and will not be discussed here.

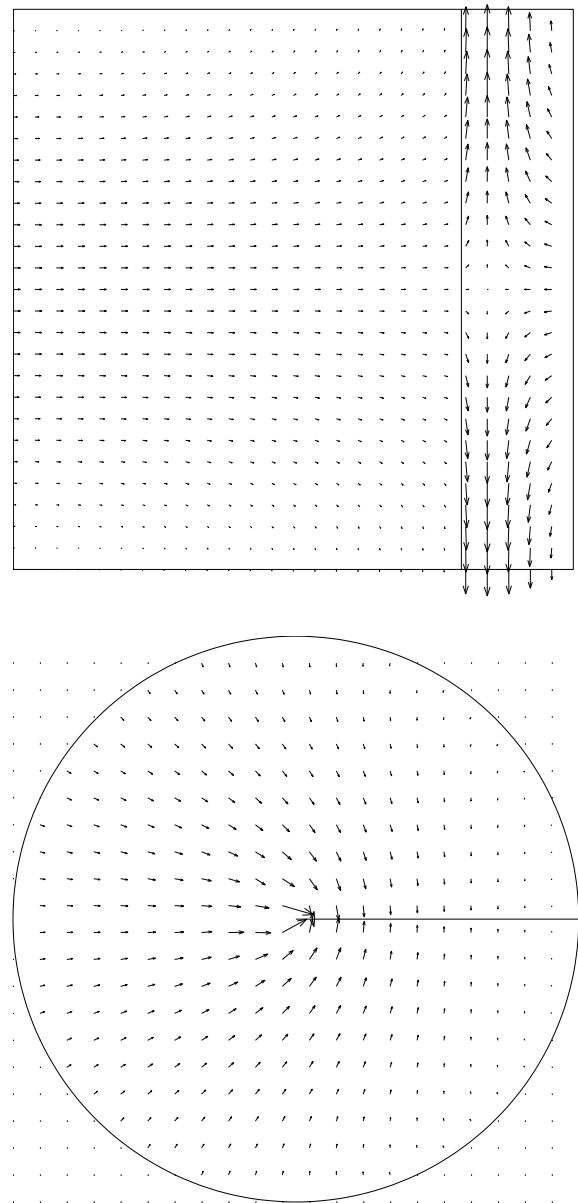


Figure 1. The dominant modes in the square and circular cavities.

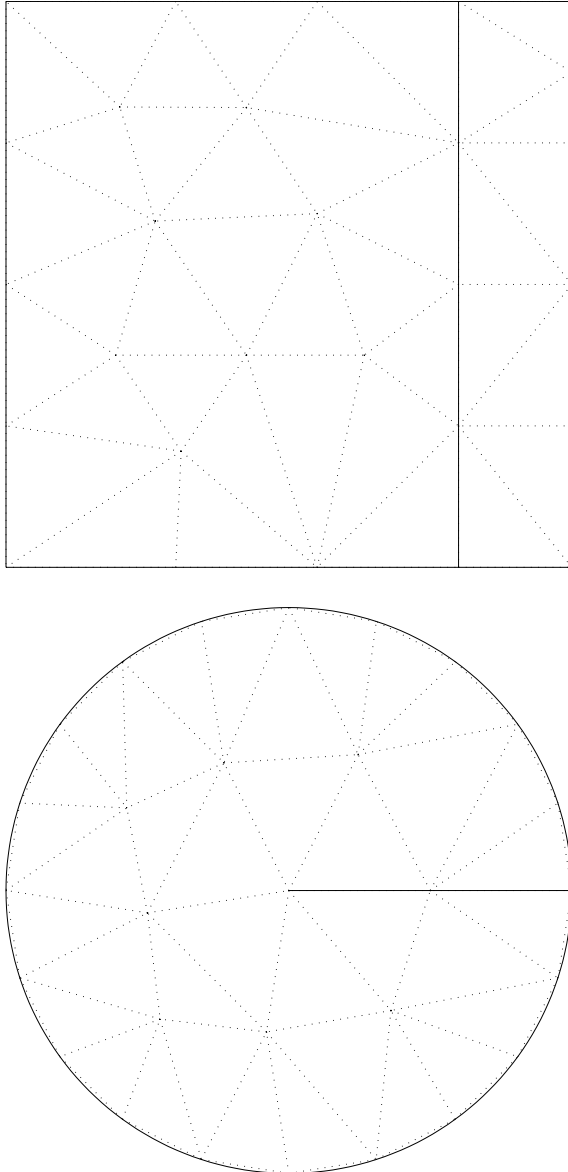


Figure 2. The coarsest meshes for the square and circular cavities.

The reallocation of unknowns is repeated until the program can no longer decrease the standard deviation of the discontinuities in the mesh. This final distribution of unknowns is then regarded as the optimal distribution of unknowns and the error associated with this distribution of unknowns (the error in the dominant resonant wavenumber) is used in a plot of error versus number of unknowns. There is, of course, no guarantee that the result is actually optimal.

Second phase of the study

The first phase of the study investigated whether a more accurate solution was possible with a fixed number of unknowns. In the second phase of the study, we attempted to determine if one could efficiently realize a nearly optimal distribution of unknowns, while avoiding the cumbersome optimization process used in phase 1.

As a first step in the approach, we solve the problem using a uniform zero-order representation throughout the mesh. We then determine the normal discontinuity (in the \mathbf{D} -field) produced at each edge in the mesh by that zero-order representation. The second step is to use that error distribution to immediately assign a “final” polynomial order to each edge in the mesh.

The ambiguity of such an approach is in how many orders and how many edges of each order to assign, since the process is constrained by the total number of unknowns desired. For this study, we cheated — we used the results of the earlier iterative optimization procedure to determine the number of orders and percentage of each order to use. In other words, if for a particular mesh the iterative method determined (after many passes) that 15% of the edges were assigned polynomial order 4, then 15% of the edges were assigned that order in the single step algorithm. However, in the single step procedure the edges chosen for refinement were selected based solely upon the extent of the zero-order normal discontinuity at that edge. Thus, the procedure is not a complete p-refinement algorithm at this point, and our specific approach is not practical for implementation. Data presented below suggest, however, that an efficient algorithm for distributing the unknowns among several orders is possible. The second phase of the study, while not a self contained single step p-refinement capability, does provide insight into the accuracy possible with relatively little computational effort.

Results

Figures 3-8 show the percent error in the dominant cavity resonant frequency determined by various methods versus number of unknowns. Each figure depicts the “homogeneous order solution,” the error obtained using a $p=0$

representation, a $p=1$ representation, etc., throughout the entire mesh.

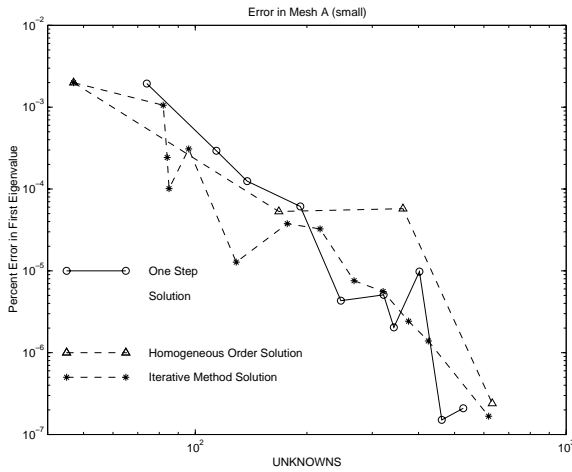


Figure 3. Error Versus Unknowns for Square Cavity, Mesh A, Iterative and One Step Methods.

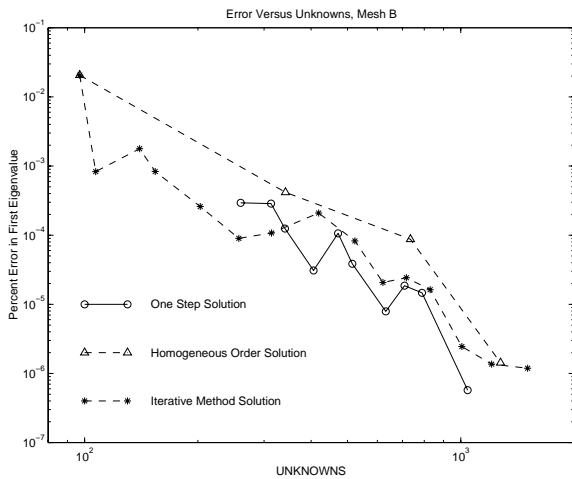


Figure 4. Error Versus Unknowns for Square Cavity, Mesh B, Iterative and One Step Methods.

Each figure also shows the error produced by the iterative optimization process, which employed a mixture of various polynomial orders throughout the mesh. The iterative process attempted to minimize the standard deviation of the normal discontinuity within the dominant mode. For most of the data, the iterative process produced better accuracy for a given number of unknowns (using a mixture of polynomial orders) than the homogeneous solution (a single polynomial order).

Figures 3-8 also show the “one step” solution obtained by jumping from the zero-order result directly to the final distribution of unknowns. The one step solution is usually as good (and occasionally better) than that produced by the gradual iterative process. This suggests that the local error associated with the zero-order solution is a meaningful predictor for the distribution of unknowns in the final result.

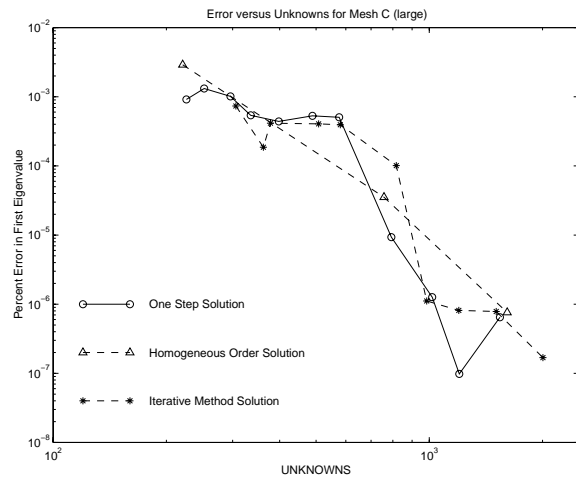


Figure 5. Error Versus Unknowns for Square Cavity, Mesh C, Iterative and One Step Methods.

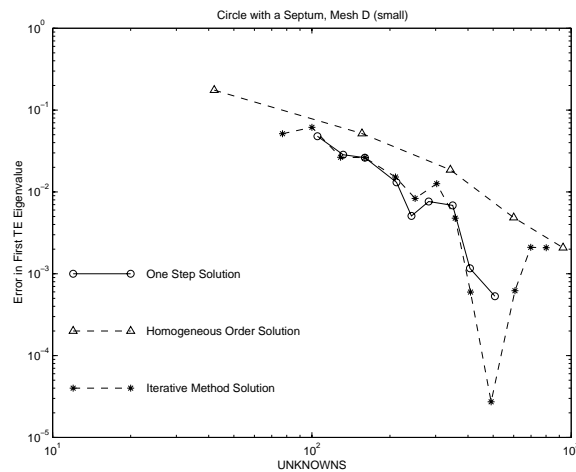


Figure 6. Error Versus Unknowns for Circular Cavity, Mesh D, Iterative and One Step Methods.

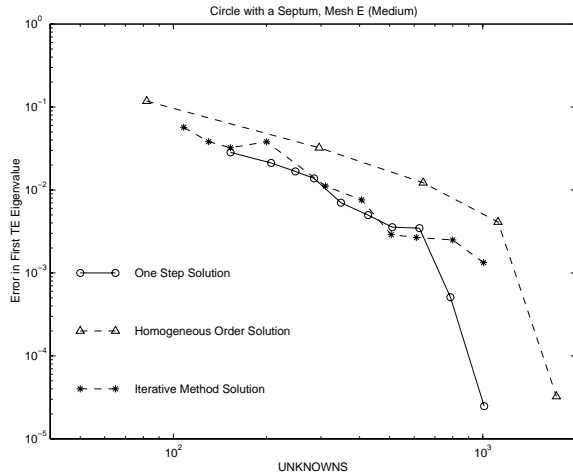


Figure 7. Error Versus Unknowns for Circular Cavity, Mesh E, Iterative and One Step Methods.

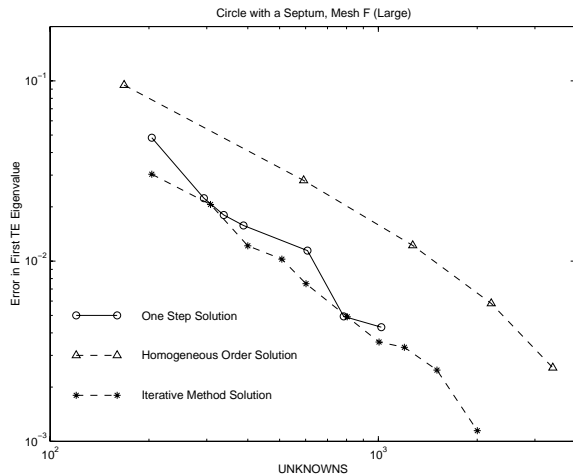


Figure 8. Error Versus Unknowns for Circular Cavity, Mesh F, Iterative and One Step Methods.

For Figures 3-5, representing the square cavity, the optimal distribution of unknowns tended to be that with a single order throughout the air-filled part of the cavity and a higher order throughout the dielectric part. The error curves tend to zigzag up and down as the number of unknowns is increased, due to the fact that a single order in the air filled part of the cavity and a higher order throughout the dielectric part can only be achieved for specific numbers of unknowns. When the algorithm is forced to optimize to a number of unknowns for which this distribution is not possible, it is less efficient. In contrast, the error curves in Figures 6-8 for the circular cavity

show a more uniform behavior. Figure 9 illustrates the distribution of degrees of freedom for mesh F, when optimized for 1000 unknowns.

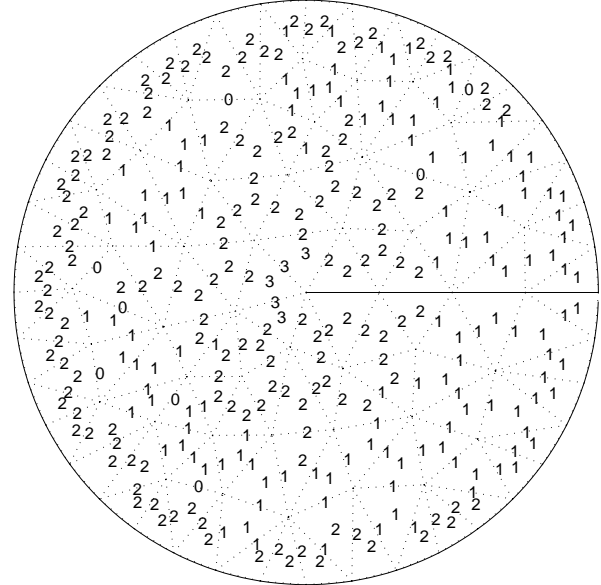


Figure 9. Distribution of degrees of freedom for mesh F when optimized at 1000 unknowns.

As an initial step in developing a control algorithm for p-refinement, we present several plots showing the distribution of polynomial order associated with a given number of unknowns. Figures 10 and 11 show the transition profiles for the square dielectric-loaded cavity (Mesh B) and the circular cavity with a baffle (Mesh E), respectively. The transition profiles show the percentage of the total number of unknowns assigned to each polynomial order for a given number of unknowns. These data are produced using the iterative optimization process. The number of unknowns is normalized to the number of unknowns in the homogeneous zero order case. For example, a normalized number of unknowns of “3” corresponds to three times as many unknowns as in the zero order homogeneous case.

Figures 12 and 13 show the percentage of edges of each polynomial order in terms of a “transition point.” The local error (discontinuity in \mathbf{D} -field) level is organized into a list by edges; the transition point is the position in that list where the transition between orders is assigned. The unknowns in the one step method are assigned

directly by the ordered list of discontinuities. For example, mesh A has 37 edges. If it is determined that there are to be 30 zero order edges and 7 first order edges after refinement, the 0/1 normalized transition point would be $30 / 37 = 0.81$.

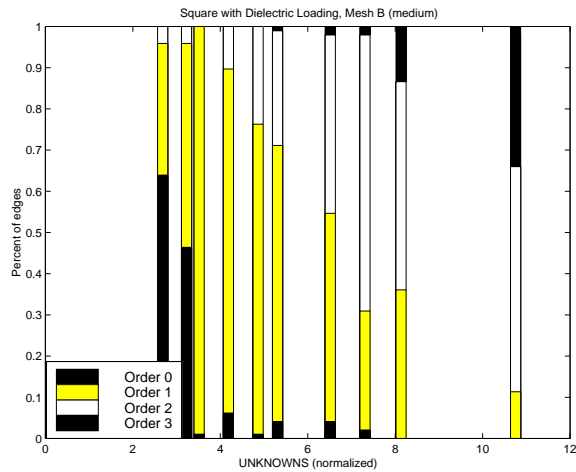


Figure 10. Transition Profile for Square Cavity, Mesh B.

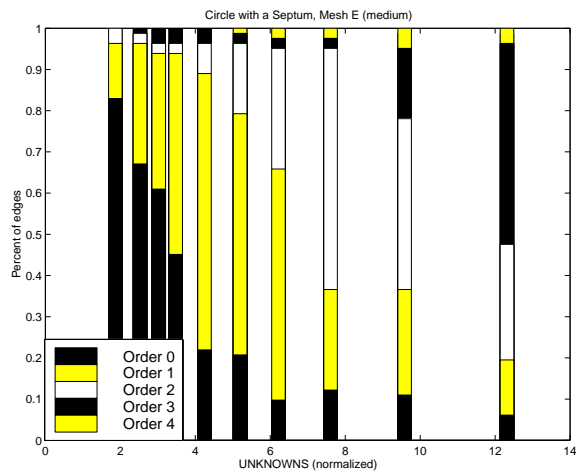


Figure 11. Transition Profile for Circular Cavity, Mesh E.

Because the unknowns in the one step method are assigned directly by the ordered list of discontinuities, the normalized transition point also corresponds to the percentage of edges to which each order is assigned. The 1/2 transition point corresponds to the percentage of edges with

order less than two in the optimized distribution of unknowns. Thus, the difference between the 1/2 transition point and the 0/1 transition point is the percentage of edges with order one in the optimized distribution. Thus, the bar graphs show the percentage of edges assigned to each order.

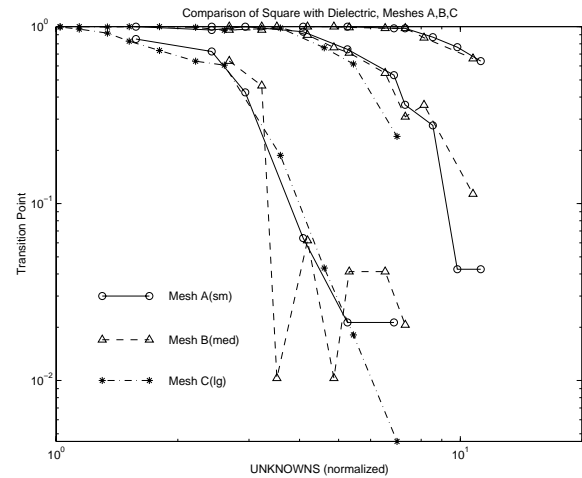


Figure 12. Comparison of Transition Profiles for the Square Cavity, Meshes A, B and C.

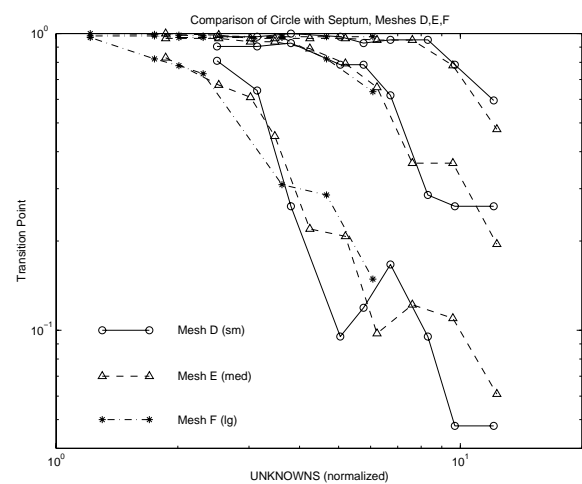


Figure 13. Comparison of Transition Profiles for the Circular Cavity, Meshes D, E and F.

It appears from Figure 12 that the normalized transition points of the different meshes for the square dielectric-loaded cavity occur at roughly the same point. Figure 13 suggests that the normalized transition points of the different meshes of the circular cavity also occur at roughly

the same point. This would indicate that the optimal normalized transition points are not strongly dependent on the number of patches or their arrangement. The transition points of the circular cavity do not, however, occur at the same points as those for the square cavity. Thus, there are other variables that do change these profiles. The similarity of Figures 12 and 13 suggest that it might be possible to develop an algorithm to assign transition points, leading to an efficient implementation of the one step p-refinement procedure, applicable to a wider range of problems than those considered here. Additional research is required to determine an efficient strategy for assigning transition points.

Conclusions

Aspects of p-refinement for vector finite elements have been investigated for two-dimensional cavity applications. Data suggest that representations with mixed polynomial orders offer better accuracy than those with a uniform polynomial order throughout the mesh. A one step p-refinement strategy is studied where the final polynomial order is assigned based on the normal field discontinuity in the zero-order solution. Results suggest that the zero-order result gives meaningful information about the regions to refine, and implies that such a strategy can provide a better accuracy-versus-efficiency trade off than methods based on a uniform polynomial order.

Two further studies would prove of immediate benefit. First, a study detailing the sensitivity of the error versus unknown curves to perturbations of the transition points would give an indication of to what accuracy the transition points must be found in order to reap the gains of a one step p-refinement method. The fact that the error trends for the one step solutions did not differ appreciably from those of the iterative method suggests that there may be significant freedom in choosing these transition points.

A second route of further study would be to attempt to correlate these optimized transition points to factors in the order zero results, such as the standard deviation of the discontinuities in the

order zero solution. If these other factors could be identified, it would be possible to implement an efficient one step p-refinement scheme.

Appendix A: A set of hierarchical vector basis functions for triangles

A set of proposed hierarchical functions for triangular cells is presented in Table 1. These are defined in terms of simplex coordinates (L_1, L_2, L_3) [6]. The lower-order members of this set are similar to the Webb and Forghani functions [8], but have been modified to satisfy the Nedelec conditions [5]. Functions have been included up to order 4/5. For source-free regions, the intent is to use the entire set up to mixed order 0/1, mixed order 1/2, mixed order 2/3, and so on. In other words, a refinement would involve increasing the order from 1/2 to 2/3, not from mixed 1/2 to complete 2. In each case the highest-order members of a given mixed group satisfy the Nedelec conditions.

In Table 1, functions of degrees 3 and 4 are constructed using polynomial products such as $(3L_1 - L_2)(L_1 - L_2)(L_1 - 3L_2)$ in order to enhance the linear independence of the functions. There are a number of ways of constructing such functions, and it can be argued that $(L_1 - L_2)$ is an equally valid way of expressing an equivalent degree of freedom, although possibly not as linearly independent — consider, for instance, the similarity in the shapes of $(L_1 - L_2)$ and $(L_1 - L_2)$. Other specific products could be used.

The vector basis set reported in Table 1 appears to be equivalent to the sets of functions recently reported by Savage [11], Andersen and Volakis [12-13], and Webb [14], if those sets are converted in a fairly obvious manner to triangular cells. This equivalence implies that an appropriate combination of any of these sets of functions conform to Nedelec's curl-conforming spaces. However, the specific elements of each set are different and parameters such as the associated matrix condition numbers may be different as a consequence.

Table 1 Proposed Hierarchal Vector Bases		
mixed order 0/1:	$L_2 \nabla L_3 - L_3 \nabla L_2$ $L_3 \nabla L_1 - L_1 \nabla L_3$ $L_1 \nabla L_2 - L_2 \nabla L_1$	3 edge-based functions total degrees of freedom = 3
complete order 1:	$\nabla(L_1 L_2)$ $\nabla(L_1 L_3)$ $\nabla(L_2 L_3)$	3 edge-based functions total degrees of freedom = 6
mixed order 1/2:	$L_1 (L_2 \nabla L_3 - L_3 \nabla L_2)$ $L_2 (L_3 \nabla L_1 - L_1 \nabla L_3)$	2 cell-based functions total degrees of freedom = 8
complete order 2:	$\nabla\{L_1 L_2 (L_1 - L_2)\}$ $\nabla\{L_1 L_3 (L_1 - L_3)\}$ $\nabla\{L_2 L_3 (L_2 - L_3)\}$ $\nabla\{L_1 L_2 L_3\}$	3 edge-based functions 1 cell-based function total degrees of freedom = 12
mixed-order 2/3:	$L_1 L_2 (L_2 \nabla L_3 - L_3 \nabla L_2)$ $L_1 L_3 (L_2 \nabla L_3 - L_3 \nabla L_2)$ $L_2 L_3 (L_3 \nabla L_1 - L_1 \nabla L_3)$	3 cell-based functions total degrees of freedom = 15
complete order 3:	$\nabla\{L_1 L_2 (2L_1 - L_2) (L_1 - 2L_2)\}$ $\nabla\{L_1 L_3 (2L_1 - L_3) (L_1 - 2L_3)\}$ $\nabla\{L_2 L_3 (2L_2 - L_3) (L_2 - 2L_3)\}$ $\nabla\{L_1 L_2 L_3 (L_1 - L_2)\}$ $\nabla\{L_1 L_2 L_3 (L_1 - L_3)\}$	3 edge-based functions, 2 cell-based functions total degrees of freedom = 20
mixed-order 3/4:	$L_1 L_2 (L_1 - L_2) (L_2 \nabla L_3 - L_3 \nabla L_2)$ $L_1 L_3 (L_1 - L_3) (L_2 \nabla L_3 - L_3 \nabla L_2)$ $L_2 L_3 (L_2 - L_3) (L_3 \nabla L_1 - L_1 \nabla L_3)$ $L_1 L_2 L_3 (L_3 \nabla L_1 - L_1 \nabla L_3)$	4 cell-based functions total degrees of freedom = 24

Table 1, cont.		
Proposed Hierarchal Vector Bases		
complete order 4:	$\nabla\{L_1 L_2 (3L_1 - L_2) (L_1 - L_2) (L_1 - 3L_2)\}$ $\nabla\{L_1 L_3 (3L_1 - L_3) (L_1 - L_3) (L_1 - 3L_3)\}$ $\nabla\{L_2 L_3 (3L_2 - L_3) (L_2 - L_3) (L_2 - 3L_3)\}$ $\nabla\{L_1 L_2 L_3 (2L_1 - L_2) (L_1 - 2L_2)\}$ $\nabla\{L_1 L_2 L_3 (2L_1 - L_3) (L_1 - 2L_3)\}$ $\nabla\{L_1 L_2 L_3 (2L_2 - L_3) (L_2 - 2L_3)\}$	3 edge-based functions, 3 cell-based functions total degrees of freedom = 30
mixed-order 4/5:	$L_1 L_2 (2L_1 - L_2) (L_1 - 2L_2) (L_2 \nabla L_3 - L_3 \nabla L_2)$ $L_1 L_3 (2L_1 - L_3) (L_1 - 2L_3) (L_2 \nabla L_3 - L_3 \nabla L_2)$ $L_2 L_3 (2L_2 - L_3) (L_2 - 2L_3) (L_3 \nabla L_1 - L_1 \nabla L_3)$ $L_1 L_2 L_3 (L_1 - L_2) (L_3 \nabla L_1 - L_1 \nabla L_3)$ $L_1 L_2 L_3 (L_1 - L_3) (L_3 \nabla L_1 - L_1 \nabla L_3)$	5 cell-based functions total degrees of freedom = 35

References

- [1] J. E. Akin, *Finite Elements for Analysis and Design*, Academic Press, San Diego, 1994.
- [2] O. C. Zienkiewicz and R. L. Taylor, *The Finite Element Method*. McGraw-Hill, New York, 1989.
- [3] M. Salazar-Palma et al., *Iterative and Self-Adaptive Finite Elements in Electromagnetic Modeling*. Boston: Artech House, 1998.
- [4] *Ansoft HFSS Users Manual*, October 1999.
- [5] J. C. Nedelec, "Mixed finite elements in R3," *Num. Math.*, vol. 35, pp. 315-341, 1980.
- [6] A. F. Peterson, S. L. Ray and R. Mittra, *Computational Methods For Electromagnetics*, IEEE Press, New York, 1998.
- [7] R. D. Graglia, D. R. Wilton and A. F. Peterson, "Higher Order Interpolatory Vector Bases for Computational Electromagnetics," *IEEE Transactions on Antennas and Propagation*, vol. 45, no. 3, pp. 329-342, March 1997.
- [8] J. P. Webb and B. Forghani, "Hierarchal Scalar and Vector Tetrahedra," *IEEE Trans. Magnetics*, vol. 29, pp. 1495-1498, March 1993.
- [9] J. S. Wang, "Hierarchic 'Edge' Elements for High-Frequency Problems," *IEEE Transactions on Magnetics*, vol. 33, no. 2, pp. 1536-1539, March 1997.
- [10] C. Carrie and J. P. Webb, "Hierarchal Triangular Edge Elements Using Orthogonal Polynomials," *Digest of the*

- 1997 *IEEE Antennas and Propagation International Symposium*, vol. 2, pp. 1310-1313, July 1997.
- [11] J. S. Savage, "Comparing high order vector basis functions," *Proceedings of the 14th Annual Review of Progress in Applied Computational Electromagnetics*, Monterey, CA, pp. 742-749, 1998.
- [12] L. S. Andersen and J. L. Volakis, "Hierarchical Tangential Vector Finite Elements for Tetrahedra," *IEEE Microwave and Guided Wave Letters*, vol. 8, pp.127-129, March 1998.
- [13] L. S. Andersen and J. L. Volakis, "Development and application of a novel class of hierarchical tangential vector finite elements for electromagnetics," *IEEE Transactions on Antennas and Propagation*, vol. 47, pp. 112-120, January 1999.
- [14] J. P. Webb, "Hierarchical vector basis functions of arbitrary order for triangular and tetrahedral finite elements," *IEEE Transactions on Antennas and Propagation*, vol. 47, pp. 1244-1253, August 1999.
- [15] R. S. Preissig, *Local P Refinement in Two Dimensional Vector Finite Elements*, Master's Thesis, Georgia Institute of Technology, Atlanta, GA, 1998.



Steve Preissig graduated from Duke University in Durham, North Carolina in 1996 with a B.S.E. in Biomedical Engineering and went on to earn Masters Degrees in Electrical Engineering and Physics from the Georgia Institute of Technology in Atlanta, Georgia in 1998. Since that time he has worked for Texas Instruments in a field support role and is currently located in Atlanta, Georgia.



Andrew F. Peterson received the B.S., M.S., and Ph.D. degrees in Electrical Engineering from the University of Illinois, Urbana-Champaign in 1982, 1983, and 1986 respectively. Since 1989, he has been a member of the faculty of the School of Electrical and Computer Engineering at the Georgia Institute of Technology, where he is now Professor and Associate Chair for Faculty Development. Within ACES, he served for six years (1991-1997) as a member of the Board of Directors, and has been the Finance Committee Chair and the Publications Committee Chair.

THE USE OF SURFACE IMPEDANCE BOUNDARY CONDITIONS IN TIME DOMAIN PROBLEMS: NUMERICAL AND EXPERIMENTAL VALIDATION

Sami Barmada⁽¹⁾, Luca Di Rienzo⁽²⁾, Nathan Ida⁽³⁾ and Sergey Yuferev⁽⁴⁾

⁽¹⁾ Università di Pisa, Via Diotisalvi 2, 56126 Pisa, ITALY; e-mail: sami.barmada@dsea.unipi.it

⁽²⁾ Politecnico di Milano, Piazza L. da Vinci, 32, 20133 Milano, ITALY; e-mail: luca.dirienzo@polimi.it

⁽³⁾ The University of Akron, Akron OH, 44325-3904, USA; e-mail: ida@uakron.edu

⁽⁴⁾ Nokia Corporation, P.O.Box 86, Salo FIN-24101, FINLAND; e-mail: sergey.yuferev@nokia.com

Abstract: This paper analyzes the limits of applicability of the time domain surface impedance concept. Numerical results obtained by the boundary element formulation employing time domain surface impedance boundary conditions (SIBCs) of different orders of approximation are compared with experimental data and numerical results obtained using the finite element method. An analytical formula for evaluation of the error due to application of the various SIBCs is proposed.

Keywords: Time Domain Solution, Surface Impedance Boundary Conditions, BEM method.

1. Introduction

Transient analysis of skin effect eddy current problems is of significant interest in practice. There are two basic approaches to solve transient problems: (1) by obtaining the solution in the frequency domain for the time-harmonic exciting source and using inverse Fourier transform techniques to calculate the required transient data and (2) by formulating the problem directly in the time domain. In [1, 2] the arguments in favor of the second method are discussed. However, time domain techniques remain computationally expensive in most cases. The problem is simplified if the electromagnetic penetration depth in the conducting body is so short that the variation of the field in the direction tangential to the body's surface is much less than the field variation in the normal direction, so that the complete equation of the electromagnetic field diffusion into the body can be replaced by a one-dimensional equation in the direction normal to the surface of the body. The solution of the reduced equation can be then used to derive the so-called surface impedance boundary conditions (SIBC) involving only the external fields imposed at the outer surface to simulate the material properties of the body and thereby to convert a two (or more) media problem into a one medium problem.

Existence of such conditions follows directly from Snell's law of refraction: if the electromagnetic wave propagates from a low-conductive medium to a high-

conductive medium, the reflection angle is about 90 degrees and it practically does not depend on the incident angle. Suppose the conducting region is so large that the wave attenuates completely inside the region. Then the electromagnetic field distribution in the conductor's skin layer can be described as a damped plane wave propagating into the depth of the conductor, normal to its surface. In other words, the behavior of the electromagnetic field in the conducting region may be assumed known *a priori*. The electromagnetic field is continuous across the real conductor's surface so the intrinsic impedance of the wave remains the same at the interface. Therefore, the ratio E_x/H_y at the xy -plane of the dielectric/conductor interface is assumed to be equal to the intrinsic impedance of the plane wave propagating in the homogeneous conducting body in the positive z -direction:

$$\left. \frac{E_x}{H_y} \right|_{\text{interface}} = Z_\omega = \sqrt{\frac{j\omega\mu}{\sigma + j\omega\epsilon}} \approx \frac{1+j}{2} \mu\omega\delta \Big|_{\sigma \gg \omega\epsilon};$$

$$\delta = \sqrt{\frac{2}{\omega\sigma\mu}} \quad (1)$$

where ω is the angular frequency of the field source, δ is the electromagnetic penetration depth, and σ , ϵ and μ are the electrical conductivity, permittivity and magnetic permeability of the body, respectively.

The SIBC for planar surfaces can be applied as long as the smallest radius of curvature of the surface is much larger than the wavelength inside the conductor. Leontovich developed the SIBC with a first order correction term that accounted for the curvature of the interface [3]. However, usually only the simplified form (1) of his condition is quoted so the SIBC for the planar surface is also called Leontovich's condition. A further correction has been introduced by Mitzner [4], who developed the conditions, now known by his name, for any smooth surface of a conducting body. The Mitzner's SIBC is written in the form:

$$\frac{E_x}{H_y} \Big|_{\text{interface}} = \frac{1+j}{2} \mu \omega \delta \left[1 + \frac{1-j}{4} \delta (d_y^{-1} - d_x^{-1}) \right] \quad (2)$$

where d_x and d_y are the local radii of curvature of the coordinate lines. More information about origins of the surface impedance concept can be found in [5-7].

Note that the condition (2) includes the term containing δ^2 whereas the condition (1) contains δ only. It is natural to expect that the SIBC of the approximation order exceeding the order of the Mitzner's approximation should include terms containing δ^3 and higher. The way to obtain these terms was suggested by Rytov [8] more than sixty years ago. He applied the perturbation method and used the following time-harmonic solution of the one-dimensional equation of the magnetic field diffusion into a perfect conductor as an initial approximation

$$H_y(z) = H_y \Big|_{z=0} \exp(-z/\delta)$$

where $H_y \Big|_{z=0}$ is the tangential magnetic field at the surface of the body. By substituting the solution into Maxwell's equations for the conducting region, Rytov derived the boundary conditions at the planar surface of a highly conducting body in the following form of asymptotic expansions in the skin depth taken as a small parameter

$$E_x \Big|_{\text{interface}} = \frac{1+j}{2} \mu \omega \delta \cdot \left[H_y + \frac{\delta^2}{4j} \left(-\frac{\partial^2 H_y}{\partial x^2} + \frac{\partial^2 H_y}{\partial y^2} + 2 \frac{\partial^2 H_x}{\partial x \partial y} \right) + \dots \right] \Big|_{\text{interface}} \quad (3)$$

The main advantage of the expression in (3) is that the variation of the magnetic field in the direction *tangential* to the body surface is taken into account under the concept of the surface impedance based on the solution of the reduced 1-D problem in the direction *normal* to the body surface. The generality of the condition (3) is not appreciated since only the SIBC of lower order of approximation were used until recently.

The SIBC concepts can also be used in transient problems, when, for instance, the duration of the incident pulse is so short that the field has no time to diffuse deeply into the body and remains concentrated in the thin layer near the body surface. The simplest SIBC in the time domain is obtained directly from (1) by using the inverse Laplace transformation and written in the form of the convolution with respect to time:

$$E_x \Big|_{\text{interface}} = -\sqrt{\mu/(4\pi\sigma)} * H_y \Big|_{\text{interface}} \quad (4)$$

Although condition (4) is mostly applied in analysis of high-frequency problems using the finite difference time domain method [9-11], it was also used in combination with the finite element method [12] and the boundary integral equation method [13-15].

Following the perturbation approach proposed by Rytov, the following time domain SIBC of high order of approximation has been developed [16]:

$$E_x \Big|_{\text{interface}} = \left\{ \hat{T}_1 * H_x + \frac{d_x - d_y}{2d_x d_y} \hat{T}_2 * H_x + \frac{3d_x^2 - d_y^2 - 2d_x d_y}{8d_x^2 d_y^2} \hat{T}_3 * H_x + \frac{\hat{T}_3}{2} * \left(-\frac{\partial^2 H_y}{\partial x^2} + \frac{\partial^2 H_y}{\partial y^2} + 2 \frac{\partial^2 H_x}{\partial x \partial y} \right) \right\} \Big|_{\text{interface}} \quad (5a)$$

Here $*$ denotes a time domain convolution product $U(t)$ is the unit step function and time-dependent functions \hat{T}_k are defined as follows:

$$\hat{T}_1(t) = -(4\pi\sigma/\mu)^{-1/2} t^{-3/2}; \quad \hat{T}_2(t) = U'(t)/\sigma \\ \hat{T}_3(t) = (\pi\sigma^3\mu)^{-1/2} t^{-1/2} \quad (5b)$$

where $U'(t)$ is the delta function.

In some cases it is more convenient to use another SIBC relating normal and tangential components of the magnetic field on the conductor's surface:

$$H_z \Big|_{\text{interface}} = \left\{ T_1 * \left(\frac{\partial H_x}{\partial x} + \frac{\partial H_y}{\partial y} \right) + \frac{d_y - d_x}{2d_x d_y} T_2 * \left(\frac{\partial H_x}{\partial x} - \frac{\partial H_y}{\partial y} \right) + T_3 * \left(\frac{3d_y^2 - d_x^2 - 2d_x d_y}{8d_x^2 d_y^2} \frac{\partial H_x}{\partial x} + \frac{3d_x^2 - d_y^2 - 2d_x d_y}{8d_x^2 d_y^2} \frac{\partial H_y}{\partial y} \right) + \frac{T_3}{2} * \left(-\frac{\partial^2 H_x}{\partial x \partial y^2} - \frac{\partial^2 H_y}{\partial y \partial x^2} + \frac{\partial^3 H_x}{\partial x^3} + \frac{\partial^3 H_y}{\partial y^3} + 2 \frac{\partial^3 H_x}{\partial x \partial y^2} + 2 \frac{\partial^3 H_y}{\partial y \partial x^2} \right) \right\} \quad (6a)$$

$$T_1(t) = (\pi\sigma\mu)^{-1/2} t^{-1/2}, \quad T_2(t) = U(t)/(\sigma\mu), \\ T_3 = (\pi\sigma^3\mu^3)^{-1/2} t^{1/2}. \quad (6b)$$

Although conditions (5) and (6) allow for such effects as curvature of the surface and variation of the field in the tangential direction, the SIBC (4) of lowest (Leontovich's) order of approximation only has been used until now in the time domain calculations (current situation in frequency domain analysis is better:

Mitzner's SIBC (2) is widely used). The matter has uncertain limits of applicability of the surface impedance concept. Indeed, under definition the surface impedance boundary conditions can be used when the skin depth δ is much less than characteristic size D of the conductor's surface:

$$\delta \ll D; \quad D = \min(d_x, d_y, R_{source}, R_{cond}) \quad (7)$$

where R_{source} and R_{cond} are the distances to the source and or neighboring conductor (if the system of conductors is considered), respectively. Condition (7) is usually used to check applicability of the concept. But it does give us neither an approximation error due to application of SIBC nor the rule which SIBC (for example, (4) or (5)) should be used in a given problem. In addition, SIBCs have been originally derived for smooth surfaces whereas real geometries include corners and edges. Although rigorous and practical technique to extend the concept to this kind of problems has not been developed so far, in practice, SIBCs are frequently applied to all kinds of bodies supposing that the errors due to singularities near edges are local. The situation is worse in the time domain due to lack of accurate mathematical definition for the skin depth in the transient case. Thus detailed validation of the SIBCs is of great importance for the concept. This problem has been frequently considered in the past [17-19], but almost all reported works are focused on the frequency domain SIBCs of low order of approximation. According to our knowledge, time domain SIBCs of high orders have not been validated using experimental methods so far. In the present paper limits of applicability of the low-frequency high order time domain SIBCs for homogeneous conductors are investigated by using experimental and numerical techniques.

2. Statement of Transient Problem

Consider a pair of identical long parallel aluminum ($\sigma = 3.82 \times 10^7 \text{ (}\Omega\text{m)}^{-1}$) conductors of circular cross section of the radius D equal to 30 mm. Distance between centers of the conductors is equal to 120 mm. Conductors are connected in series and the circuit is fed by a dc voltage source that provides equal and oppositely directed currents $I_1(t)$ and $I_2(t)$ flowing through the conductors:

$$I_1(t) = -I_2(t). \quad (8)$$

The duration of the source current has been chosen so that

$$\tau \ll \sigma \mu D^2 \quad (9)$$

where τ is the pulse duration. Clearly, (9) is time domain analog of (7).

3. Boundary Element Formulation Employing Time Domain SIBC

Presence of condition (9) enables the surface impedance concept being applied. It is natural to consider the problem as two-dimensional in the plane of cross sections of the conductors. The magnetic scalar potential in free space can be introduced as follows:

$$\vec{H} = \vec{H}^{fil} - \nabla \phi \quad (10)$$

where $\vec{H}^{fil} = \sum_{i=1}^N \vec{H}_i^{fil}$ and \vec{H}_i^{fil} is the magnetic field created by a filamentary conductor carrying the current I_i and placed at position \vec{r}_i and it is expressed by the Biot-Savart law as

$$\left| \vec{H}_i^{fil}(\vec{r}, t) \right| = \frac{I_i(t)}{2\pi |\vec{r} - \vec{r}_i|}. \quad (11)$$

Hence in free space the governing equation is

$$\nabla^2 \phi = 0 \quad (12)$$

and application of the boundary element method yields the following set of integral equations over the contours of cross sections of conductors:

$$\frac{1}{2} \phi + \sum_{i=1}^N \int_{L_i} \phi \frac{\partial G}{\partial \vec{n}'} ds' = \sum_{i=1}^N \int_{L_i} G \frac{\partial \phi}{\partial \vec{n}'} ds' \quad (13)$$

$$\frac{1}{2} \vec{n} \times \vec{H} + \vec{n} \times \sum_{i=1}^N \iint_{L_i, 0}^t \vec{H} \frac{\partial T}{\partial \vec{n}'} dt' ds' = \vec{n} \times \sum_{i=1}^N \iint_{L_i, 0}^t K \frac{\partial \vec{H}}{\partial \vec{n}'} dt' ds' \quad (14)$$

$$\frac{1}{2} \vec{n} \cdot \vec{H} + \vec{n} \cdot \sum_{i=1}^N \iint_{L_i, 0}^t \vec{H} \frac{\partial T}{\partial \vec{n}'} dt' ds' = \vec{n} \cdot \sum_{i=1}^N \iint_{L_i, 0}^t K \frac{\partial \vec{H}}{\partial \vec{n}'} dt' ds' \quad (15)$$

$$\partial \phi / \partial \vec{n} = \vec{n} \cdot (\vec{H}^{fil} - \vec{H}). \quad (16)$$

Here L_i is the contour of the cross section of the conductor i , $s=s(x,y)$ is the coordinate directed along the

contour of the conductor's cross section, \vec{n} is the normal unit vector directed inside a conductor, c is the coefficient depending on the shape of the contour. G and K are the fundamental solutions of the two-dimensional Laplace and diffusion equations, respectively [20]:

$$G(s, s') = \frac{1}{2\pi} \ln \left(\frac{1}{|\vec{r}(s) - \vec{r}(s')|} \right)$$

$$K(s, s') = \frac{(\sigma\mu)^{1/2}}{4\pi(t_F - t)} \exp \left[-\frac{|\vec{r}(s) - \vec{r}(s')|^2 (\sigma\mu)^{1/2}}{4(t_F - t)} \right] \quad (17)$$

with t_F the final time of analysis.

Solution of (13)-(16) yields distributions of ϕ , $(\vec{n} \times \vec{H})$, $(\vec{n} \cdot \vec{H})$ and $\partial(\vec{n} \times \vec{H})/\partial\vec{n}$ over the contour of the conductor's cross sections. Hence, for our problem, ne being the number of elements in which the contour of each conductor is discretized, the system to be solved is a square system of dimension $5 \cdot 2ne$. However, the number of unknowns can be reduced by application of SIBC (6) that in our 2-D case is written in the form:

$$H_n = \frac{\partial H_s}{\partial s} * T_1 + \frac{1}{2D} \frac{\partial H_s}{\partial s} * T_2$$

$$+ \left(\frac{3}{8D^2} \frac{\partial H_s}{\partial s^3} + \frac{1}{2} \frac{\partial^3 H_s}{\partial s^3} \right) * T_3. \quad (18)$$

SIBC (18) can be used instead of integral equations (14)-(15) so the BEM-SIBC formulation consists of equations (13), (16) and (18) and can be solved with respect to ϕ , $(\vec{n} \times \vec{H})$, $(\vec{n} \cdot \vec{H})$. If ne is the total number of nodes, 3 linear systems of ne equations and ne unknowns must be solved in order to calculate the scalar potential over the nodes.

4. Experimental Setup

The experimental set-up is described in Fig. 1. The transient is obtained closing a circuit breaker so that the resulting source current is exponential (see Figure 2). Commercial magnetoresistive sensors (Philips KMZ10A) of nominal sensitivity $S = 80$ mV/(kA/m) lie over the conductors, as described in Fig. 1. Sensor No 1 is in position (-121 mm, 54.2 mm), sensor No. 2 is in position (-73 mm, 54.2 mm) and sensor No. 3 is in position (-25 mm, 54.6 mm). Measurement standard uncertainty of the positions has been estimated 0.5 mm. Sensors are oriented with their sensitivity axis parallel to x -axis. Six low drift, high accuracy instrument amplifiers (INA 128,

Burr Brown) have been employed in order to process and amplify the signals generated by each magnetoresistive sensor. The output signals are sampled and acquired by an 8 channels data acquisition system, with 12-bit resolution and 32 ksamples/s rate for each channel

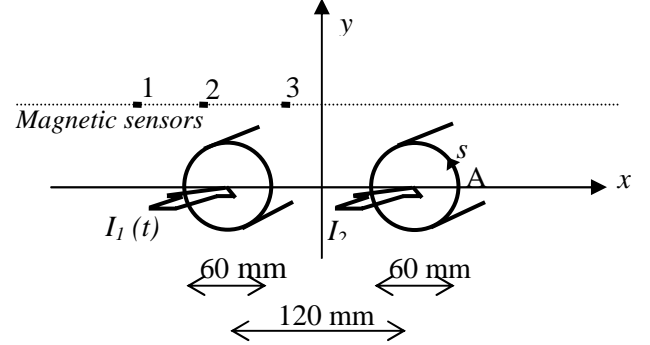


Fig. 1. Experimental set-up.

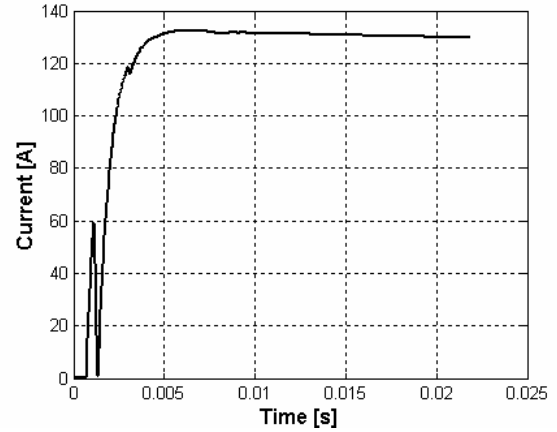


Fig. 2. Current waveform $I_1(t)$.

5. Comparison of Numerical and Experimental Results

In this section the experimental data together with numerical results obtained using BEM formulation employing SIBCs of different orders of approximation and commercial finite element software [21] are presented. Figures 3, 4 and 5 give the magnetic fields at the position of sensors 1, 2 and 3, respectively. Figures 6, 7 and 8 report the difference between calculated and measured fields.

In Figures 9, 10 and 11 distributions of the tangential magnetic field over the surface of the conductor obtained using PEC, Leontovich's, Mitzner's and Rytov's boundary conditions are compared with data obtained using commercial FEM software. BEM code uses 80 nodes per conductor, numbered starting from A along s , and constant elements. From the results shown in Figures

3-11 it can be concluded that the SIBC formulation allows an efficient and accurate simulation of the test case. The hypothesis of perfect electric conductor gives definitely worse results. Increasing the order of the SIBC formulation, numerical results are closer and to the FEM solution and to the experimental measurements, considering uncertainty in the latter. However, it is unclear a priori, until which times BEM-SIBC formulation may be used. For this purpose an analytical formula giving approximate limit of applicability of the surface impedance concept is derived in the next Section. Note that the error (difference between results obtained using BEM-SIBC and FEM) is higher in Figures 9-11 than in Figures 3-8. It occurs because the field in free space has been calculated by performing integration of the scalar potential over the surface of the conductors that reduces computational error.

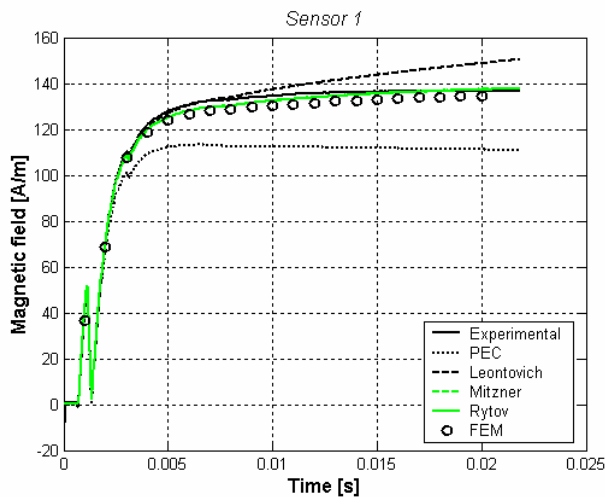


Fig. 3 The magnetic field near the sensor No. 1.

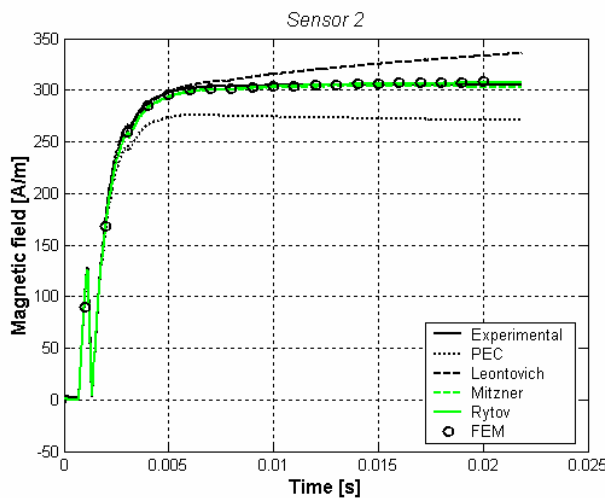


Fig. 4 The magnetic field near the sensor No. 2.

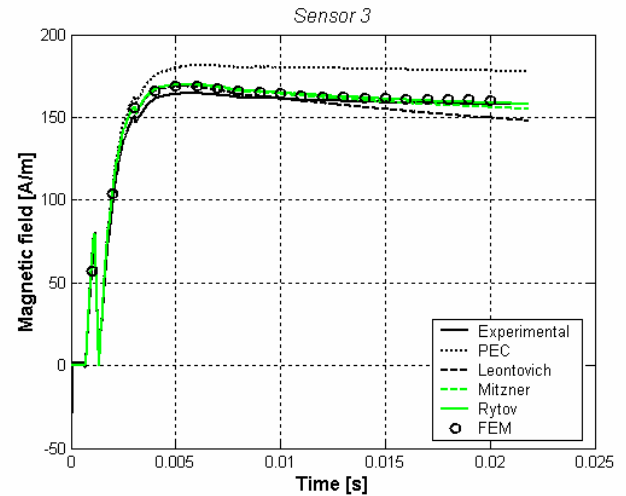


Fig. 5 The magnetic field near the sensor No. 3.

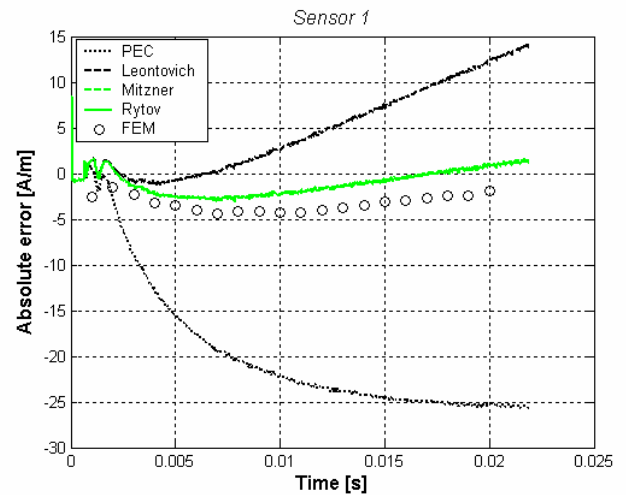


Fig. 6 Difference between computed and measured fields in the case of sensor No. 1.

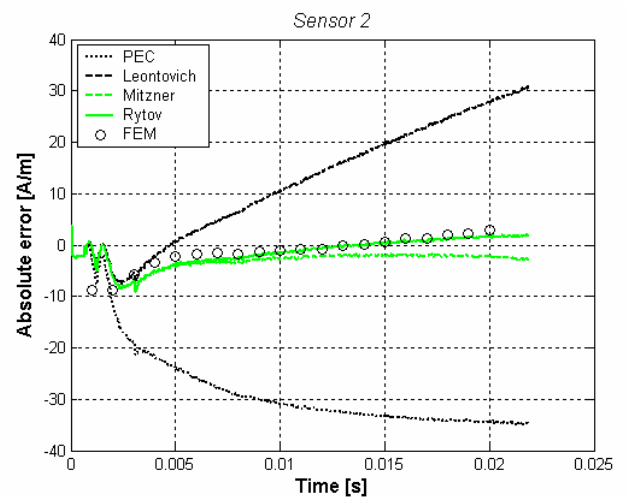


Fig. 7 Difference between computed and measured fields in the case of sensor No. 2.

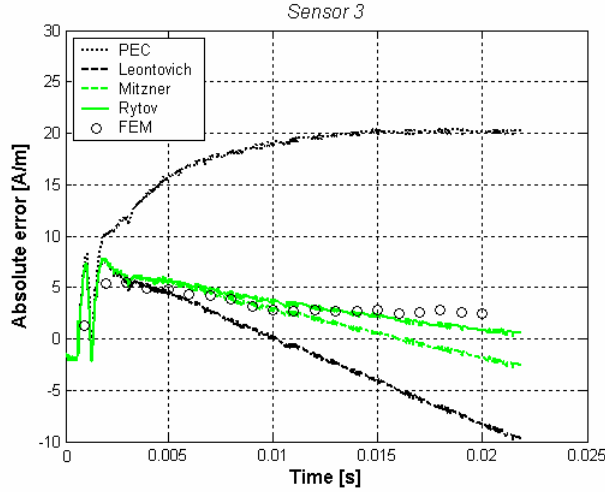


Fig. 8 Difference between computed and measured fields in the case of sensor No. 3.

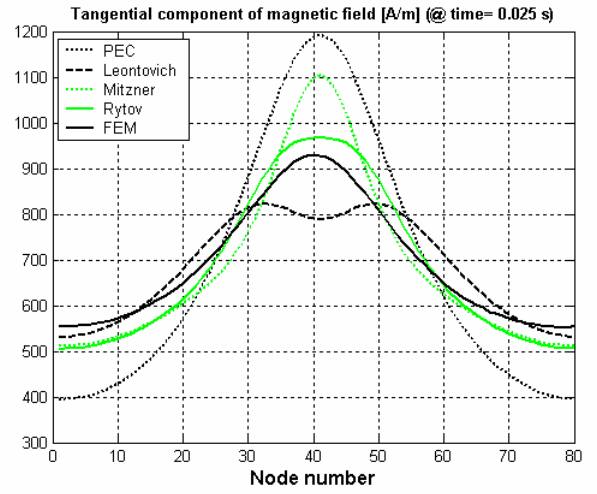


Fig. 11 Distribution of the tangential magnetic field over the conductor's surface at 0.025 s.

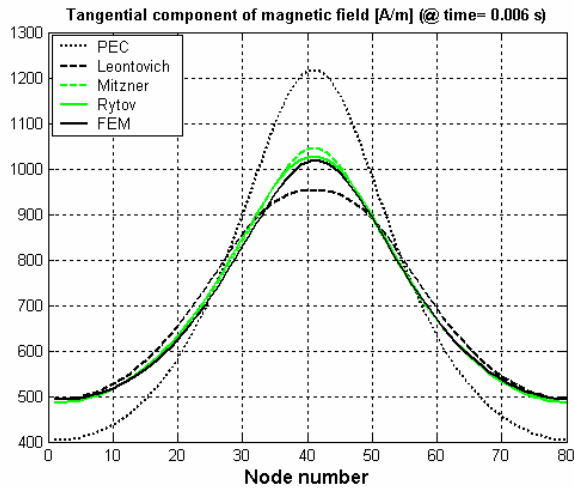


Fig. 9 Distribution of the tangential magnetic field over the conductor's surface at 0.006 s.

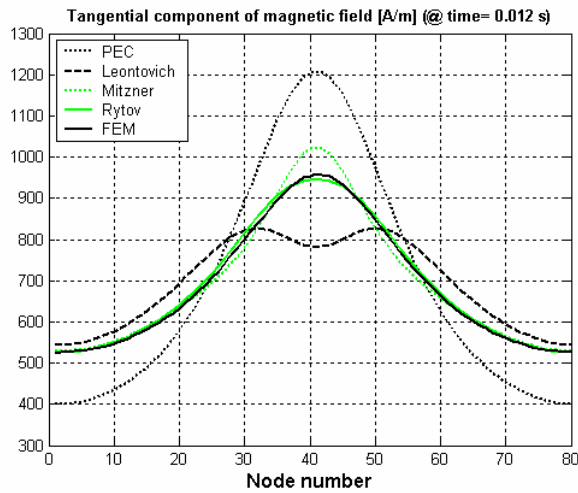


Fig. 10 Distribution of the tangential magnetic field over the conductor's surface at 0.012 s.

6. Conditions of Applicability

Since the surface impedance approach gives the solution in the form of asymptotic expansions, a natural question is limits of their applicability. Basic condition giving an error of approximation of the surface impedance boundary condition is derived from (9) and written in the form:

$$p^k = \left[\tau / (\sigma \mu D^2) \right]^{k/2} \ll 1 \quad (19)$$

where values of k equal to 1, 2, 3 correspond to PEC-limit, Leontovich's SIBC, Mitzner's SIBC and Rytov's SIBC respectively. Small parameter p is combination of two values, τ and D . In our experimental setup the duration τ of the pulse may vary whereas the conductor's radius D is constant. Thus condition (19) can be represented in the form:

$$\varepsilon_k = \alpha^k \tau^{k/2}, \quad \alpha = (\sigma \mu D^2)^{-1/2}, \quad k=1,2,3 \quad (20)$$

where ε_k is the error of approximation k . Figure 10 shows distribution of the errors corresponding to PEC-limit, Leontovich's, Mitzner's and Rytov's approximations. For example, application of Leontovich's SIBC for simulations with the pulse duration equal to 0.0065 s leads to the 10% error. Use of Rytov's SIBC allows to perform simulations for longer pulse of the duration equal to 0.021 s with the same error.

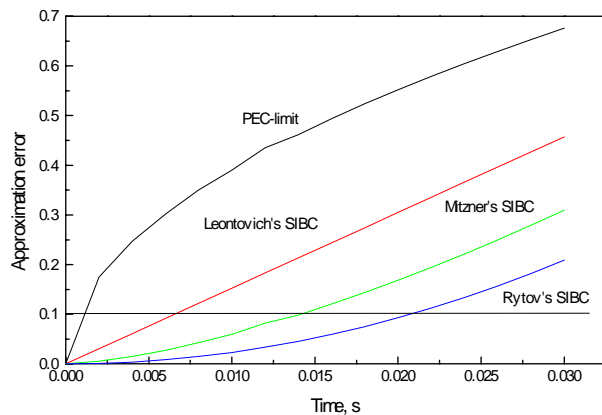


Fig. 12. The approximation error as a function of the pulse duration.

Note that the disagreement between results obtained using the SIBCs and measured data is actually less than the error predicted by the formula (20) since it does not take into account such effects as symmetry of the problem, shape of the pulse and the proximity effect. Nevertheless, (20) gives quick evaluation of the applicability of the surface impedance concept for a given problem and can be used for selection of the approximation order.

7. Conclusions

Experimental and numerical verification of the time domain surface impedance concept has been performed by simulation and measurement of the transient electromagnetic field around a system of two long parallel conductors with oppositely directed currents. The time domain surface impedance boundary conditions of different orders of approximation have been coupled with the boundary element code based on the fundamental solution in free space (the Laplace equation). The results have been compared with measured data and numerical results obtained using the boundary element code employing the fundamental solutions of the Laplace and diffusion equations. A formula for quick evaluation of applicability of the surface impedance concept for a given problem has been proposed and analyzed.

References

[1] C. L. Bennet and G. F. Ross, "Time-domain electromagnetics and its applications", *Proc. IEEE*, Vol. 66, No. 3, pp. 299-318, 1978.
 [2] D. A. Vechinski, S. M. Rao and T. K. Sarkar, "Transient scattering from three-dimensional

arbitrary shaped dielectric bodies", *J. Opt. Soc. Am. A.*, Vol. 11, No. 4, pp. 1458-1470, April 1994.

- [3] M. A. Leontovich, "On the approximate boundary conditions for the electromagnetic field on the surface of well conducting bodies", in *Investigations of Radio Waves*, B.A.Vvedensky Ed., Moscow: Acad. of Sciences of USSR, 1948.
 [4] K. M. Mitzner, "An integral equation approach to scattering from a body of finite conductivity", *Radio Science*, Vol. 2, No. 12, pp. 1459-1470, 1967.
 [5] S. A. Shelkunoff, "The impedance concept and its application to problems of reflection, radiation, shielding and power absorption", *Bell Syst. Tech. J.*, Vol. 17, pp. 17-48, 1938.
 [6] Z. Godzinski, "The surface impedance concept and the theory of radio waves over real earth", *Proc. IEE*, Vol. 108C, pp. 362-373, March 1961.
 [7] J.R. Wait, "The scope of impedance boundary conditions in radio propagation", *IEEE Trans. Geoscience Remote Sensing*, Vol. 28, No. 4, pp. 721-723, 1990.
 [8] S. M. Rytov, "Calculation of skin effect by perturbation method" *J. Experimental'noi i Teoreticheskoi Fiziki*, Vol. 10, No. 2, pp. 180-189, 1940 (in Russian).
 [9] J. G. Maloney and G.S. Smith, "The use of surface impedance concepts in the finite-difference imedomain method", *IEEE Trans. Antennas and Propagation*, Vol. 40, No. 1, pp. 38-48, 1992.
 [10] K. S. Oh and J.E. Schutt-Aine, "An efficient implementation of surface impedance boundary conditions for the finite-difference time-domain method", *IEEE Trans. Antennas Propag.*, Vol. 43, No. 7, pp. 660-666, 1995.
 [11] J. H. Beggs, "A FDTD surface impedance boundary condition using Z-transform", *Applied Comput. Electromagn. Society J.*, Vol. 13, No. 3, pp. 14-24, 1998.
 [12] S. Celozzi and M. Feliziani, "Time domain finite element simulation of conductive regions", *IEEE Trans. Magnetics.*, Vol. 29, No. 2, pp. 1705-1710, March 1993.
 [13] F. M. Tesche, "On the inclusion of loss in time-domain solutions of electromagnetic interaction problems", *IEEE Trans. Electromagn. Compat.*, Vol. 32, No. 1, pp. 1-4, 1990.
 [14] S. Yuferev, "Generalized BIE-BLA formulation of skin and proximity effect problems for an arbitrary regime of the magnetic field generation", *Proc. 2d IEE Intern. Conf. on Computation in Electromagnetics*, IEE publication No. 384, pp. 307-310, 1994.
 [15] S. Yuferev and L. Kettunen, "A unified surface impedance concept for both linear and non-linear

skin effect problems”, *IEEE Trans. on Magnetics*, Vol. 35, No. 3, pp. 1454-1457, 1999.

- [16] S. Yuferev and N. Ida, “Time domain surface impedance boundary conditions of high order of approximation”, *IEEE Trans. on Magnetics*, Vol. 34, No. 5, pp. 2605-2608, 1998.
- [17] N. G. Alexopoulos and G.A. Tadler, “Accuracy of the Leontovich boundary condition for continuous and discontinuous surface impedance”, *J. Appl. Phys.*, Vol. 46, pp. 3326-3332, 1975.
- [18] D-S. Wang, “Limits and validity of the impedance boundary condition on penetrable surfaces”, *IEEE Trans. Antennas and Propagation*, Vol. AP-35, No. 4, pp. 453-457, 1987.
- [19] S. R. H. Hoole, “Experimental validation of the impedance boundary condition and a review of its limitations”, *IEEE Trans. on Magnetics*, Vol. 25, No. 4, pp.3028-3030, 1989.
- [20] C. A. Brebbia, J. C. F. Telles, L. C: Wrobel, *Boundary Element Techniques*, Springer Verlag, 1984.
- [21] *Maxwell 2D Transient*, Ansoft Corporation.



Sami Barmada was born in Livorno, Italy on November 18, 1970. He received his master degree in Electrical Engineering from the University of Pisa in 1995. He worked from 1995 to 1997 at ABB Teknologi (Oslo, Norway), on distribution network analysis and

optimization. In 2001 he received the Ph. D. in Electrical Engineering at the Department of Electrical System and Automation of the University of Pisa.

He is currently working on numerical computation of electromagnetic fields, in particular on the modeling of MTL and to the application of the wavelet expansion to computational electromagnetics.



Luca Di Rienzo was born in Foggia, Italy, in 1971. He received the Laurea degree in Electrical Engineering in 1996 and the Ph. D. degree in Electrical Engineering in 2001, both from the Politecnico di Milano. Currently he is research assistant at Dipartimento di Elettrotecnica of Politecnico di Milano. At

present, his research interests include validation and application of time domain Surface Impedance Boundary Conditions and numerical analysis of inverse problems in electromagnetics.



Nathan Ida is currently Professor of electrical engineering at The University of Akron, Akron, Ohio, USA, where he has been since 1985. His current research interests are in the areas of numerical

modeling of electromagnetic fields, electromagnetic wave propagation, nondestructive testing of materials at low and microwave frequencies and in computer algorithms. Dr. Ida received his B.Sc. in 1977 and M.S.E.E. in 1979 from the Ben-Gurion University in Israel and his Ph.D. from Colorado State University in 1983.

Sergey Yuferev was born in St.Petersburg, Russia, in 1964. He received M.Sc. degree from St.Petersburg Technical University in 1987 and Ph.D degree from A. F. Ioffe Physical-Technical Institute, St.Petersburg, in 1992. From 1987 to 1996, he was with Dense Plasma Dynamics Laboratory of A. F. Ioffe Institute. From 1996 to 1998 he was Visiting Researcher at Tampere University of Technology. From 1999 to 2000 he was Visiting Associate Professor at The University of Akron, Ohio. Since 2000, he has been with Nokia Mobile Phones, Finland. His current research interests include time domain methods of computational electromagnetics and their application to numerical modeling of EMC problems of mobile phones.

ANALYSIS OF TRANSIENT SCATTERING FROM CONDUCTORS USING LAGUERRE POLYNOMIALS AS TEMPORAL BASIS FUNCTIONS

Baek Ho Jung¹, Young-seek Chung², Mengtao Yuan² and Tapan K. Sarkar²

¹Department of Information and Communication Engineering, Hoseo University
Asan, Chungnam 336-795, Korea
e-mail: bhjung@office.hoseo.ac.kr

²Department of Electrical Engineering and Computer Science, Syracuse University
Syracuse, NY 13244-1240
e-mail: ychung05@syr.edu, myuan@syr.edu, tk Sarkar@syr.edu

ABSTRACT

In this paper, a new method is presented for analyzing the transient electromagnetic response from a three-dimensional (3-D) perfectly electric conducting body using the time-domain electric field integral equation (TD-EFIE). Instead of the conventional marching-on in time (MOT) technique, the solution method in this paper is based on the Galerkin's method that involves separate spatial and temporal testing procedure. Triangular patch basis functions are used for spatial expansion and testing functions for arbitrarily shaped 3-D structures. The time-domain unknown coefficient is approximated as an orthonormal basis function set that is derived from the Laguerre functions. These basis functions are also used as the temporal testing. With the representation of the derivative of the time-domain coefficient in an analytic form, the time derivative of the vector potential in the TD-EFIE can be handled analytically. We also propose an alternative formulation to solve the differential form of the TD-EFIE. Two methods presented in this paper result in very accurate and stable transient responses from conducting objects. Detailed mathematical steps are included and representative numerical results are presented and compared.

I. INTRODUCTION

For a time-domain integral equation formulation, the MOT method is usually employed [1]. A serious drawback of this algorithm is the occurrence of late-time instabilities in the form of high frequency oscillation. Several MOT formulations have been presented for the solution of the TD-EFIE to calculate the electromagnetic scattering from arbitrarily shaped three-dimensional structures using triangular patch modeling technique. An explicit solution has been presented by differentiating the TD-EFIE and using second order finite difference [2]. But the results become unstable for late times. Its late time oscillations could be eliminated by approximating the average value of the current [3]. In addition, to overcome this, a backward finite difference approximation for the magnetic vector potential term has

been presented for the explicit technique [4]. Recently an implicit scheme has been proposed to improve the stability problem [5]-[8], in addition matrix pencil is used in [9] to extrapolate the late time data. Even though employing an implicit technique, the accuracy and stability are dependent on the choice of the time step.

In this paper, we present a new technique to obtain accurate and stable responses of the TD-EFIE for arbitrarily shaped 3-D conducting objects using the associate Laguerre polynomials as temporal basis functions. The associate Laguerre series is defined only over the interval from zero to infinity and, hence, are considered to be more suited for the transient problem, as they naturally enforce causality [10], [11]. Using the associate Laguerre polynomials, we construct a set of orthogonal basis functions. Transient quantities that are functions of time can be spanned in terms of these orthogonal basis functions. The temporal basis functions used in this work are completely convergent to zero as time increases to infinity. Therefore, transient response spanned by these basis functions is also convergent to zero as time progresses. Using the Galerkin's method, we introduce a temporal testing procedure, which is similar to the spatial testing procedure of the method of moments (MoM). By applying the temporal testing procedure to the TD-EFIE, we can eliminate the numerical instabilities. Instead of the MOT procedure, we employ a marching-on in-degree manner as increasing the degree of temporal testing functions. Therefore, we can obtain the unknown coefficients by solving a matrix equation recursively with a finite number of basis functions. The minimum degree or number of basis functions is dependent on the time duration and the frequency bandwidth product of an incident wave. We also propose an alternative formulation to solve the differential form of TD-EFIE, which has been used in [2].

This paper is organized as follows. In the next section, we describe the general TD-EFIE and set up a matrix equation by applying MoM with spatial and temporal testing procedure. In section III, an alternative technique

for TD-EFIE formulation is presented. In section IV, we discuss some numerical results. Finally, some conclusions based on this work are presented in section V.

II. FORMULATION

In this section we discuss the TD-EFIE and derive a matrix equation to obtain induced currents on the conducting scatterer. Let S denote the surface of a closed or open conducting body illuminated by a transient electromagnetic wave. Since the total tangential electric field is zero on the surface for all times, we have

$$\left[\mathbf{E}^i(\mathbf{r}, t) + \mathbf{E}^s(\mathbf{r}, t) \right]_{\text{tan}} = 0, r \in S, \quad (1)$$

where \mathbf{E}^i is the incident field and \mathbf{E}^s is the scattered field due to the induced current \mathbf{J} . The subscript 'tan' denotes the tangential component. The scattered field is

$$\mathbf{E}^s(\mathbf{r}, t) = -\frac{\partial}{\partial t} \mathbf{A}(\mathbf{r}, t) - \nabla \Phi(\mathbf{r}, t), \quad (2)$$

where \mathbf{A} and Φ are the magnetic vector and the electric scalar potential given by, respectively,

$$\mathbf{A}(\mathbf{r}, t) = \frac{\mu}{4\pi} \int_S \frac{\mathbf{J}(\mathbf{r}', \tau)}{R} dS' \quad (3)$$

$$\Phi(\mathbf{r}, t) = \frac{1}{4\pi\epsilon} \int_S \frac{q(\mathbf{r}', \tau)}{R} dS'. \quad (4)$$

In (3) and (4), $R = |\mathbf{r} - \mathbf{r}'|$ represents the distance between the arbitrarily located observation point \mathbf{r} and the source point \mathbf{r}' , $\tau = t - R/c$ is the retarded time, μ and ϵ are permeability and permittivity of the space, and c is the velocity of propagation of the electromagnetic wave in that space. The electric surface charge density q is related to the surface current density \mathbf{J} by the equation of continuity

$$\nabla \cdot \mathbf{J}(\mathbf{r}, t) = -\frac{\partial}{\partial t} q(\mathbf{r}, t). \quad (5)$$

Combining (1) and (2) gives

$$\left[\frac{\partial}{\partial t} \mathbf{A}(\mathbf{r}, t) + \nabla \Phi(\mathbf{r}, t) \right]_{\text{tan}} = \left[\mathbf{E}^i(\mathbf{r}, t) \right]_{\text{tan}}, r \in S. \quad (6)$$

Equation (6) with (3) and (4) constitutes a TD-EFIE from which the unknown current \mathbf{J} may be determined.

1. SPATIAL TESTING PROCEDURE

The surface of the structure to be analyzed is approximated by planar triangular patches. As in [12], we define the vector basis function associated with the n -th common edge as

$$\mathbf{f}_n(\mathbf{r}) = \mathbf{f}_n^+(\mathbf{r}) + \mathbf{f}_n^-(\mathbf{r}) \quad (7-1)$$

$$\mathbf{f}_n^\pm(\mathbf{r}) = \begin{cases} \frac{l_n}{2A_n^\pm} \boldsymbol{\rho}_n^\pm, & \mathbf{r} \in T_n^\pm \\ 0, & \mathbf{r} \notin T_n^\pm \end{cases}, \quad (7-2)$$

where l_n and A_n^\pm are the length of the edge and the area of triangle T_n^\pm . $\boldsymbol{\rho}_n^\pm$ is the position vector defined with respect to the free vertex of T_n^\pm . The electric current \mathbf{J} on the scattering structure may be approximated in terms of the vector basis function as

$$\mathbf{J}(\mathbf{r}, t) = \sum_{n=1}^N J_n(t) \mathbf{f}_n(\mathbf{r}), \quad (8)$$

where N represents the number of common edges, discounting the boundary edges in the triangulated model of the conducting object. When (8) is used in (6), we meet a time integral term from the relation (4) and (5). For convenience to avoid this problem and to handle the time derivative of a vector potential analytically, we introduce a new source vector $\mathbf{e}(\mathbf{r}, t)$ defined by

$$\mathbf{J}(\mathbf{r}, t) = \frac{\partial}{\partial t} \mathbf{e}(\mathbf{r}, t), \quad (9)$$

where the relation between this source vector and charge density is given as

$$q(\mathbf{r}, t) = -\nabla \cdot \mathbf{e}(\mathbf{r}, t). \quad (10)$$

By using (8) and (9), we may express

$$\mathbf{e}(\mathbf{r}, t) = \sum_{n=1}^N e_n(t) \mathbf{f}_n(\mathbf{r}). \quad (11)$$

We now solve (6) by applying Galerkin's method in the MoM context and hence the testing functions are same as the expansion functions. By choosing the spatial expansion function $\mathbf{f}_m(\mathbf{r})$ also as the spatial testing functions, we have from (6)

$$\langle \mathbf{f}_m(\mathbf{r}), \frac{\partial}{\partial t} \mathbf{A}(\mathbf{r}, t) \rangle + \langle \mathbf{f}_m(\mathbf{r}), \nabla \Phi(\mathbf{r}, t) \rangle \quad (12)$$

$$= \langle \mathbf{f}_m(\mathbf{r}), \mathbf{E}^i(\mathbf{r}, t) \rangle,$$

where $m = 1, 2, \dots, N$. The next step in the MoM procedure is to substitute the unknown expansion functions defined in (11) into (12). In computing the inner product integrals in (12), we assume that the unknown quantity does not appreciably change within a triangle patch so that

$$\tau = t - \frac{R}{c} \rightarrow \tau_{mn}^{pq} = t - \frac{R_{mn}^{pq}}{c}, R_{mn}^{pq} = |\mathbf{r}_m^{cp} - \mathbf{r}_n^{cq}| \quad (13)$$

where p and q are + or -. $\mathbf{r}_m^{c\pm}$ is the position vector of the center in triangle T_n^\pm . With the assumption (13) and using (3), (4), and (9)-(11), (12) can be written as

$$\sum_{n=1}^N \sum_{p,q} \left[\mu a_{mn}^{pq} \frac{d^2}{dt^2} e_n(\tau_{mn}^{pq}) + \frac{b_{mn}^{pq}}{\varepsilon} e_n(\tau_{mn}^{pq}) \right] = V_m(t),$$

$$m = 1, 2, \dots, N, \quad (14)$$

where

$$a_{mn}^{pq} = \frac{1}{4\pi} \int_S \mathbf{f}_m^p(\mathbf{r}) \cdot \int_S \frac{\mathbf{f}_n^q(\mathbf{r}')}{R} dS' dS \quad (15)$$

$$b_{mn}^{pq} = \frac{1}{4\pi} \int_S \nabla \cdot \mathbf{f}_m^p(\mathbf{r}) \int_S \frac{\nabla' \cdot \mathbf{f}_n^q(\mathbf{r}')}{R} dS' dS \quad (16)$$

$$V_m(t) = \int_S \mathbf{f}_m(\mathbf{r}) \cdot \mathbf{E}^i(\mathbf{r}, t) dS. \quad (17)$$

The integrals (15)-(17) may be evaluated by the method described in [12] and [13].

2. TEMPORAL BASIS FUNCTIONS

Consider the set of functions [14],

$$L_j(t) = \frac{e^{-t}}{j!} \frac{d^j}{dt^j} (t^j e^{-t}), \quad 0 \leq t < \infty, \quad j = 0, 1, 2, \dots \quad (18)$$

These are the Laguerre functions of degree j . They are causal, i.e., exist for $t \geq 0$. They can be computed in a stable fashion recursively through

$$L_0(t) = 1 \quad (19-1)$$

$$L_1(t) = 1 - t \quad (19-2)$$

$$L_j(t) = \frac{1}{j} \left[(2j-1-t)L_{j-1}(t) - (j-1)L_{j-2}(t) \right], \quad j \geq 2. \quad (19-3)$$

The Laguerre functions are orthogonal as

$$\int_0^\infty e^{-t} L_i(t) L_j(t) dt = \delta_{ij} = \begin{cases} 1, & i = j \\ 0, & i \neq j \end{cases} \quad (20)$$

An orthonormal basis function set can be derived from the Laguerre function through the representation

$$\phi_j(t) = e^{-t/2} L_j(t). \quad (21)$$

These functions can approximate a causal response quite well. A causal electromagnetic response function $f(t)$ at a particular location in space for $t \geq 0$ can be expanded using (21) as

$$f(t) = \sum_{j=0}^\infty f_j \phi_j(t). \quad (22)$$

By multiplying a function $f(t)$ with (21) and integrating from zero to infinity, which we call a Laguerre transform here, we get

$$\int_0^\infty \phi_i(t) f(t) dt = f_i. \quad (23)$$

In obtaining (23), the orthogonal relation (20) was used. Also, we can obtain the result of the Laguerre transform for the derivative of the function $f(t)$ as

$$\int_0^\infty \phi_i(t) \frac{d}{dt} f(t) dt = \frac{1}{2} f_i + \sum_{k=0}^{i-1} f_k, \quad (24)$$

where $f(0) = 0$ was assumed and $\phi_i(\infty) = 0$ was used.

Using a similar relation between (22) and (23), we can expand the derivative of the function $f(t)$ using (24) as

$$\frac{d}{dt} f(t) = \sum_{j=0}^\infty \left(\frac{1}{2} f_j + \sum_{k=0}^{j-1} f_k \right) \phi_j(t). \quad (25)$$

Similarly, if we assume $f'(0) = 0$, the result of expanding the second derivative of the function $f(t)$ can be obtained as

$$\frac{d^2}{dt^2} f(t) = \sum_{j=0}^\infty \left[\left(\frac{1}{4} f_j + \sum_{k=0}^{j-1} (j-k) f_k \right) \right] \phi_j(t). \quad (26)$$

3. TEMPORAL TESTING PROCEDURE

The transient coefficient introduced in (11) can be expanded as

$$e_n(t) = \sum_{j=0}^\infty e_{n,j} \phi_j(st), \quad (27)$$

where s is a scaling factor. By controlling this factor s , the support provided by the expansion can be increased or decreased. Using (26), therefore, the expression of expanding the second derivative of the coefficient is given as

$$\frac{d^2}{dt^2} e_n(t) = s^2 \sum_{j=0}^\infty \left[\frac{1}{4} e_{n,j} + \sum_{k=0}^{j-1} (j-k) e_{n,k} \right] \phi_j(st). \quad (28)$$

Substituting (27) and (28) into (14) and taking a temporal testing with $\phi_i(st)$, which is the Laguerre transform defined in (23), we have

$$\sum_{n=1}^N \sum_{p,q} \sum_{j=0}^\infty \left[\left(\frac{s^2}{4} \mu a_{mn}^{pq} + \frac{b_{mn}^{pq}}{\varepsilon} \right) e_{n,j} + s^2 \mu a_{mn}^{pq} \sum_{k=0}^{j-1} (j-k) e_{n,k} \right] I_{ij} \left(s \frac{R_{mn}^{pq}}{c} \right) = V_{m,i}, \quad (29)$$

where

$$I_{ij} \left(s \frac{R_{mn}^{pq}}{c} \right) = \int_0^\infty \phi_i(st) \phi_j \left(st - s \frac{R_{mn}^{pq}}{c} \right) d(st); \quad (30)$$

$$V_{m,i} = \int_0^\infty \phi_i(st) V_m(t) d(st). \quad (31)$$

Now, we consider the integral defined in (30). For simplicity, we rewrite (30) as

$$I_{ij}(y) = \int_0^\infty \phi_i(x) \phi_j(x-y) dx. \quad (32)$$

Through the following change of variable $z = x - y$ in (32), we have

$$I_{ij}(y) = e^{-y/2} \int_{-y}^{\infty} e^{-z} L_i(z+y) L_j(z) dz. \quad (33)$$

Using the formula (8.971) and (8.974) in [15], we obtain

$$L_i(z+y) = \sum_{k=0}^i L_k(z) [L_{i-k}(y) - L_{i-k-1}(y)]. \quad (34)$$

Substituting (34) into (33), we obtain

$$I_{ij}(y) = e^{-y/2} \sum_{k=0}^i [L_{i-k}(y) - L_{i-k-1}(y)] \int_{-y}^{\infty} e^{-z} L_k(z) L_j(z) dz. \quad (35)$$

Because the Laguerre function is defined for $z \geq 0$, the lower limit of the integral in (35) may be changed from $-y$ to zero, and the integral can be computed easily using (20). Finally, we have

$$I_{ij}(y) = \begin{cases} e^{-y/2} [L_{i-j}(y) - L_{i-j-1}(y)], & j \leq i \\ 0, & j > i \end{cases}. \quad (36)$$

We note that $I_{ij} = 0$ when $j > i$. Therefore we can write the upper limit for the summation symbol as i instead of ∞ in (29). In this result, moving the terms including $e_{n,j}$, which is for $j < i$, to the right-hand side, we obtain

$$\begin{aligned} & \sum_{n=1}^N \sum_{p,q} \left(\frac{s^2}{4} \mu \alpha_{mn}^{pq} + \frac{b_{mn}^{pq}}{\epsilon} \right) e_{n,i} I_{ii} \left(s \frac{R_{mn}^{pq}}{c} \right) = \\ & V_{m,i} - \sum_{n=1}^N \sum_{p,q} \sum_{j=0}^{i-1} \left(\frac{s^2}{4} \mu \alpha_{mn}^{pq} + \frac{b_{mn}^{pq}}{\epsilon} \right) e_{n,j} I_{ij} \left(s \frac{R_{mn}^{pq}}{c} \right) \\ & - \sum_{n=1}^N \sum_{p,q} \sum_{j=0}^i s^2 \mu \alpha_{mn}^{pq} \sum_{k=0}^{j-1} (j-k) e_{n,k} I_{ij} \left(s \frac{R_{mn}^{pq}}{c} \right). \end{aligned} \quad (37)$$

Rewriting (37) in a simpler form, we have

$$\sum_{n=1}^N \alpha_{mn} e_{n,i} = V_{m,i} + P_{m,i}, \quad m = 1, 2, \dots, N, \quad (38)$$

where

$$\begin{aligned} \alpha_{mn} &= \sum_{p,q} \left(\frac{s^2}{4} \mu \alpha_{mn}^{pq} + \frac{b_{mn}^{pq}}{\epsilon} \right) \exp \left(-s \frac{R_{mn}^{pq}}{2c} \right) \\ P_{m,i} &= - \sum_{n=1}^N \sum_{p,q} \left[\left(\frac{s^2}{4} \mu \alpha_{mn}^{pq} + \frac{b_{mn}^{pq}}{\epsilon} \right) \sum_{j=0}^{i-1} e_{n,j} I_{ij} \left(s \frac{R_{mn}^{pq}}{c} \right) + \right. \\ & \left. s^2 \mu \alpha_{mn}^{pq} \sum_{j=0}^i \sum_{k=0}^{j-1} (j-k) e_{n,k} I_{ij} \left(s \frac{R_{mn}^{pq}}{c} \right) \right]. \end{aligned} \quad (40)$$

In obtaining (39), we used $I_{ii}(y) = e^{-y/2}$ from (36).

Finally, we can write (38) in a matrix form as

$$[\alpha_{mn}] [e_{n,i}] = [\gamma_{m,i}], \quad i = 0, 1, \dots, \infty, \quad (41)$$

where $\gamma_{m,i} = V_{m,i} + P_{m,i}$. It is important to note that $[\alpha_{mn}]$ is not a function of the degree of the temporal testing

function. Therefore, we can obtain the unknown coefficients by solving (41) by increasing the degree of the temporal testing functions. The coefficients of the current $J_n(t)$ oscillate for low degrees and die down for high degrees. We can solve the coefficients recursively until they are small enough. Therefore, this formulation is marching on in degree as opposed to marching on-in time for an implicit procedure. The matrix equation is first solved for $i = 0$ and then continued for different values for i which corresponds to different order of the Laguerre functions.

We need the minimum degree or number of temporal basis functions, M in computing (41). This parameter is dependent on the time duration of the transient response and the bandwidth of the excitation signal. We consider a signal with a bandwidth B in frequency-domain and the duration T_f in the time-domain. When we represent this signal by a Fourier series, the range of the sampling frequency is $-B \leq k\Delta f \leq B$, where k is an integer and $\Delta f = 1/T_f$. So we get $|k| \leq B/T_f$. Hence the minimum number of temporal basis functions becomes $M = 2BT_f + 1$. We note that the upper limit of the integral in (31) can be replaced by a time duration sT_f instead of infinity.

4. CURRENT AND FAR FIELD

By solving the matrix equation (41) in a marching-on in degree manner, the electric transient current coefficient in (8) is expressed using the relation (9) and (11) with (25) as

$$J_n(t) = \frac{d}{dt} e_n(t) = s \sum_{j=0}^{M-1} \left(\frac{1}{2} e_{n,j} + \sum_{k=0}^{j-1} e_{n,k} \right) \phi_j(st). \quad (42)$$

Once the current coefficients have been obtained, we can compute the far field. We explain the analytic method to compute the far field directly by using the coefficient $e_n(t)$ obtained from (41). Neglecting the scalar potential term, the far field is given by

$$\mathbf{E}(\mathbf{r}, t) \approx -\frac{\partial}{\partial t} \mathbf{A}(\mathbf{r}, t). \quad (43)$$

Substituting (3), (9), and (11) into (43) with (7-1), we get

$$\mathbf{E}(\mathbf{r}, t) \approx -\frac{\mu}{4\pi} \sum_{n=1}^N \sum_q \int_s \frac{d^2}{dt^2} e_n(\tau) \frac{\mathbf{f}_n^q(\mathbf{r}')}{R} dS'. \quad (44)$$

We make the following approximation in the far field:

$R \approx r - \mathbf{r}' \cdot \hat{\mathbf{r}}$ for the time retardation term $\tau = t - R/c$, $R \approx r$ for the amplitude term $1/R$, where $\hat{\mathbf{r}} = \mathbf{r}/r$ is a unit vector in the direction of the radiation. The integral in (44) is evaluated by approximating the integrand by the value at the center of the source triangle T_n^q .

Substituting (7-2) into (44) and approximating $\mathbf{r}' \approx \mathbf{r}_n^{cq}$ and $\boldsymbol{\rho}_n^q \approx \boldsymbol{\rho}_n^{cq}$, we obtain

$$\mathbf{E}^s(\mathbf{r}, t) \approx -\frac{\mu}{8\pi r} \sum_{n=1}^N l_n \sum_q \boldsymbol{\rho}_n^{cq} \frac{d^2}{dt^2} e_n(\tau_n^q), \quad (45)$$

where $\tau_n^q \approx t - (r - \mathbf{r}_n^{cq} \cdot \hat{\mathbf{r}}) / c$ and

$$\frac{d^2}{dt^2} e_n(t) = s^2 \sum_{j=0}^{M-1} \left[\frac{1}{4} e_{n,j} + \sum_{k=0}^{j-1} (j-k) e_{n,k} \right] \phi_j(s\tau_n^q). \quad (46)$$

III. ALTERNATIVE FORMULATION

In this section, we present an alternative method of solving TD-EFIE as given in (1), which has been extensively used in the literature. The goal is to see which form provides more accurate solution as this method contains double derivatives. By differentiating (6), we get

$$\left[\frac{\partial^2}{\partial t^2} \mathbf{A}(\mathbf{r}, t) + \nabla \frac{\partial}{\partial t} \Phi(\mathbf{r}, t) \right]_{\tan} = \left[\frac{\partial}{\partial t} \mathbf{E}^i(\mathbf{r}, t) \right]_{\tan}, \quad \mathbf{r} \in S. \quad (47)$$

In a similar manner as in (12), we obtain the result of the spatial testing from (47) as

$$\begin{aligned} & \langle \mathbf{f}_m(\mathbf{r}), \frac{\partial^2}{\partial t^2} \mathbf{A}(\mathbf{r}, t) \rangle + \langle \mathbf{f}_m(\mathbf{r}), \nabla \frac{\partial}{\partial t} \Phi(\mathbf{r}, t) \rangle \\ & = \langle \mathbf{f}_m(\mathbf{r}), \frac{\partial}{\partial t} \mathbf{E}^i(\mathbf{r}, t) \rangle. \end{aligned} \quad (48)$$

Substituting (3)-(5), (7), and (8) into (48) and with the use of (13), we get

$$\sum_{n=1}^N \sum_{p,q} \left[\mu a_{mn}^{pq} \frac{d^2}{dt^2} J_n(\tau_{mn}^{pq}) + \frac{b_{mn}^{pq}}{\epsilon} J_n(\tau_{mn}^{pq}) \right] = V_m(t), \quad (49)$$

where a_{mn}^{pq} and b_{mn}^{pq} are same as to (15) and (16), respectively, and

$$V_m(t) = \int_S \mathbf{f}_m(\mathbf{r}) \cdot \frac{\partial}{\partial t} \mathbf{E}^i(\mathbf{r}, t) dS. \quad (50)$$

The transient current coefficient can be written as

$$J_n(t) = \sum_{j=0}^{\infty} J_{n,j} \phi_j(st), \quad (51)$$

where s is a scaling factor. Using (26), the second derivative of the current coefficient is given as

$$\frac{d^2}{dt^2} J_n(t) = s^2 \sum_{j=0}^{\infty} \left[\frac{1}{4} J_{n,j} + \sum_{k=0}^{j-1} (j-k) J_{n,k} \right] \phi_j(st). \quad (52)$$

Substituting (51) and (52) into (49) with the temporal testing with $\phi_i(st)$, we get

$$\sum_{n=1}^N \sum_{p,q} \sum_{j=0}^{\infty} \left[\left(\frac{s^2}{4} \mu a_{mn}^{pq} + \frac{b_{mn}^{pq}}{\epsilon} \right) J_{n,j} \right. \\ \left. + s^2 \mu a_{mn}^{pq} \sum_{k=0}^{j-1} (j-k) J_{n,k} \right] I_{ij} \left(s \frac{R_{mn}^{pq}}{c} \right) = V_{m,i}, \quad (53)$$

where $V_{m,i}$ is of the same form given in (31), but $V_m(t)$ is different. Changing the upper limit of the summation symbol to i instead of ∞ in (53) and moving the terms including $J_{n,j}$, which is for $j < i$, to the right-hand side, we obtain

$$\begin{aligned} & \sum_{n=1}^N \sum_{p,q} \left(\frac{s^2}{4} \mu a_{mn}^{pq} + \frac{b_{mn}^{pq}}{\epsilon} \right) J_{n,i} I_{ii} \left(s \frac{R_{mn}^{pq}}{c} \right) \\ & = V_{m,i} - \sum_{n=1}^N \sum_{p,q} \sum_{j=0}^{i-1} \left(\frac{s^2}{4} \mu a_{mn}^{pq} + \frac{b_{mn}^{pq}}{\epsilon} \right) J_{n,j} I_{ij} \left(s \frac{R_{mn}^{pq}}{c} \right) \\ & \quad - \sum_{n=1}^N \sum_{p,q} \sum_{j=0}^i s^2 \mu a_{mn}^{pq} \sum_{k=0}^{j-1} (j-k) J_{n,k} I_{ij} \left(s \frac{R_{mn}^{pq}}{c} \right). \end{aligned} \quad (54)$$

Rewriting (54) in a simple form, we have

$$\sum_{n=1}^N \alpha_{mn} J_{n,i} = V_{m,i} + P_{m,i}, \quad m = 1, 2, \dots, N, \quad (55)$$

where α_{mn} is same as (39) and

$$P_{m,i} = - \sum_{n=1}^N \sum_{p,q} \left[\left(\frac{s^2}{4} \mu a_{mn}^{pq} + \frac{b_{mn}^{pq}}{\epsilon} \right) \sum_{j=0}^{i-1} J_{n,j} I_{ij} \left(s \frac{R_{mn}^{pq}}{c} \right) \right. \\ \left. + s^2 \mu a_{mn}^{pq} \sum_{j=0}^i \sum_{k=0}^{j-1} (j-k) J_{n,k} I_{ij} \left(s \frac{R_{mn}^{pq}}{c} \right) \right]. \quad (56)$$

Lastly, we can write (55) in a matrix form as

$$[\alpha_{mn}] [J_{n,i}] = [\gamma_{m,i}], \quad (57)$$

where $\gamma_{m,i} = V_{m,i} + P_{m,i}$. By solving (57) by a marching-on in degree algorithm with M temporal basis functions, we can obtain the current coefficient directly, which is given as

$$J_n(t) = \sum_{j=0}^{M-1} J_{n,j} \phi_j(st). \quad (58)$$

Substituting (3) and (8) into (43) with (7), and using (25), the far field is given as

$$\mathbf{E}^s(\mathbf{r}, t) \approx -\frac{\mu}{8\pi r} \sum_{n=1}^N l_n \sum_q \boldsymbol{\rho}_n^{cq} \frac{d}{dt} J_n(\tau_n^q), \quad (59)$$

where

$$\frac{d}{dt} J_n(\tau_n^q) = s \sum_{j=0}^{M-1} \left(\frac{1}{2} J_{n,j} + \sum_{k=0}^{j-1} J_{n,k} \right) \phi_j(st). \quad (60)$$

The formulation provided in this section computes the coefficients of $J_n(t)$ directly. We don't need to convert $e_n(t)$ to $J_n(t)$ by (42). However, this formulation

requires the derivative of the incident wave as in (50). Gaussian wave is used extensively in transient analysis, and we have the analytic form of derivative of Gaussian wave. Two formulations will obtain the same performance by using Gaussian wave, as shown in the next section. If we have an arbitrary input, the formulation introduced in section II is preferred.

It's important to notice that the minimum degree can be obtained at the optimal scaling factor s . We can estimate the range for convergence and the optimal scaling factor s by B and Tf , and solve $J_{n,i}$ recursively, until $J_{n,i}$ converges to zero ([16]). Stable performance can be obtained by this way.

IV. NUMERICAL EXAMPLES

In this section, we present the numerical results for three representative 3-D scatterers, viz. a sphere, a cube, and a cylinder, as shown in Fig. 1. The scatterers are illuminated by a Gaussian plane wave, in which the electric field is given by

$$\mathbf{E}^i(\mathbf{r}, t) = \mathbf{E}_0 \frac{4}{\sqrt{\pi T}} e^{-\gamma^2}, \quad (61)$$

$$\gamma = \frac{4}{T}(ct - ct_0 - \mathbf{r} \cdot \hat{\mathbf{k}}), \quad (62)$$

where $\hat{\mathbf{k}}$ is the unit vector in the direction of wave propagation, T is the pulse width of the Gaussian impulse, and t_0 is a time delay which represents the time at which the pulse peaks at the origin. In this work, the field is incident from $\phi = 0^\circ$ and $\theta = 0^\circ$ with $\hat{\mathbf{k}} = -\hat{\mathbf{z}}$ and $\mathbf{E}_0 = \hat{\mathbf{x}}$. To avoid problems with the internal resonance of the structure, we use a pulse of width $T = 8$ lm with $ct_0 = 12$ lm, which has a frequency spectrum of 125 MHz. The unit 'lm' denotes a light meter. A light meter is the length of time taken by the electromagnetic wave to travel 1 m. We set $s = 10^9$ and $M = 80$, which is sufficient to get accurate solutions. For comparison, we present MOT solutions using the method in [8] and the results obtained by taking the IDFT solution calculated from the frequency-domain EFIE. In all figures to be shown, the legends 'form1' and 'form2' implies results computed by the formulation in section II and section III, respectively.

As a first example, we consider a conducting sphere of radius 0.5 m centered at the origin as shown in Fig. 1(a). The first resonant frequency of this sphere is 262 MHz. There are twelve and twenty-four divisions along the θ and ϕ directions with equal angular intervals. This results in a total of 528 patches and 792 common edges, and $R_{\min} = 2.23$ cm, where R_{\min} represents the minimum distance between any two distinct patch centers. The

θ -directed current at $\theta = 90^\circ$ and $\phi = 7.5^\circ$, and ϕ -directed current at $\theta = 7.5^\circ$ and $\phi = 90^\circ$ on the sphere are indicated by arrows in Fig. 1(a). Fig. 2 shows the transient response for the θ -directed and ϕ -directed current. The time step in the MOT computation is chosen such that $c\Delta t = 4R_{\min}$ in order to generate an implicit solution. It is important to note that all the four solutions show good agreements except the late-time oscillation in the MOT solution. We can see that solutions of the presented method 1 and 2 are stable and the agreement between each other is very good. Fig. 3 compares the transient response of two presented methods with the Mie series solution and the IDFT of the frequency-domain EFIE solution for the far scattered field from the sphere along the backward direction. All the four solutions agree well as is evident from the figure.

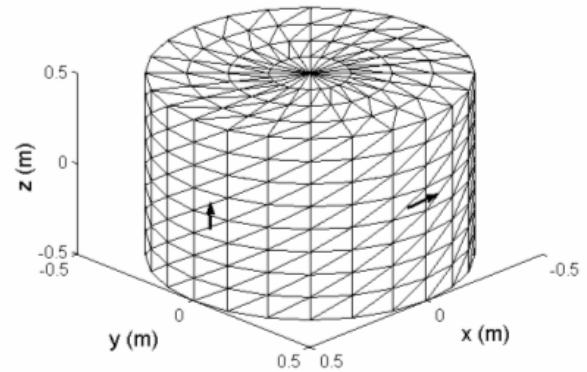
As a second example, consider a conducting cube, 1 m on a side, centered about the origin shown in Fig. 1(b). The first resonant frequency of this cube is 212 MHz. There are eight divisions along the x , y and z directions, respectively. This represents a total of 768 patches and 1,152 common edges, and $R_{\min} = 5.57$ cm. The z - and x -directed current at the side faces are indicated by arrows in Fig. 1(b). Fig. 4 shows the transient response for the z - and x -directed currents. The time step in the MOT computation is chosen as $c\Delta t = 2R_{\min}$ in order to generate an implicit solution. Here the agreement between the results from the IDFT and two presented methods is very good. It is important to note that the MOT solution shows some instability. Fig. 5 compares the transient response of two presented methods and the IDFT of the frequency-domain EFIE solution for the far scattered field from the cube along the backward direction. All the three solutions agree well.

As a final example, we show the transient response from a conducting cylinder with a radius of 0.5 m and height 1 m, centered at the origin as shown in Fig. 1(c). We subdivide the cylinder into four, twenty-four, and eight divisions along r , ϕ and z directions, respectively. This represents a total of 720 patches with 1,080 common edges, and $R_{\min} = 2.15$ cm. The z - and ϕ -directed current at the side faces are indicated by arrows in Fig. 1(c). Fig. 6 shows the transient response for the z - and ϕ -directed currents. The time step in MOT computation is chosen as $c\Delta t = 4R_{\min}$ in order to generate an implicit solution. Here the agreement between the results from the IDFT and two presented methods is very good, while MOT solution shows

instability. Fig. 7 compares the transient response of two presented methods and the IDFT of the frequency-domain EFIE solution for the far scattered field from the cylinder along the backward direction. All the three solutions agree well without late-time oscillation.

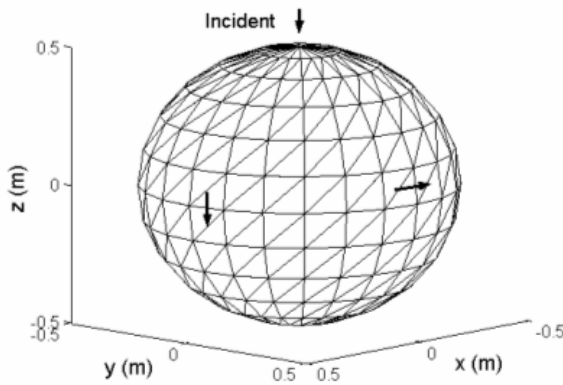
V. CONCLUSION

We presented two methods to solve the time-domain electric field integral equation for three-dimensional arbitrarily shaped conducting structures. To apply MoM procedure, we used triangular patch functions as spatial basis and testing functions. We introduced temporal basis function set derived from Laguerre polynomials. The advantages of proposed method is to guarantee the late time stability. The temporal derivative can be treated analytically. Transient electric current and far field obtained by the two presented methods are accurate and stable. The agreement between the solutions obtained using the two proposed methods and the IDFT of the frequency domain is excellent.

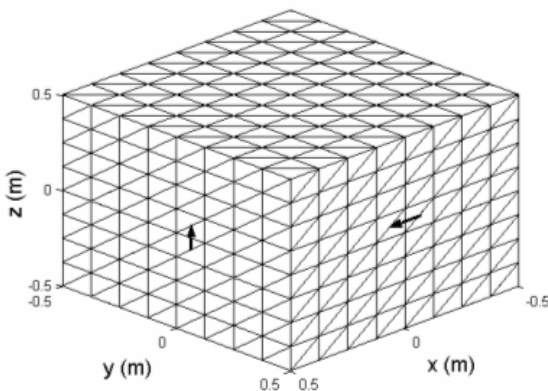


(c)

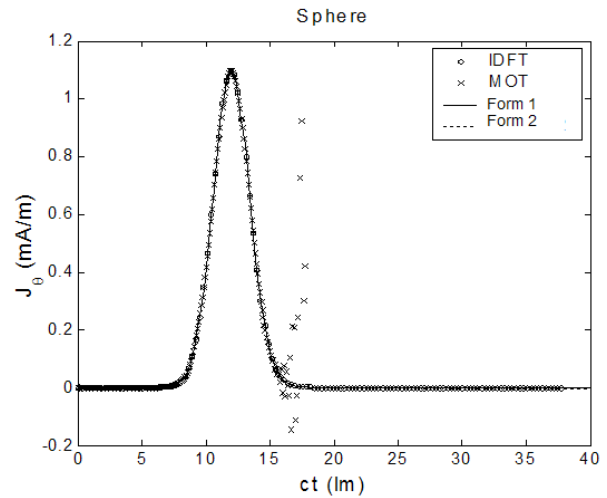
Fig. 1. Triangle patching of a conducting objects. (a) sphere. (b) cube. (c) cylinder.



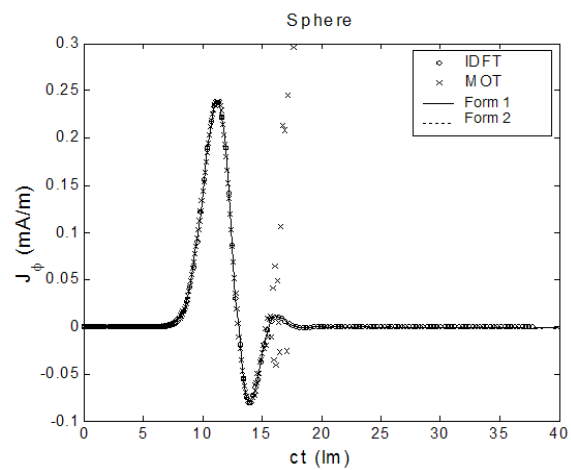
(a)



(b)



(a)



(b)

Fig. 2. Transient current on the sphere. (a) θ – directed current. (b) ϕ – directed current.

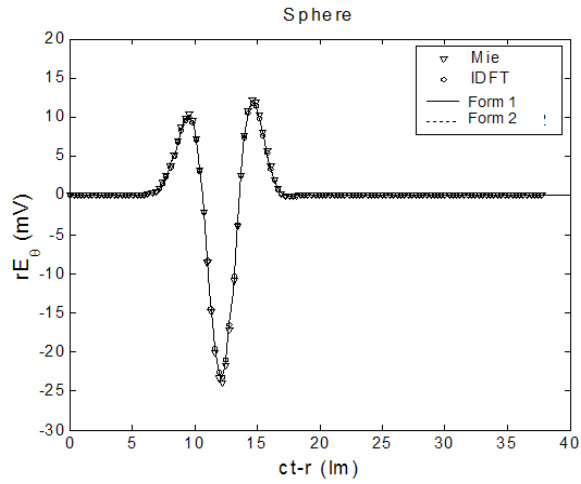


Fig. 3. Scattered far field from the sphere along backward direction.

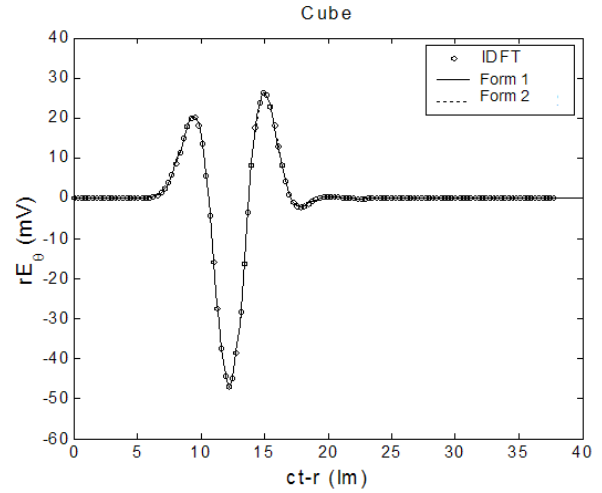
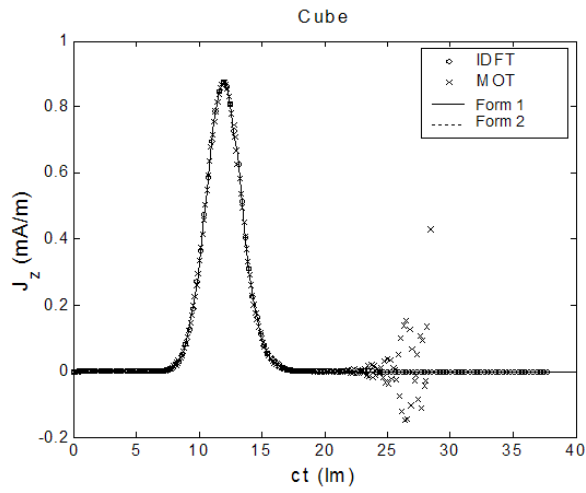
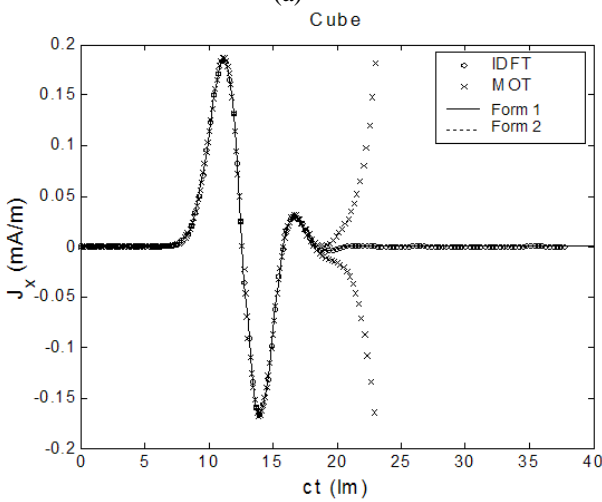


Fig. 5. Scattered far field from the cube along backward direction.

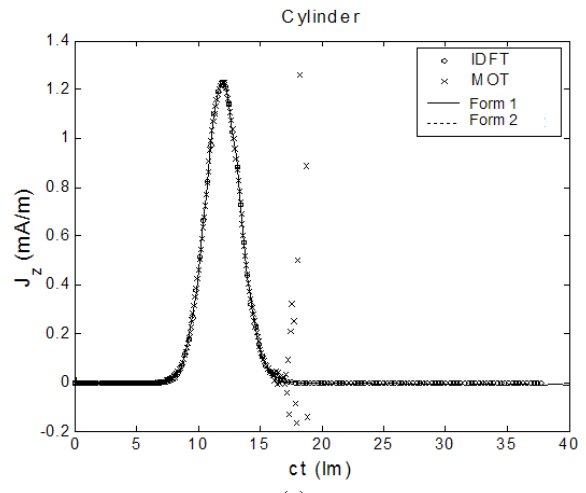


(a)

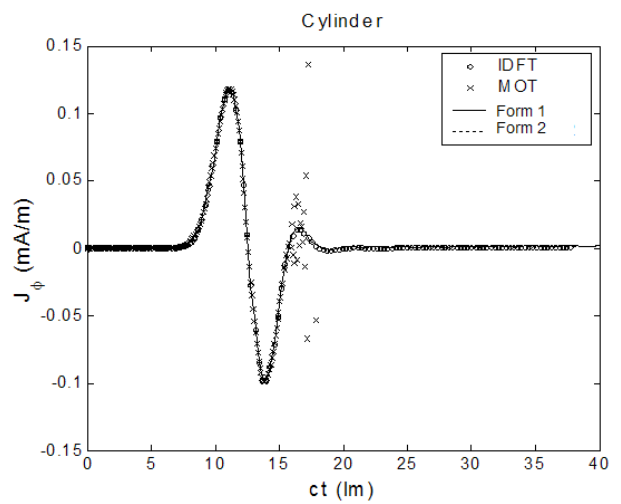


(b)

Fig. 4. Transient current on the cube. (a) z – directed current. (b) x – directed current.



(a)



(b)

Fig. 6. Transient current on the cylinder. (a) z – directed current. (b) ϕ – directed current.

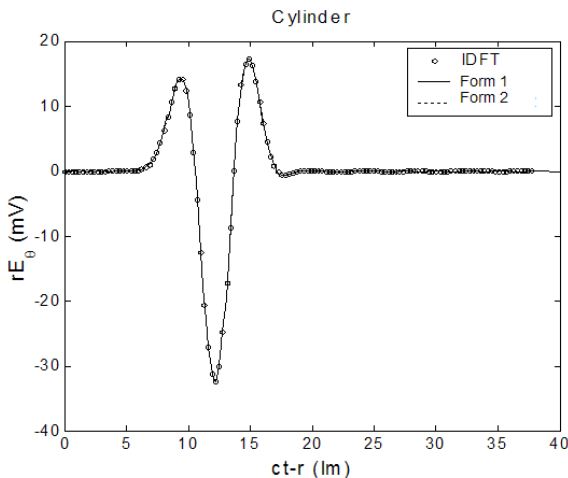


Fig. 7. Scattered far field from the cylinder along backward direction.

REFERENCES

- [1] S. M. Rao, *Time Domain Electromagnetics*. Academic Press, 1999.
- [2] S. M. Rao and D. R. Wilton, "Transient scattering by conducting surfaces of arbitrary shape," *IEEE Trans. Antennas Propagat.*, vol. 39, no. 1, pp. 56-61, Jan. 1991.
- [3] D. A. Vechinski and S. M. Rao, "A stable procedure to calculate the transient scattering by conducting surfaces of arbitrary shape," *IEEE Trans. Antennas Propagat.*, vol. 40, no. 6, pp. 661-665, June 1992.
- [4] S. M. Rao and T. K. Sarkar, "An alternative version of the time-domain electric field integral equation for arbitrarily shaped conductors," *IEEE Trans. Antennas Propagat.*, vol. 41, no. 6, pp. 831-834, June 1993.
- [5] S. M. Rao and T. K. Sarkar, "An efficient method to evaluate the time-domain scattering from arbitrarily shaped conducting bodies," *Microwave Opt. Technol. Lett.*, vol. 17, no. 5, pp. 321-325, April 1998.
- [6] S. M. Rao and T. K. Sarkar, "Transient analysis of electromagnetic scattering from wire structures utilizing an implicit time-domain integral-equation technique," *Microwave Opt. Technol. Lett.*, vol. 17, no. 1, pp. 66-69, Jan. 1998.
- [7] T. K. Sarkar, W. Lee, and S. M. Rao, "Analysis of transient scattering from composite arbitrarily shaped complex structures," *IEEE Trans. Antennas Propagat.*, vol. 48, no. 10, pp. 1625-1634, Oct. 2000.
- [8] B. H. Jung and T. K. Sarkar, "Time-domain electric-field integral equation with central finite difference," *Microwave Opt. Technol. Lett.*, vol. 31, no. 6, pp. 429-435, Dec. 2001.
- [9] R. S. Adve, T.K. Sarkar, O. M. Pereira-Filho and S. M. RAO, "Extrapolation of time domain responses from three-dimensional conducting objects utilizing the matrix pencil technique," *IEEE Trans. Antennas Propagat.*, vol. 45, No. 1, pp. 147-156, Jan. 1997.
- [10] T. K. Sarkar and J. Koh, "Generation of a wide-band electromagnetic response through a Laguerre expansion using early-time and low-frequency data," *IEEE Trans. Microwave Theory Tech.*, vol. 50, no. 5 pp. 1408-1416, May 2002.
- [11] Y. S. Chung, T. K. Sarkar, B. H. Jung and M. Salazar-Palma, "An unconditionally stable scheme for the finite-difference time-domain method," *IEEE Trans. Microwave Theory Tech.*, vol. 51, No. 3, pp. 697-704, Mar. 2003.
- [12] S. M. Rao, D. R. Wilton, and A. W. Glisson, "Electromagnetic scattering by surfaces of arbitrary shape," *IEEE Trans. Antennas Propagat.*, vol. 30, no. 3, pp. 409-418, May 1982.
- [13] D. R. Wilton, S. M. Rao, A. W. Glisson, D. H. Schaubert, O. M. Al-Bundak, And C. M. Butler, "Potential integrals for uniform and linear source distributions on polygonal and polyhedral domains," *IEEE Trans. Antennas Propagat.*, vol. 32, no. 3, pp. 276-281, March 1984.
- [14] A. D. Poularikas, *The Transforms and Applications Handbook*. IEEE Press, 1996.
- [15] I. S. Gradshteyn and I. M. Ryzhik, *Table of Integrals, Series, and Products*. New York: Academic Press, 1980.
- [16] M. Yuan, T. K. Sarkar and J. Koh, "Modeling of ultra-wideband electromagnetic signals arising in computational electromagnetics". Submitted to *IEEE Trans. Antennas Propagat.*.

Fast Converging Graded Mesh for Bodies of Revolution with Tip Singularities

Kueichien Hill

Air Force Research Laboratory
2591 K St., AFRL/SNS
WPAFB, OH 45433

Tri Van

Mission Research Corporation
3975 Research Blvd.
Dayton, OH 45430

Abstract— In this paper, we study the plane wave scattering from perfectly electric conducting (PEC) bodies of revolution (BOR) with tip singularities. It is known that solutions to surface integral equations such as magnetic, electric, and combined field integral equations (MFIE, EFIE, and CFIE, respectively) are singular near the tips. Consequently, the convergence of method of moments (MoM) based on those surface integral equations is not optimal or guaranteed. By using appropriate graded meshes, one can retain the optimal convergence rate in MoM.

Keywords—Tip Singularity, Graded Mesh, Optimal Convergence, Integral Equations, Method of Moments, Radar Cross Section.

I. INTRODUCTION

Computational electromagnetics (CEM) technology has made tremendous progress in the last decade due largely to the advancement of fast solver and high performance computing technology. Consequently, CEM tools are being applied to ever more complex problems. Even though CEM tools still rely on radar cross section (RCS) measurements for validation, the measurement community is increasingly relying on CEM tools, especially those based on the method of moments (MoM), to validate their measured data to minimize measurement uncertainty. To provide prediction data for measurement validation, one typically needs to compute the RCS from 2 to 18 GHz using very fine grids to ensure solution convergence. This presents quite a challenge for MoM codes even for canonical targets of moderate sizes, especially if computation is required at every 10 MHz and every 0.1 degree. Instead of using a uniform mesh, one would like to use a non-uniform mesh that is denser near the singularities and coarser elsewhere to minimize the number of unknowns. In this paper, we investigate the choices of non-uniform mesh that give fast converging solutions for bodies of revolution (BOR). The theorem that defines the constraint for the graded mesh will be discussed and

followed by numerical examples, particularly those of a 10-foot ogive and a 10-inch ogive with gap.

II. SOLUTIONS NEAR GEOMETRY SINGULARITIES

It is known that the solution of the scattering problem by the perfectly conducting ogive is singular due to the ogive tips. In fact, if r is the distance from the tip, the solution near the tip behaves as

$$|E| \sim r^{\mu_1-1}, \quad |H| \sim r^{\mu_2-1}, \quad 0 < \mu_1, \mu_2 < 1,$$

where μ_1 and μ_2 depend on the angle of the tip (see, for example, [1] and [2]). If piecewise polynomial basis functions defined on a uniform mesh are used to approximate the solutions, the convergence of MoM is not optimal due to the singular behavior of the solutions near the ogive tips. To retain the optimal convergence rate, one can either include the singular basis functions in the approximation or discretize the ogive with a graded mesh. It is easier to construct graded meshes and apply them to the existing MoM codes. Here we apply graded meshes to Cicero [1] which is a MoM computer code for bodies of revolution (BOR) (see [4], [5], [6], and references therein). We will need the following result in approximating the singular function $r^{-\alpha}$ on $[0, 1]$, $0 < \alpha < 1$ (see [7]):

Theorem 1: Let p be such that $\alpha < 1/p$. Define the following partition τ_n^q of $[0, 1]$

$$r_i = (i/n)^q, \quad i = 0, 1, 2, 3, \dots, n,$$

where $q = \frac{1+p}{1-\alpha p}$ and is called the grading exponent of τ_n .

Let $S(\tau_n^q)$ be the set of functions that are constant on each subinterval $[r_i, r_{i+1}]$. Then

$$\inf_{\zeta \in S(\tau_n^q)} \left\| r^{-\alpha} - \zeta(r) \right\|_{L^p[0,1]} = O(1/n).$$

In fact, if $\zeta(r) \in S(\tau_n^q)$ is such that

$$\zeta(r) = r_i^{-\alpha} \quad \text{in } [r_i, r_{i+1}], \quad i = 0, 1, 2, \dots, n-1, \text{ then}$$

$$\left\| r^{-\alpha} - \zeta(r) \right\|_{L^p[0,1]} \leq C/n.$$

The norm of $f \in L^p[0,1]$ is $\|f\|_{L^p[0,1]} = \sqrt[p]{\int_0^1 |f|^p dx}$. In engineering application, L^2 -norm (i.e., $p = 2$) is usually used. In this case, Theorem 1 states that, when $r^{-\alpha}$, for $0 < r < 1$, and $\alpha < 1/2$, is approximated by step functions, the best approximation in L^2 -norm is obtained when these step functions are defined on a graded grid with grading exponent $q = \frac{3}{1-2\alpha}$. Note that the above theorem can be applied to singularities of arbitrary order such as vertices, edges, corners, etc. The singularity order α of field solutions near the ogive tips can be approximated by that of the field near the tip of the cone whose interior angle is the same as the angle of the ogive tip.

III. GRADED MESH AND CONVERGENCE

Let S be the surface of the PEC ogive which is parameterized by arc-length

$$(l, \phi) \rightarrow (\rho(l), \phi, z(l)), \quad l \in [0, L], \quad \phi \in [0, 2\pi]$$

where L is the total arc-length of the generating curve and the axis of rotation is along the z direction. The tips occur at $l=0$ and $l=L$ with $\rho(0) = \rho(L) = 0$. The components J_t and J_ϕ of the surface current $J = \hat{n} \times H$ behave like $l^{-\alpha}$ and $(L-l)^{-\alpha}$ near the tips, where $0 < \alpha < 1$. A graded mesh is constructed as follows. First, we divide $[0, L]$ into three subintervals $[0, \varepsilon]$, $[\varepsilon, L - \varepsilon]$, and $[L - \varepsilon, L]$ where $\varepsilon < L/4$ and is a rational. Let $\beta(x)$ be a twice differentiable function defined as

$$\beta(x) = \begin{cases} \varepsilon(x/\varepsilon)^q & \text{for } x \in [0, \varepsilon], \\ b(x) & \text{for } x \in [\varepsilon, L - \varepsilon], \\ L - \varepsilon \left(\frac{L-x}{\varepsilon} \right)^q & \text{for } x \in [L - \varepsilon, L], \end{cases}$$

where $q = \frac{1+p}{1-\alpha p}$, $0 < p < 1/\alpha$, and $b(x)$ is a ‘‘connecting function’’ which is monotonically increasing and has two continuous derivatives. (Such a function is constructed from a perfect spline in [8]). Then the nodes in the graded mesh τ_N^q is defined as

$$l_i = \beta(x_i), \quad x_i = L(i/N), \quad i = 0, 1, 2, \dots, N,$$

where x_i 's represent a uniform mesh and l_i 's are the mapped points in the graded mesh. Note that ε needs to be chosen so that ε and $L - \varepsilon$ coincide with one of the x_i 's. It is common in MoM codes to approximate the fields with pulse functions (or piecewise constant), i.e. $S(\tau_N^q)$. Let $P_n : L^p([0, L]) \rightarrow S(\tau_N^q)$ be the orthogonal projection, that is,

$$\langle P_n u, v_n \rangle = \langle u, v_n \rangle, \quad \forall v_n \in S(\tau_n^q).$$

Then Galerkin approximation problem is to find $u_n \in S(\tau_N^q)$ such that

$$P_n A u_n = P_n f,$$

where A is the integral operator defined as in the combined field integral equation (CFIE) and f is the given incident field. We assume that the integral equation $Au = f$ has a unique solution. It can be shown that Galerkin approximation scheme is stable [9], that is,

$$\|P_n A v_n\|_{L^2(0, 2\pi, L^p[0, L])} \geq C \|v_n\|_{L^2(0, 2\pi, L^p[0, L])},$$

for all $v_n \in S(\tau_N^q)$ and some $C > 0$ independent of v_n .

Consequently, we obtain the error estimate [9]

$$\|u - u_n\|_{L^2(0, 2\pi, L^p[0, L])} \leq C \inf_{v_n \in S(\tau_N^q)} \|u - v_n\|_{L^2(0, 2\pi, L^p[0, L])},$$

where u is the solution of the continuous problem and $u_n \in S(\tau_N^q)$ is the approximating solution. This implies that convergence rate for the graded mesh is optimal (for L^p -norm). In other words, the approximating solutions $u_n \in S(\tau_N^q)$ converges to u at the rate

$\inf_{v_n \in S(\tau_N^q)} \|u - v_n\|_{L^2(0, 2\pi, L^p[0, L])}$ which is the best possible for

elements in $S(\tau_N^q)$. It is possible to show that the optimality holds for a more familiar weighted Sobolev space, $L_\alpha^2([0, L])$, whose norm is defined as

$$\|u\|_{L_\alpha^2([0, L])} = \left(\int_0^L |x^\alpha u|^2 dx \right)^{1/2}.$$

Hence, if $J_{t,n}$ and $J_{\phi,n}$ are the approximate solutions of J_t and J_ϕ , respectively, then the following error estimates also hold

$$\|J_t - J_{t,n}\|_{L^2(0, 2\pi, L_\alpha^2[0, L])} \leq C/n,$$

$$\|J_\phi - J_{\phi,n}\|_{L^2(0, 2\pi, L_\alpha^2[0, L])} \leq C/n,$$

where α is the order of singularity.

IV. NUMERICAL RESULTS

In this section, we illustrate the benefits of using properly graded meshes with Cicero code in computing RCS of a 10-foot ogive and a 10-inch ogive with gap. Cicero is a MoM code with pulse basis and testing functions. In each of the following figures, the numbers in the legend are the number of sampling points per wavelength (ppw) used. For graded meshes, the ‘‘ppw’’ means that the total number of grid points are the same as that of the uniform mesh with the ‘‘ppw’’. All results are computed using CFIE.

A. The 10-foot ogive

The 10-foot ogive is 10-foot long from tip to tip and 1-foot

wide at the waist. The tips of the ogive are at $z = \pm 1.524$ meters. The meshes are either uniform ($q = 1$) or graded with the grading exponents $q = 2$. We first compute the electric current components J_t and J_ϕ at 0.5 GHz. In Figure 1 and Figure 2, we plot $|J_t|$, $|J_\phi|$ for θ -polarized incident field at $\theta^i = 0^\circ$ and $\theta^i = 20^\circ$, respectively.

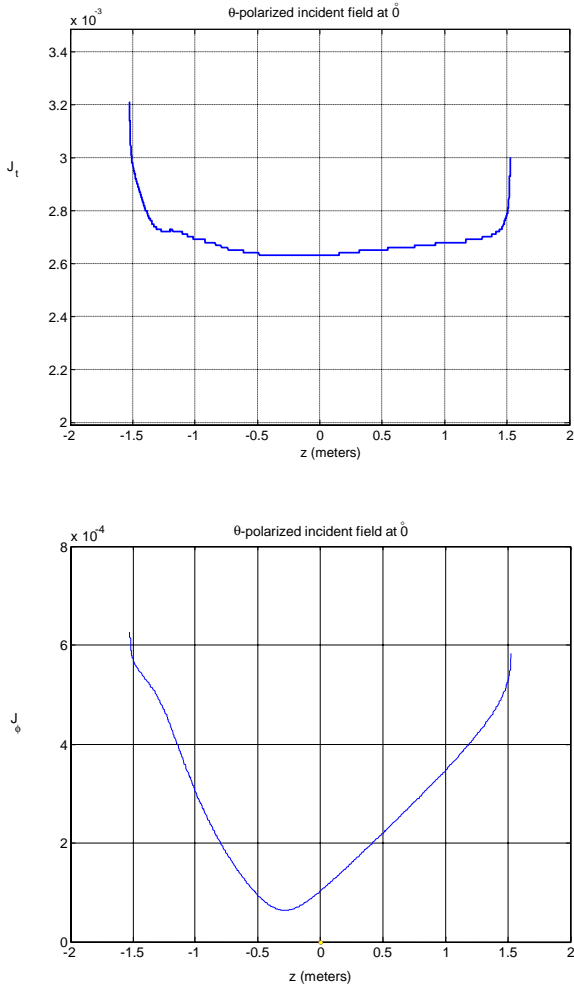


Figure 1: Magnitude J_t and J_ϕ for θ -polarized incidence field at $\theta = 0^\circ$. Tips of the 10-foot ogive are at $z=1.524$ m and $z=-1.524$ m.

Due to numerical limitations in Cicero such as piecewise approximations to the roof-top basis functions, we can only observe that J_t and J_ϕ and their derivatives tend to infinity at the tips instead of become infinity as expected in [2]. In any case, these singularities cause slow convergence in MoM using uniform meshes.

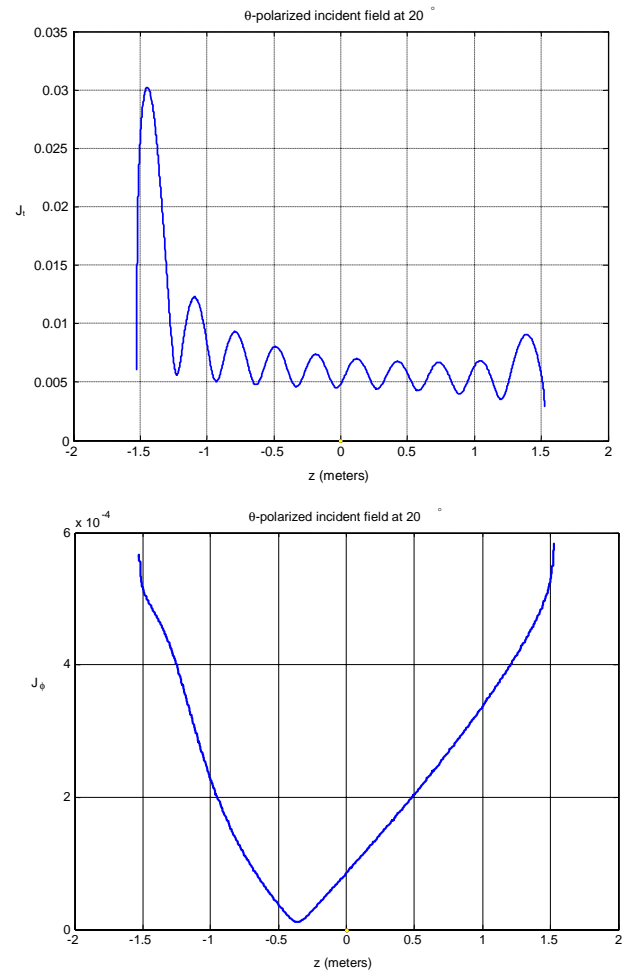


Figure 2: Magnitude J_t and J_ϕ for θ -polarized incidence field at $\theta = 20^\circ$.

We assume that the electric currents computed with 640 points per wavelength are “exact” and plot the relative errors e_{h_n} in Figure 3 and Figure 4

$$e_{h_n} = \frac{\|J_\nu^{h_n} - J_\nu^{h_{min}}\|_{L^{1/2}(0,L)}}{\|J_\nu^{h_n}\|_{L^{1/2}(0,L)}}, \quad n = 1, 2, \dots, 5$$

where ν is either t or ϕ , h_n is the mesh size corresponding to the number of points per wavelength $ppw = 2^n \times 10$, and h_{min} is the mesh size for $n = 6$ (or 640 points per wavelength). It is observed that the errors in graded meshes are smaller than their uniform counterparts for sufficiently large ppw and decrease at a faster rate.

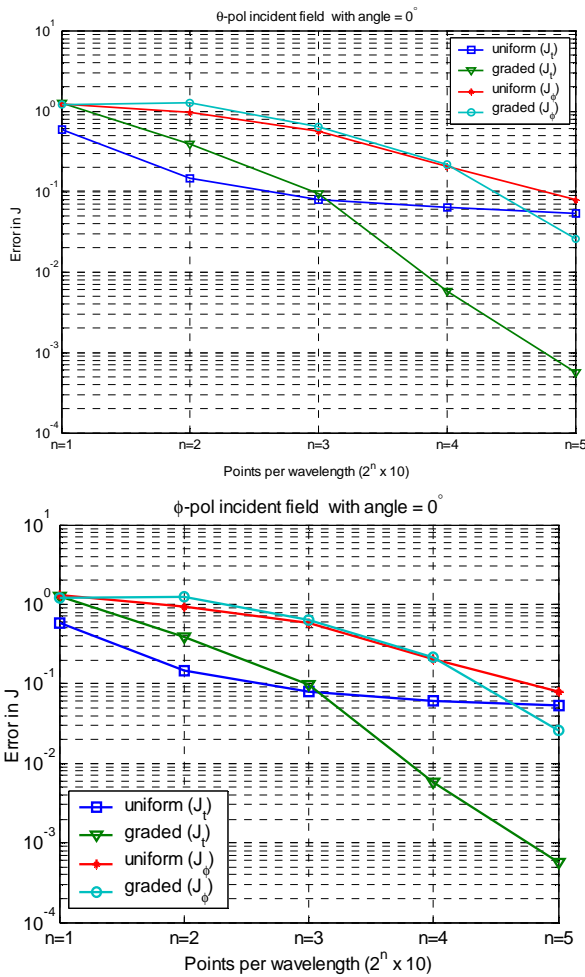


Figure 3: Logarithmic relative error for (J_t, J_ϕ) at $\theta = 0^\circ$ in graded meshes are smaller and decrease faster than those in uniform meshes.

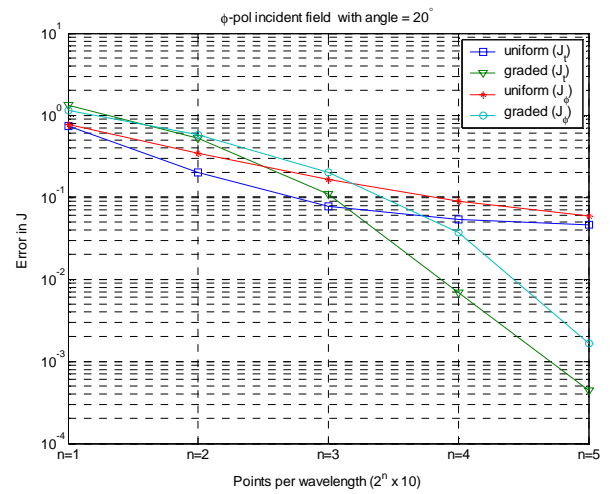
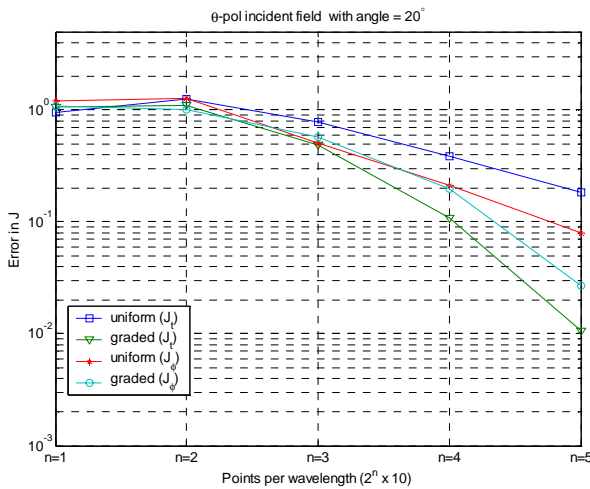


Figure 4: Logarithmic relative error for (J_t, J_ϕ) at $\theta = 20^\circ$ in graded meshes are smaller and decrease faster than those in uniform meshes.

Next we compare the RCS results for different meshes. It can be seen from the below figures that the graded mesh performs better than the uniform one with the same number of unknowns, that is, RCS results of the graded meshes converge at a faster rate. In Figure 5, RCS at 0.5 GHz for $\theta\theta$ polarization computed with the 640 ppw-uniform mesh is viewed as the “exact” result. The zero-degree angle corresponds to the tip scattering direction while the 90-degree angle corresponds to the broadside scattering. We observe that the result computed with the graded mesh at 60 ppw already overlaps with the “exact” solution while the RCS curve computed with the uniform mesh at 60 ppw has not converged, especially near $\theta = 20^\circ$. In fact, it requires at least 160 ppw in a uniform mesh to yield the same accuracy as the 60 ppw in a graded mesh.

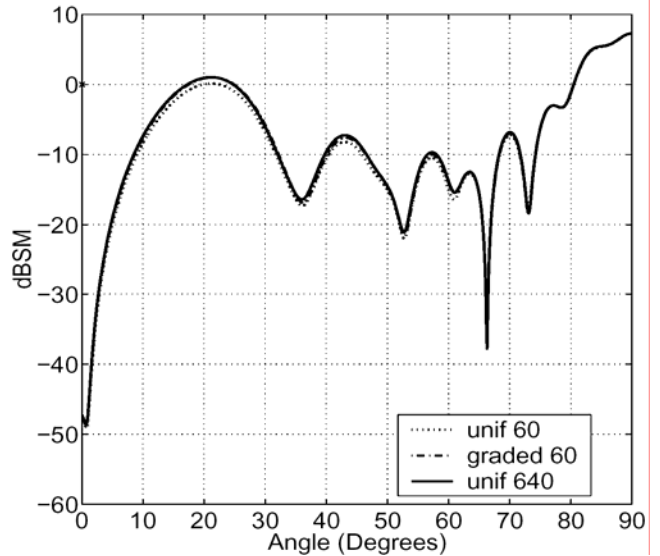


Figure 5: RCS of the 10-foot ogive at 0.5 GHz ($\theta\theta$ polarization). The “exact” solution is represented by the 640 ppw-uniform mesh (solid line). At 60 ppw, the uniform-mesh solution has not converged (dotted line) while the graded-mesh solution (dash-dotted line) overlaps with the “exact” solution.

At higher frequencies, tip singularity becomes more problematic. In Figure 6, RCS at 5 GHz for the 10-foot ogive is computed near the nose-on (grazing) angular region by using uniform meshes of different grid densities. The curves oscillate near -69.5 dBsm.

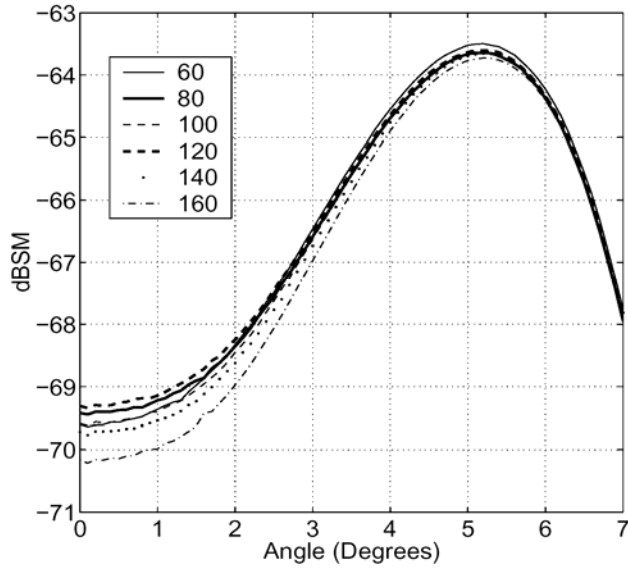


Figure 6: Uniform mesh - RCS of the 10-foot ogive at 5 GHz near the grazing angle ($\phi\phi$ polarization).

However, RCS at 5 GHz for the 10-foot ogive computed with graded meshes approaches monotonically to a converged solution as seen in Figure 7.

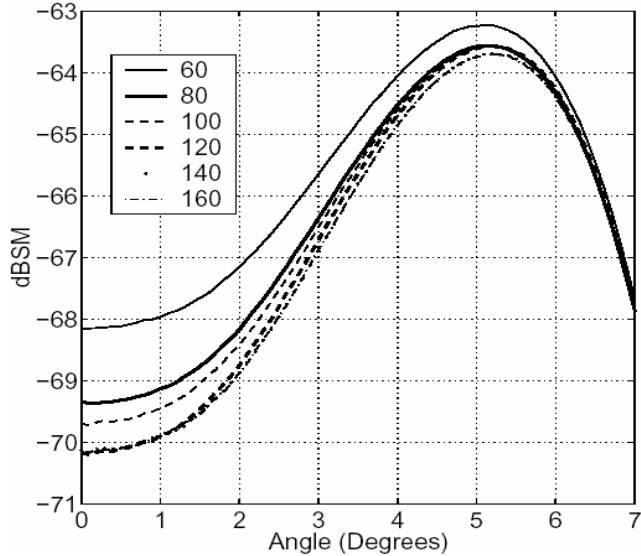


Figure 7: Graded mesh - RCS of the 10-foot ogive at 5 GHz near the grazing angle ($\phi\phi$ polarization).

B. The 10-inch ogive with gap

To examine further the advantage of graded meshes, we also consider the ogive with gap (see Figure 8), one of the test targets proposed by Electromagnetic Code Consortium [10], [11]. The ogive is 10 inches long, subtending a half

angle of 22.62 degree, and with a maximum radius of 1 inch at the middle. The generating curve for this ogive is part of a circular arc with a 13 inch radius. A small rectangular groove cut out around the middle of the ogive. The circumferential groove is 0.25 inches wide by 0.25 inches deep. The bottom of the groove forms a ring 0.75 inches in radius.

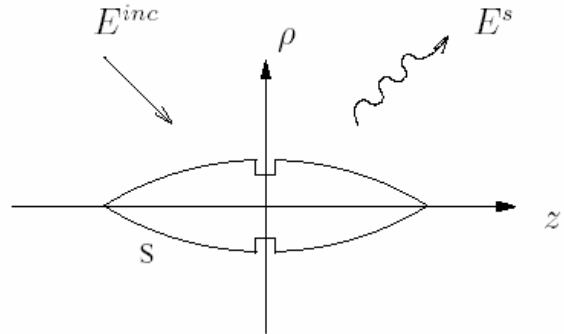


Figure 8: Ogive with gap.

Here, the solutions to the integral equations have both edge and tip singularities due to the groove and the ogive tips. As in the case of the 10-foot ogive, we design appropriate graded meshes to improve the convergence rate in MoM solutions. There are three corners in the generating arc and each has different angles. Thus, we construct a graded mesh with three grading exponents (q_1, q_2, q_3) . For example, the distribution of points in a graded mesh with $(q_1, q_2, q_3) = (2, 2, 2)$ is plotted in Figure 9.

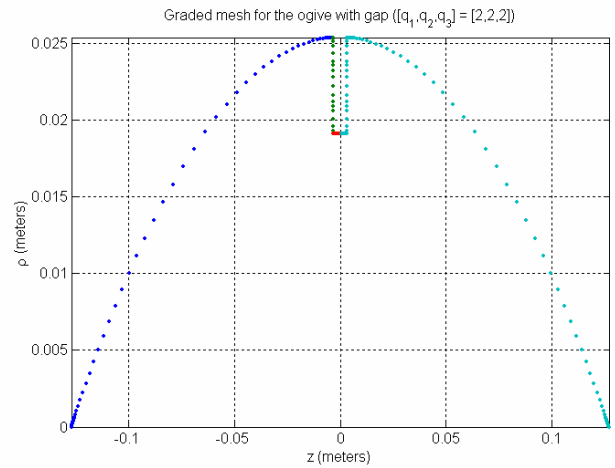


Figure 9: Point distribution of a graded mesh on the generating arc of ogive with gap.

In Figure 10 and Figure 11, RCS curves at 2 GHz are plotted. Uniform-mesh solutions converge much slower than graded-mesh solutions, especially near the grazing angular region. We see that at 80 ppw, RCS of the graded mesh already converges while that of uniform mesh does not.

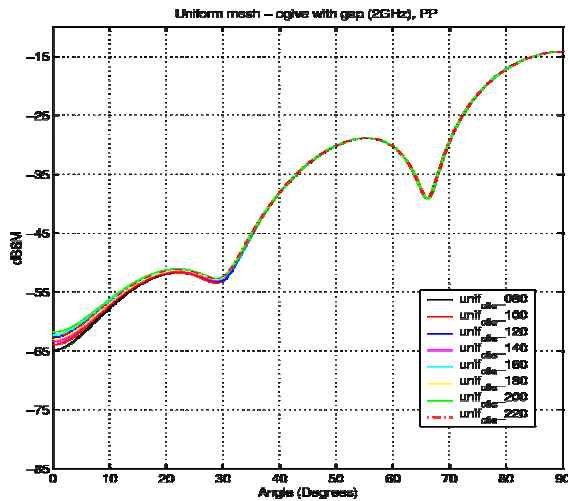


Figure 10: Uniform mesh - RCS of ogive with gap at 2 GHz ($\phi\phi$ polarization).

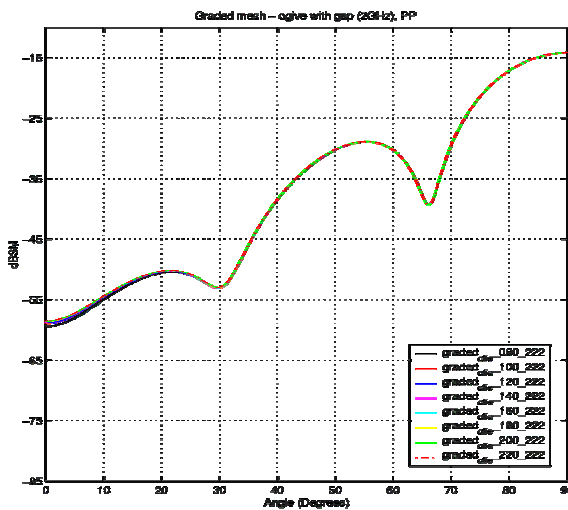


Figure 11: Graded mesh - RCS of ogive with gap at 2 GHz ($\phi\phi$ polarization).

Furthermore, the RCS differences at $\phi = 0^\circ$ (the grazing angle) decrease for graded meshes while oscillate for the uniform meshes as seen in Figure 12 and Figure 13.

V. CONCLUSIONS

In this paper, we present a construction of graded meshes that enable a faster convergence using MoM for BOR targets with tip singularities. Numerical results are given for the PEC ogive with and without gap using CFIE. These preliminary results show that faster convergence can be achieved if one chooses a graded mesh using the technique outlined in this paper. We have also observed the similar improvement in convergence for other types of integral equations. The technique can be easily generalized to non-BOR targets which have tip and edge singularities. This will be reported in the future.

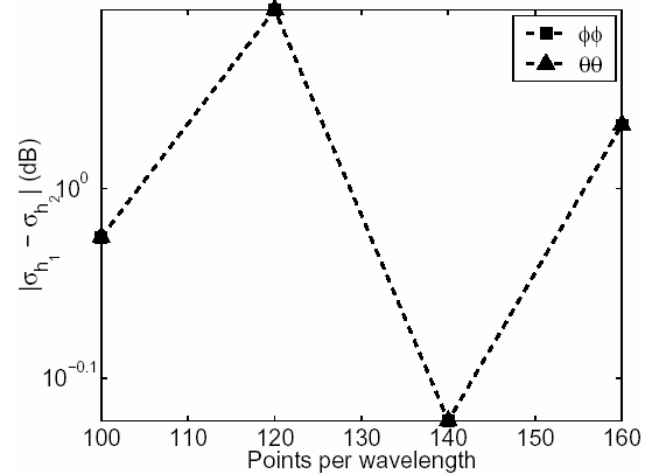


Figure 12: Uniform mesh at 2 GHz - RCS errors in ogive with gap at $\theta = 0^\circ$.

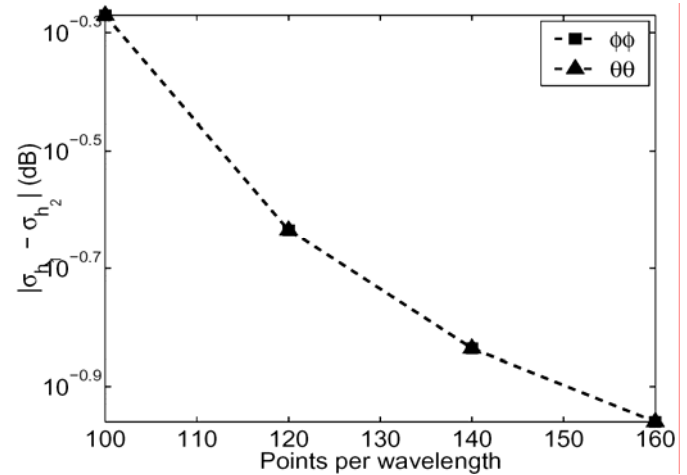


Figure 13: Graded mesh at 2 GHz - RCS errors in ogive with gap at $\theta = 0^\circ$.

ACKNOWLEDGMENT

The author would like to thank the reviewer for helpful suggestions and comments.

REFERENCES

- [1] J. Van Bladel, *Singular Electromagnetic Fields and Sources*, IEEE Press, 1996
- [2] J. J. Bowman, T. B. A. Senior, P. L. E. Uslenghi, and J. S. Asvestas, *Electromagnetic and Acoustic Scattering by Simple Shapes*, Hemisphere Pub. Corp., NY, 1987
- [3] J. M. Putnam and L. N. Medgyesi-Mitschang, *Combined Field Integral Equation Formulation for Axially Inhomogeneous Bodies of Revolution (Combined Field Formulation of CICERO)*, McDonnell Douglas Research Laboratories, December 1987.
- [4] J. R. Mautz and R. F. Harrington, *Electromagnetic scattering from a homogeneous material body of revolution*, Arch. Elektron. Ubertragungstech, 33, 1979, pp71-80.
- [5] M. G. Andreasen, *Scattering from bodies of revolution*, IEEE Trans. Antennas Propagat. , AP-13, Mar. 1965, pp.303-310
- [6] L. N. Medgyesi-Mitschang and J. Putnam, *Electromagnetic scattering from axially inhomogeneous bodies of revolution*, IEEE Trans. Antennas Propagat., AP-32, Aug. 1984, pp. 797-806

- [7] J. Rice, *On the degree of convergence of nonlinear spline approximation*, Approximations with Special Emphasis on Spline Functions (I. J. Schoenberg, ed.), Academic Press, 1969, pp. 349–365.
- [8] L. L. Schumaker, *Spline Functions. Basis Theory*, Wiley, 1981.
- [9] S. Prossdorf and B. Silbermann, *Numerical Analysis for Integral and Related Operator Equations*, Akademie-Verlag, Berlin, 1991
- [10] A. Woo, H. Wang, M. Schuh, and M. Sanders, *Benchmark radar targets for the validation of computational electromagnetics programs*, IEEE Antenna and Propagation Magazine, 34, Dec. 1992, pp. 52–56.
- [11] A. Woo, H. Wang, M. Schuh, and M. Sanders, *Benchmark radar targets for the validation of computational electromagnetics programs*, IEEE Antenna and Propagation Magazine, 35, Feb. 1993, pp. 84–89.

Kueichien Hill received her M.S. and Ph.D. degrees in electrical engineering from the Ohio State University in 1984 and 1990,

respectively. She was a research engineer and instructor at the University of Dayton from 1984 to 1986 and joined the Air Force Research Laboratory in 1991 as a research and project engineer. Her area of research focuses on CEM code validation and benchmark, and CEM techniques that incorporate fast solver and high performance computing technology. Dr. Hill is an AFRL Fellow.

Tri Van received the B.A. in mathematics from New College-University of South Florida in 1992, the M.S. in mathematics from State University of New York - Stony Brook in 1994 and the Ph.D. in applied mathematics from the University of Florida in 1999. From 1999 to 2001, he was with the Air Force Institute of Technology, WPAFB, as a Research Associate. He is presently a Senior Research Engineer at Mission Research Corporation-Dayton, OH. His current research interests include computational electromagnetics and mathematical modelling in fiber optics and electromagnetics.

TM Electromagnetic Scattering from 2D Multilayered Dielectric Bodies – Numerical Solution

F. Seydou^{1,2}, *R. Duraiswami*², *N.A. Gumerov*² & *T. Seppänen*¹

1. Department of Electrical and Information Engineering University of Oulu, P.O. Box 3000, 90401 Finland
2. Institute for Advanced Computer Studies University of Maryland, College Park, MD

Abstract

An integral equation approach is derived for an electromagnetic scattering from an M arbitrary multilayered dielectric domain. The integral equation is valid for the 2D and 3D Helmholtz equation. Here we show the numerical solution for the 2D case by using the Nyström method. For validating the method we develop a mode matching method for the case when the domains are multilayered circular cylinders and give numerical results for illustrating the algorithm.

Introduction

Problems of electromagnetic scattering in layered media are of significant importance in many areas of technology such as optics, geophysical probing, communication, etc. (see [6] and the references therein). In this paper we discuss some analytical and computational results for the problem of approximating the scattered electromagnetic field from M layered two-dimensional scatterer. The scatterer is a nested body consisting of a finite number of homogeneous layers (annular regions) with boundary conditions on the interfaces. For the case when the boundaries are circular, closed form solutions can be obtained via a mode matching approach (see [9], [16] and [6], Chapter 6). For boundaries of arbitrary shapes, one of the most efficient techniques to tackle the problem is using (volume or surface) integral equation methods. There are also other type of methods such as the domain decomposition methods [12] and k-space methods (Cf. [3] and [4]). In this paper we choose the surface integral equation method since the inhomogeneities are piecewise constants in each re-

gion. The problem can thus be solved (via a boundary element method) on surfaces. It has an advantage over the volume integral equation method, where the whole multilayered domain has to be discretized and the unknowns are in a volume rather than on a surface (see [13]). The straightforward way for solving this type of problems via boundary element methods is by using Green's theorem in each domain [6]. Another alternative is to consider the use of single and/or double layer potentials [7]. In the case of one interface, both methods yield a single integral equation for a single unknown if the interface is impenetrable (e.g., impedance core). However, when the body is penetrable with one interface (e.g., dielectric core), they lead to a pair of integral equations for a pair of unknowns [7]. We deduce that, by using these approaches in the multilayered dielectric domain, for N interfaces we have $2N$ unknown functions to determine. From a computational point of view, it is highly desirable to obtain less equations and less unknowns. In the case of one interface, the so called transmission problem, one integral equation involving one unknown was obtained by a

few authors (see [10], [14] and the references therein). In [10] the single integral equation for one unknown was obtained for the transmission problem by using a hybrid of Green's theorem and layer potentials. In [6], Chapter 8.3, single integral equations are obtained for multilayered domains by using the extended boundary condition method. But this method suffers from ill-conditioned equations and is mainly convenient for a scatterer where the fields around it are expandable to cylindrical harmonics. The purpose of this paper is to obtain Fredholm type single integral equations on each interface for the multilayered domain case. To this end, we alternate the layer potentials and Green's theorems in the multilayered domain and implement numerical computations using the Nyström method. For a theoretical study of the problem, see [1] and [2]. Our results are validated by developing a mode matching approach for the case of a multilayered circular cylinder and comparing the two algorithms.

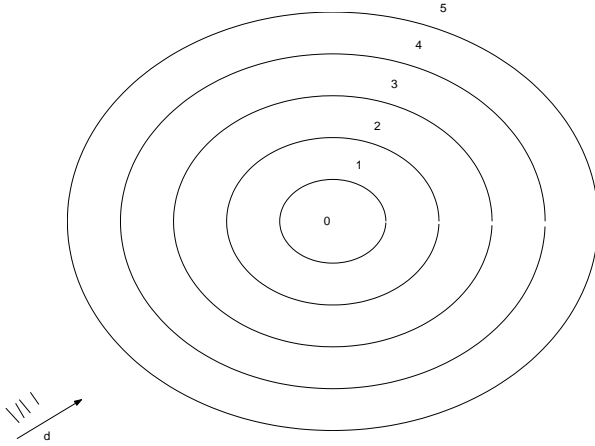


Figure 1: The geometry for the case of five concentric layered cylinder. The incident field is a plane wave propagating in a direction \mathbf{d} .

1 The mathematical formulation of the problem

Let \mathbf{D}_l , $l = 0, 1, \dots, M-1$ be M bounded domains in \mathbf{R}^2 such that $\overline{\mathbf{D}}_{l-1} \subset \mathbf{D}_l$, $l = 1, 2, \dots, M-1$. Let Γ_l

be the C^2 boundaries of \mathbf{D}_{l-1} , $l = 1, \dots, M$. Now let $\Omega_1 = \mathbf{D}_0$, $\Omega_l = \mathbf{D}_l \setminus \overline{\mathbf{D}}_{l-1}$, $l = 1, \dots, M-1$, and $\Omega_M = \mathbf{R}^2 \setminus \overline{\mathbf{D}}_{M-1}$. We assume that Ω_M is simply connected. See Figure 1 for Ω_l , $l = 0, 1, \dots, 5$. This is a special case of the general geometry where we have the cross section of ($M = 5$) concentric cylinders that are infinite in length and their axes are parallel to the z direction.

Each of the regions Ω_l is a dielectric material of constant complex permittivity and permeability ϵ_l and μ_l ($l = 0, \dots, M$), respectively. This geometry is illuminated by an incident field which is a plane wave with direction $\mathbf{d} = (\cos \phi_0, \sin \phi_0)$.

It can be shown that we have to solve the following type of boundary value problem for the Helmholtz equation.

$$(\Delta + \kappa_l^2)u_l = 0 \quad \text{in } \Omega_l, \quad l = 0, \dots, M,$$

where the wave numbers κ_l are given by $\kappa_l = \omega \sqrt{\epsilon_l \mu_l}$, ω is the frequency, with the following continuity conditions on the internal interfaces:

$$\frac{\partial}{\partial \nu} u_l = \rho_l \frac{\partial}{\partial \nu} u_{l-1} \quad \text{on } \Gamma_l, \quad l = 1, \dots, M-1,$$

$$u_l = u_{l-1} \quad \text{on } \Gamma_l, \quad l = 1, \dots, M-1,$$

with $\rho_l = \frac{\hat{\rho}_l}{\hat{\rho}_{l-1}}$, $l = 1, 2, \dots, M$, where $\hat{\rho}_l = \sqrt{\frac{\mu_l}{\epsilon_l}}$ is the intrinsic impedance.

On the outermost interface we have

$$\frac{\partial u}{\partial \nu} = \rho_M \frac{\partial}{\partial \nu} u_{M-1} \quad \text{on } \Gamma_M,$$

$$u = u_{M-1} \quad \text{on } \Gamma_M,$$

where,

$$u = u_M + u^i \quad \text{in } \Omega_M$$

and the given incident field, u^i , satisfies

$$\Delta u^i + \kappa_M^2 u^i = 0$$

everywhere. In addition, u_M must satisfy the Sommerfeld radiation condition, i.e.,

$$\lim_{|\mathbf{x}| \rightarrow \infty} |\mathbf{x}|^{1/2} \left(\frac{\partial u_M}{\partial |\mathbf{x}|} - i \kappa_M u_M \right) = 0.$$

The unit outward normal ν to Γ_l is assumed to be directed towards the exterior domain. The above problem is known as the TM mode. The TE mode is obtained by replacing ρ_l by $\frac{1}{\rho_l}$. We denote the fundamental solution to the Helmholtz equations (the free-space source) by

$$\Phi_k(\mathbf{x}, \mathbf{y}) = -\frac{i}{2} H_0^{(1)}(\kappa_k |\mathbf{x} - \mathbf{y}|), \quad k = 0, 1, \dots, M,$$

where $H_0^{(1)}$ is the Hankel function of the first kind and order zero. Throughout this paper i will denote the complex constant satisfying $i^2 = -1$.

2 The integral equation approach

First, for non-zero functions ϕ_l , $l = 1, 2, \dots, M$, define the single and double layer potentials as

$$S_k^l \phi_l(\mathbf{x}) = \int_{\Gamma_l} \Phi_k(\mathbf{x}, \mathbf{y}) \phi_l(\mathbf{y}) ds(\mathbf{y}), \quad \mathbf{x} \in \mathbf{R}^2 \setminus \Gamma_l,$$

and

$$D_k^l \phi_l(\mathbf{x}) = \int_{\Gamma_l} \frac{\partial}{\partial \nu_l(\mathbf{y})} \Phi_k(\mathbf{x}, \mathbf{y}) \phi_l(\mathbf{y}) ds(\mathbf{y}), \quad \mathbf{x} \in \mathbf{R}^2 \setminus \Gamma_l,$$

respectively, for $k = 0, 1, \dots, M$. Their normal derivatives are denoted by P_k^l and Q_k^l , respectively, for $k = 0, 1, \dots, M$.

We have the continuity relations

$$S_k^l = \hat{S}_k^l, \quad Q_k^l = \hat{Q}_k^l,$$

and the jump relations

$$D_k^l = \mp I + \hat{D}_k^l \quad \text{and} \quad P_k^l = \pm I + \hat{P}_k^l,$$

where, the upper (lower) sign corresponds to the limit when \mathbf{x} approaches Γ_l from the outside (inside). The hat on each operator represents it on the boundary Γ_l .

To arrive at the desired integral equation we define a layer ansatz by $E_k^l := D_k^l - i\eta_l S_k^l$ for $l \neq 0$ and $E_k^0 = 0$ (with normal derivative $H_k^l := \partial E_k^l / \partial \nu$) in Ω_k , where η_l s are nonzero complex constants chosen to obtain well-posedness, $k = 0, 2, 4, \dots$, and Green's theorem in $\Omega_{k'}$, $k' = 1, 3, 5, \dots$. In particular, let us

assume that M is odd. Then, in the core region Ω_0 we define

$$u_0(\mathbf{x}) = E_0^1 \phi_1(\mathbf{x}), \quad \mathbf{x} \in \Omega_0. \quad (2.1)$$

In the outermost domain, we use Green's theorem ([7] pp. 68-70) to obtain

$$\begin{cases} 2u_M(\mathbf{x}) = S_M^M \frac{\partial}{\partial \nu} u(\mathbf{x}) - D_M^M u(\mathbf{x}), & \mathbf{x} \in \Omega_M, \\ -2u^i(\mathbf{x}) = S_M^M \frac{\partial}{\partial \nu} u(\mathbf{x}) - D_M^M u(\mathbf{x}), & \mathbf{x} \in \mathbf{R}^2 \setminus \bar{\Omega}_M. \end{cases} \quad (2.2)$$

In the other domains, for $l = 2, 4, \dots, M-1$, we define

$$u_l(\mathbf{x}) = E_l^l \phi_l(\mathbf{x}) + E_l^{l+1} \phi_{l+1}(\mathbf{x}), \quad \mathbf{x} \in \Omega_l, \quad (2.3)$$

and, using Green's theorem for $l = 1, 3, \dots, M-2$ we have

$$\begin{cases} 2u_l(\mathbf{x}) = S_l^l \frac{\partial}{\partial \nu} u_l(\mathbf{x}) - S_l^{l+1} \frac{\partial}{\partial \nu} u_l(\mathbf{x}) - \\ (D_l^l - D_l^{l+1}) u_l(\mathbf{x}), & \mathbf{x} \in \Omega_l, \\ 0 = S_l^l \frac{\partial}{\partial \nu} u_l(\mathbf{x}) - S_l^{l+1} \frac{\partial}{\partial \nu} u_l(\mathbf{x}) - \\ (D_l^l - D_l^{l+1}) u_l(\mathbf{x}), & \mathbf{x} \in \mathbf{R}^2 \setminus \bar{\Omega}_l \end{cases} \quad (2.4)$$

Now, using the jump and continuity relations we obtain the second equation in (2.2) on Γ_M and the second equation in (2.4) on Γ_l and Γ_{l+1} ($l = 1, 3, 5, \dots, M-2$). Using the boundary conditions, jump properties for the single and double layer potentials together with their derivatives, and replacing u_0 (given in (2.1)) and u_l (given in (2.3)) into these equations we arrive at a set of M integral equations with M unknowns ϕ_l on Γ_l , $l = 1, 2, \dots, M$. In particular, on Γ_M we have

$$\begin{aligned} -2u^i = & (\rho_M \hat{S}_M^M \hat{H}_{M-1}^M - (\hat{D}_M^M + I) \hat{E}_{M-1}^M) \phi_M + \\ & (\rho_M \hat{S}_M^M H_{M-1}^{M-1, M} - (\hat{D}_M^M + I) E_{M-1}^{M-1, M}) \\ & \times \phi_{M-1}, \end{aligned}$$

and for $l = 1, 3, 5, \dots, M-2$, we have

$$\begin{aligned} 0 = & (\rho_l \hat{S}_l^l H_{l-1}^{l-1, l} - (\hat{D}_l^l + I) E_{l-1}^{l-1, l}) \phi_{l-1} + \\ & (\rho_l \hat{S}_l^l \hat{H}_{l-1}^l - (\hat{D}_l^l + I) \hat{E}_{l-1}^l) \phi_l - \\ & \left(\frac{1}{\rho_{l+1}} S_l^{l+1, l} \hat{H}_{l+1}^{l+1} - D_l^{l+1, l} \hat{E}_{l+1}^{l+1} \right) \phi_{l+1} - \\ & \left(\frac{1}{\rho_{l+1}} S_l^{l+1, l} H_{l+1}^{l+2, l+1} - D_l^{l+1, l} E_{l+1}^{l+2, l+1} \right) \phi_{l+2} \end{aligned}$$

on Γ_l and

$$0 = \left(\frac{1}{\rho_{l+1}} \hat{S}_l^{l+1} \hat{H}_{l+1}^{l+1} - (\hat{D}_l^{l+1} - I) \hat{E}_{l+1}^{l+1} \right) \phi_{l+1} + \left(\frac{1}{\rho_{l+1}} \hat{S}_l^{l+1} H_{l+1}^{l+2, l+1} - (\hat{D}_l^{l+1} - I) E_{l+1}^{l+2, l+1} \right) \phi_{l+2} - \left(\rho_l S_l^{l, l+1} H_{l-1}^{l-1, l} - D_l^{l, l+1} E_{l-1}^{l-1, l} \right) \phi_{l-1} - \left(\rho_l S_l^{l, l+1} \hat{H}_{l-1}^l - D_l^{l, l+1} \hat{E}_{l-1}^l \right) \phi_l \quad \text{on } \Gamma_{l+1},$$

where $\hat{E}_k^m = \mp I + \hat{D}_k^m - i\eta_m \hat{S}_k^m$, $\hat{H}_k^m = \hat{Q}_k^m - i\eta_m (\pm I + \hat{P}_k^m)$, and by $T_k^{m, n}$ (T is for S , D , E or H) we mean that T_k^m is evaluated on Γ_n when $n \neq m$. Numerically the above system has to be discretized and solved to obtain an approximation of the unknowns ϕ_l , $l = 1, 2, \dots, M$. Then the solution of the layered problem can be constructed for the discretized forms of (2.1)-(2.4).

Remark: The above system is also valid for the 3D Helmholtz equation. The only difference is that the fundamental solution is

$$\Phi_k(\mathbf{x}, \mathbf{y}) = -\frac{e^{i\kappa_k |\mathbf{x} - \mathbf{y}|}}{2\pi |\mathbf{x} - \mathbf{y}|}.$$

3 Numerical validation and results

This section is devoted to the numerical solution of the above system and its validation for the 2D case. To this end, we use the Nyström method for the numerical solution and Bessel function expansion for the validation. Then we show the numerical results.

3.1 Discretization and numerical solution

The system is discretized using the Nyström method [11]. The resulting matrix equation, that involves matrix multiplications resulted from the multiplications of layer potentials and/or their derivatives, is solved by a standard LU decomposition approach. Let us note that the assumption that M is odd is not a loss of generality. In fact, for an even M we can use the same method, but for $M+1$ regions, Γ_{M+1} encloses the scatterer, with $\kappa_{M+1} = \kappa_M$ and $\rho_{M+1} = 1$. This way has the advantage of keeping the same system of equations and the disadvantage of adding another equation and an unknown function ϕ_{M+1} . This may be overcome by starting with Green's theorem in the core region,

alternate with layer ansatz and obtain the Green's theorem in Ω_M , which gives a different system than the previous argument.

3.2 The Mode Matching Approach

This method is studied in detail in the literature (see e.g., [9]). Consider the case when the regions \mathbf{D}_l 's are circular cylinders with radii r_{l+1} and origins \mathbf{O}_{l+1} , $l = 0, 1, 2, \dots, M-1$; then we have the following expansions [6]: For the outermost region

$$u(\tilde{r}_M, \phi_M) = \sum_{n=-\infty}^{\infty} \left(b_n^M H_n^{(1)}(\kappa_M \tilde{r}_M) + J_n(\kappa_M \tilde{r}_M) \right) \times e^{-in(\phi_M - \phi_0)}$$

and for other regions we have

$$u_l(\tilde{r}_1, \phi_1) = \sum_{n=-\infty}^{\infty} \left(b_n^l H_n^{(1)}(\kappa_l \tilde{r}_1) + a_n^l J_n(\kappa_M \tilde{r}_1) \right) \times e^{-in(\phi_1 - \phi_0)}, \quad l = 0, 1, 2, \dots, M-1,$$

where $b_n^0 = 0$.

To enforce the boundary conditions we need the addition formula for u_l , $l = 1, \dots, M-1$ which means that the fields expressed in terms of $X_1 O_1 Y_1$ be translated to $X_l O_l Y_l$ coordinates. This yields, by the addition theorem (cf. [5] pp. 30-31),

$$u_l(\tilde{r}_l, \phi_l) = \sum_{n=-\infty}^{\infty} \sum_{i=-\infty}^{\infty} J_{i-n}(\kappa_l d_{l1}) \times \left[b_n^l H_i^{(1)}(\kappa_l \tilde{r}_l) + a_n^l J_i(\kappa_l \tilde{r}_l) \right] \times e^{i(\phi_0 - (i-n)\phi_{l1})},$$

where d_{l1} is the distance between \mathbf{O}_1 and \mathbf{O}_l , and ϕ_{l1} is the angle between $\mathbf{O}_1 \mathbf{O}_l$ and the x axis.

The sums in the above equations have to be truncated, at some number, N_0 , to obtain a finite system. Now we can use the expansions on the boundary together with their derivatives and the boundary conditions to obtain a linear system in the unknowns a_n^l and b_n^l . This system is also solved via LU decomposition approach.

3.3 Numerical Results

In this section, numerical solution obtained by using the integral equation (IE) and mode matching (MM)

methods are presented. We have conducted several numerical experiments.

First we try to validate the MM method by analyzing the physical properties of the waves, by plotting the absolute value of the waves against the boundaries. In this end, we consider a cylinder with radius $r = 3$ that we only have the inner and outermost domain and keep the angle of the incident field $\phi_0 = 90$ and $\rho_1 = 1$ fixed. We would expect, for real κ_1 and complex κ_2 with negative imaginary part, that the waves diverge at the boundary. If, on the other hand, we have that the two wave numbers are real and equal, the absolute value of the wave should be unity. Finally, for the case when κ_1 is real and κ_2 is complex with a positive imaginary part, because of absorption, the absolute value of the wave must decay at the boundary and the bigger the imaginary part, the faster the wave should decay. Our numerical computations show that all these properties are satisfied, and the results are summarized in Figure 2.

Next we validated the IE method for one interface, centered at $\mathbf{O} = (-0.2, 0.7)$, by plotting the absolute value of the far field pattern (measured at a fixed observation point \hat{x}) against the incidence angle for two different wave numbers using the IE and MM methods. See [8], page 20, for the definition of the far field pattern f . The result is given in Figure 3, which shows a very good agreement of the two methods. Unless otherwise stated we use 32 grid points for the Nyström solver.

Our next examples are for the two and three-layered circular cases. First we plot the absolute value of the far field against the incidence angle for the two-layered case and then for the three-layered case. The results are shown in Figure 4 and Figure 5, respectively. In these cases as well we have very good agreements of the two methods.

For the case of more circular layers we have the same conclusions, except that more grid points are needed, which is due to the errors in the computation of the layer potentials.

Our last example is for the case of three boundaries of kite type where MM method can not be performed (Figure 6). Here we investigate the convergence as well as the boundary conditions. For the former we compute the far field pattern for different wave numbers.

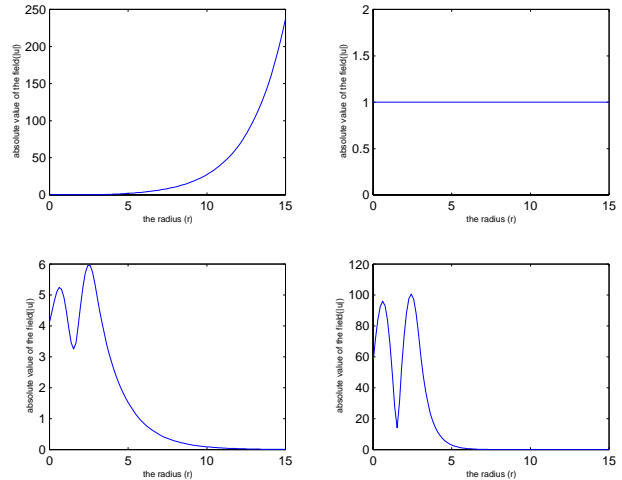


Figure 2: The case of one circular boundary ($r = 3$). The absolute value of the wave plotted against the radius. We have used $\kappa_1 = 2$ and $\kappa_2 = 2 - 0.5i$ (top left), $\kappa_1 = 2$ and $\kappa_2 = 2$ (top right), $\kappa_1 = 2$ and $\kappa_2 = 2 + 0.5i$ (bottom left), and $\kappa_1 = 2$ and $\kappa_2 = 2 + 1.5i$ (bottom right).

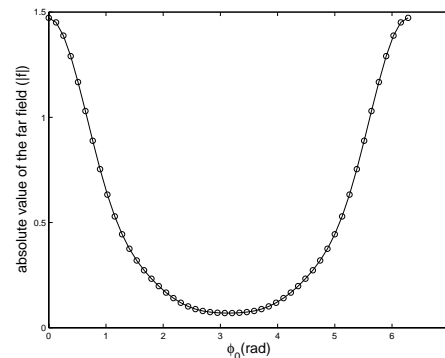


Figure 3: The absolute value of the far field pattern plotted against the incidence angle using the MM ('o') and IE (solid line) methods. The case of one interface. We used $\kappa_0 = 2$, $\kappa_1 = 3$ and the radius is $r = 1$.

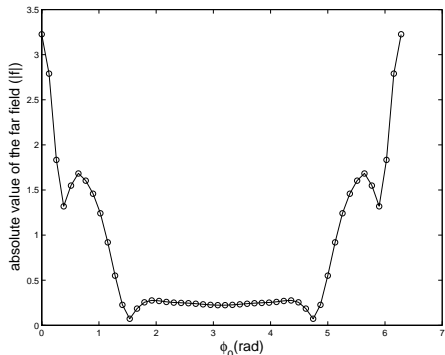


Figure 4: The absolute value of the far field pattern plotted against the incidence angle using the MM ('o') and IE (solid line) methods. The case of two-layered circular cylinders. Here $\kappa_0 = 2$, $\kappa_1 = 3$, $\kappa_2 = 4$, $r_1 = 1$ and $r_2 = 2$.

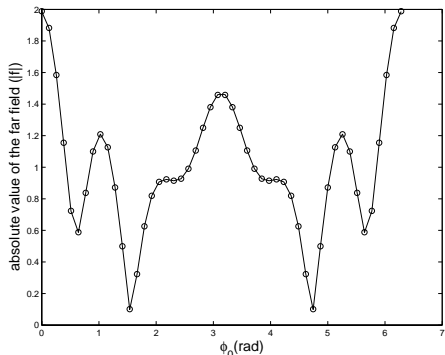


Figure 5: The absolute value of the far field pattern plotted against the incidence angle for the MM ('o') and IE (solid line) methods. The case of three-layered circular cylinder. Here $\kappa_0 = 2$, $\kappa_1 = 3$, $\kappa_2 = 4$, $\kappa_3 = 1$, $r_1 = 1$, $r_2 = 2$ and $r_3 = 3$.

The results are reported in the two tables below. We see clear convergence, and, as expected, it is fast. For the latter case we plot $|u_0|$ and $|u_1|$ on Γ_1 , $|u_1|$ and $|u_2|$ on Γ_2 , and $|u_2|$ and $|u_3 + u^i|$ on Γ_3 , against the incidence angle. From the boundary conditions we know that they must coincide. This is shown in Figures 7. One way we have used to compare the IE and MM methods in the case of 3-layered kite is by enclosing the tree layers within a circular domain and choose all the inner layers to have the same wave numbers and the outer region to have a different wave number. Physically, this is a one-layered problem; but mathematically the four layers exist. By so doing we still obtain a figure similar to Figure 3.

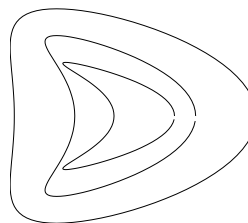


Figure 6: The geometry for the case of three boundaries of kite type.

Table 1: Parameter values and description for the geometry in Figure 6. D1, D2 and D3 are the first, the second and third data, respectively, for the numerical computation

Description	Symbol	D1	D2	D3
Wave numbers	κ_0	2	4	$1+i$
	κ_1	3	5	2
	κ_2	1.5	4.5	$2+0.5i$
	κ_3	2.5	5.5	3

4 Conclusion and future work

We have developed an integral equation approach for solving the M multilayered electromagnetic problem and used the Nyström method for the numerical computation. The algorithm was validated by a Fourier expansion method for circular (not necessarily concentric) cylinders. One may think as a disadvantage for our

Table 2: The numerical results using the integral equation (IE) approach for the geometry in Figure 6. The data are given in Table 1. The number N is the number of Nyström (grid) points.

	N	IE
D1	8	$-3.1863 + 0.4213i$
	16	$-3.5238 + 0.1952i$
	32	$-3.5215 + 0.1955i$
	64	$-3.5214 + 0.1954i$
D2	8	$-11.9843 + 15.8975i$
	16	$-3.5291 + 3.2993i$
	32	$-4.2103 + 3.5349i$
	64	$-4.2103 + 3.5344i$
D3	8	$-2.3889 + 1.6002i$
	16	$-2.5120 + 1.5746i$
	32	$-2.5126 + 1.5739i$
	64	$2.5126 + 1.5739i$

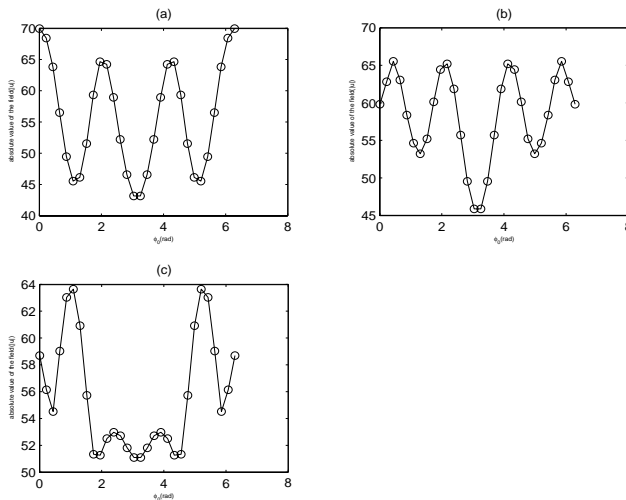


Figure 7: Here we plot $|u_j|$ ('o') and $|u_{j+1} + \frac{(j-1)(j-2)}{2}u^i|$ (solid line) on the boundary Γ_j against the incidence angle. In (a) we have the case $j=1$, in (b) $j=2$ and (c) $j=3$.

method the numerous matrix vector multiplications. This problem can be overcome by using fast multipole methods (see [15]) where these operations are done very quickly. Our results also show the (expected) fast convergence of the Nyström method for analytic boundaries. The natural expansion of our method is for the numerical solution of the three-dimensional electromagnetic problem, and to the case of multiple scatterers.



Dr. F. Seydou is a Docent (Associate Professor) in applied mathematics at the University of Oulu, Finland and a Visiting Researcher at the University of Maryland, College Park. He wrote his Ph.D. thesis at the University of Delaware and graduated at the University of Oulu in 1997.

Dr. Seydou's research interests are finite and boundary element methods applied to problems in computational electromagnetism, and inverse scattering problems.



Ramani Duraiswami is a Research Associate Professor at the University of Maryland Institute for Advanced Computer Studies. He is also Director of the Perceptual Interfaces and Reality Laboratory. Dr. Duraiswami got his Ph.D. in 1991 from The Johns

Hopkins University. His research interests include computational audio, scientific computing and computer vision. He is an associate editor of the ACM Transactions on Applied Perception.



Nail Gumerov is a Research Assistant Professor at the University of Maryland Institute for Advanced Computer Studies. He got his Ph.D. in 1987 from The Lomonosov Moscow State University and Sc.D. in 1992 from the Tyumen University in Russia.

His research interests include mathematical modeling, fluid mechanics, acoustics, and scientific computing.



Tapio Seppänen is a professor of information engineering at the University of Oulu, Finland. Dr. Seppänen got his Ph.D. in 1990 from the University of Oulu. His research interests include speech and audio signal processing, multimedia search engines,

digital rights management of multimedia, and processing of physiological signals.

References

- [1] C. Athanastadis, "On the acoustic scattering amplitude for a multi-layered scatterer," *J. Austral. Math. Soc. Ser. B* 39, pp. 431–448, 1998.
- [2] C. Athanasiadis, A.G. Ramm and I.G. Stratis, "Inverse acoustic scattering by a layered obstacle," in *Inverse Problems, Tomography, and Image Processing* (ed. A.G. Ramm), Plenum Press, New York, pp. 1–8, 1998.
- [3] N. N. Bojarski, "The k-space formulation of the scattering problem in the time domain," *J. Opt. Soc. Amer.*, Vol. 72, pp. 570–584, 1982.
- [4] O.P. Bruno and A. Sei, "A fast high-order solver for EM scattering from complex penetrable bodies: TE case," *IEEE Transactions on Antennas and Propagation*, Vol. 48, 12, pp. 1862–1864, 2000.
- [5] K. Chadán, D. Colton, L. Paivarinta and W. Rundell, *An Introduction to Inverse Scattering and Inverse Spectral Problems*, SIAM Monographs on Mathematical Modeling and Computation, 1997.
- [6] W. C. Chew, *Waves and Fields in Inhomogeneous Media*, IEEE Press, 1995.
- [7] D. Colton and R. Kress, *Integral Equation in Scattering Theory*, John Wiley & Sons, 1983.
- [8] D. Colton and R. Kress, *Inverse Acoustic and Electromagnetic Scattering Theory*, Springer Verlag, 1992.
- [9] A. Kishk, R. Parrikar and A. Elsherbeni, "Electromagnetic Scattering from an eccentric multilayered circular cylinder," *IEEE Trans. Antennas and Prop. Vol. 40*, No3 pp. 295–303, 1992.
- [10] R.E. Kleinmann and P.A. Martin, "On single integral equations for the transmission problem of acoustics," *SIAM J. Appl. Math. Vol. 48*, No. 2, pp. 307–325, 1988.
- [11] R. Kress, "On the numerical solution of a hypersingular integral equation in scattering theory," *J. Comp. Appl. Math. Vol. 61*, pp. 345–360, 1995.
- [12] E. Larsson, "A domain decomposition method for the Helmholtz equation in a multilayer domain," *SIAM J. Sci. Comput.*, Vol. 20, pp. 1713–1731, 1999.
- [13] Olivier J. F. Martin and Nicolas B. Piller, "Electromagnetic scattering in polarizable backgrounds," *Phys. Rev. E* 58, No. 3, pp. 3909–3915, 1998.
- [14] P.A. Martin and P. Ola, "Boundary integral equations for the scattering of electromagnetic waves by a homogeneous dielectric obstacle," *J. Proc. R. Soc. Edinb., Sect. A* 123, No. 1, pp. 185–208, 1993.
- [15] J.M. Song and W.C. Chew, "FMM and MLFMA in 3D and Fast Illinois Solver Code, Chapter 3" in *Fast and Efficient Algorithms in Computational Electromagnetics*, edited by Chew, Jin, Michielssen, and Song, Artech House, 2001.
- [16] Z. Wu and L. Guo, "Electromagnetic scattering from a multilayered cylinder arbitrarily located in a gaussian beam, a new recursive algorithms," *Progress In Electromagnetics Research, PIER* 18, pp. 317–333, 1998.

New Compact 3 dB $0^\circ/180^\circ$ Microstrip Coupler Configurations

Ashraf Mohra¹, Abdel Fattah Sheta², and Samir F. Mahmoud³

¹Microstrip Dept., Electronics Research Institute, Cairo, Egypt

²EE Dept., College of Eng, King Saude University, Riyadh, Saudi Arabia

³EE Dept., Kuwait University, P.O. Box 5969, Safat 13060, Kuwait

Abstract: Compact 3 dB $0^\circ/180^\circ$ microstrip couplers in ring and square configurations are proposed and discussed. In a ring form, the coupler may be designed for symmetrical ports about either one axis or two axes. The proposed configurations introduce significant size reduction, which is the most important demand for microwave integrated circuits (MICs) and monolithic microwave integrated circuits (MMICs). Different couplers are designed, and simulated at 1 GHz. The IE3D software is used in order to validate the design procedure. The designed coupler in ring shape is simulated and implemented. The experimental results agree well with the theoretical prediction.

Keywords: Compact ring coupler, Hybrid ring, Microstrip, MMICs

I. Introduction

In recent years, the rapid growth in wireless communications has increased the demand for small size RF circuits. Hybrid couplers are fundamental components in microwave circuits and include branch line couplers, parallel line couplers, hybrid ring couplers, and the rat race ring. A fundamental component of all these couplers is the $\lambda/4$ transmission line section. At the lower microwave frequencies, the size based on this $\lambda/4$ section is unsuitably large for many wireless applications. Much effort to reduce the size of hybrid couplers has been reported [1-6]. Recently, T-shaped and stepped impedance circuits equivalent to $\lambda/4$ line section have been used in hybrid quadrature branch line coupler [1]. The resultant coupler has been implemented on 36% of the area of that of the conventional one without any significant sacrifice in circuit performance. Different techniques have been used to reduce the size of the conventional ring coupler of 1.5λ circumference (see Fig. 1). A quarter wavelength pair of coupled lines short-circuited at their diagonal ends has been used to replace the three quarter wavelength line [2]. The circumference of such coupler has been reduced to one

wavelength λ . However, this technique requires a very tightly coupled line section that is difficult to fabricate with simple microstrip technology. The use of $\lambda/6$ or $\lambda/8$ sections allows reducing the circumference of the ring to 1.25λ [3]. Another approach to reduce the ring coupler size requires; (1) using a small section of transmission line with a specified characteristic impedance instead of the $\lambda/4$ line; and (2) replacing the three quarter wavelength line by a one-quarter-wavelength line with phase inverter [4, 5]. Based on this approach, the 1.5λ circumference has been reduced to 0.67λ [4]. The circuit is composed of a coplanar strip (CPS) ring and coplanar waveguide (CPW) feed lines. Air bridges are then needed to avoid the excitation of an even mode. A crossover of the two strips on the ring is also required to achieve 180° phase shift (phase inverter). These techniques tend to increase the fabrication cost which is one of the most important parameters of MIC. Compact ring $0^\circ/180^\circ$ couplers using T-shaped sections to replace the $\lambda/4$ lines have been introduced recently by the authors [6].

In this paper, we propose new small size 3 dB $0^\circ/180^\circ$ coupler configurations. The coupler can be designed in square form or ring shape with symmetric ports about either one axis or two axes. The various configurations can be fabricated with simple low cost microstrip technology. The reduced size coupler configurations are discussed in the next section followed by the simulation and experimental results. The couplers' simulations are performed using the IE3D software.

II. Reduced Size Coupler Configurations

The size of the conventional ring coupler, shown in Fig.1, can be reduced to the ring coupler with 4θ circumference shown in Fig. 2. The arms characteristic impedances Z_C are related to the electrical length θ and 50Ω port impedance Z_0 by [4]:

$$Z_c = Z_o \sqrt{2(1 - \cot^2 \theta)}. \quad (1)$$

The range of the arm electrical length is $45^\circ < \theta < 90^\circ$, where θ is the arm electrical length at the center frequency. The phase inverter has been implemented by crossing over the two strips in case of coplanar strip technique. In simple microstrip technique, the phase inverter can be implemented as a half wavelength line having the same characteristic impedance of the θ sections. In this case the resultant bandwidth is narrow and decreases as θ decreases. However, wider bandwidth can be obtained if θ is equal to 90° at the center frequency [5]. The corresponding characteristic impedance of the arms is

$$Z_c = Z_o \sqrt{2 \left(1 - \frac{2}{10 - \frac{L}{20} + 1} \right)} \quad (2)$$

where L is the maximum in-band return loss specification. For $L = \infty$ the resultant ring coupler will be similar to the conventional one. In the following, some proposed geometrical arrangements, suitable for microstrip technology, are given and they lead to the coupler structures shown in Figs 3-5:

A. Semi-circle shape with symmetric ports about one axis (Fig. 3)

In this case the $180^\circ + \theta$ line between ports 2 and 4 is designed in the free region inside the semi-circle as shown in Fig. 3. The minimum area can be achieved for $\theta = 45^\circ$, which correspond to 12.5% of that of the conventional ring coupler. However, the resultant bandwidth in this case will be almost zero. Practically, θ should be greater than 45° and can be determined for a particular BW requirement as described in the next section. A simple software program such as Puff can quickly predict the coupler performance.

B. Ring shape with symmetric ports about the two axes (Fig. 4)

The line $180^\circ + \theta$, in this case is formed inside the ring in a circular shape. However, the inner line should be far enough from the outer one to avoid any significant coupling. Denote the electrical distance between the two bending lines and the two rings by θ_1 as shown in Fig. 4. For small θ_1 , the arms electrical length can be approximated by

$$\theta \approx 0.5 (\pi \theta_1 + 90^\circ). \quad (3)$$

C. Square shape (Fig. 5)

In this case the coupler can be implemented in the square form of side length θ , where the $\theta + 180^\circ$ line takes the serpentine shape inside the square as shown in Fig. 5.

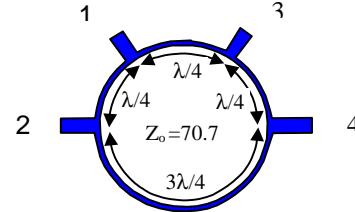


Fig. 1 Layout of the conventional ring coupler based on $\lambda_g/4$ line.

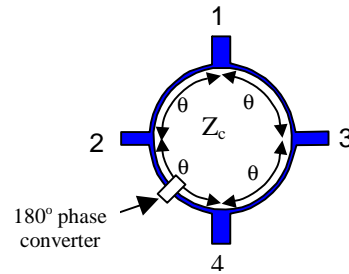


Fig. 2 Layout of a small size ring coupler derived from the theory in [4].

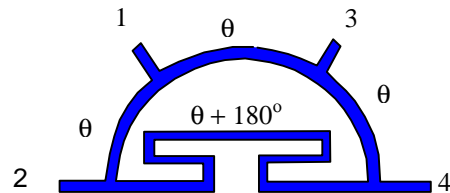


Fig. 3 Layout of small size ring coupler for asymmetrical feeding ports.

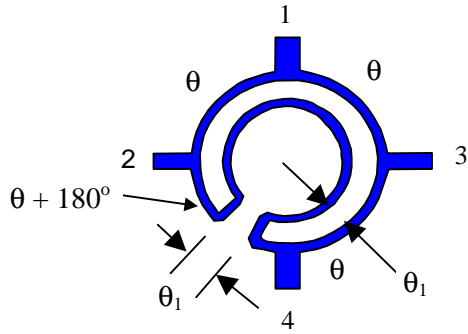


Fig. 4 Layout of small size ring coupler for symmetrical feeding ports.

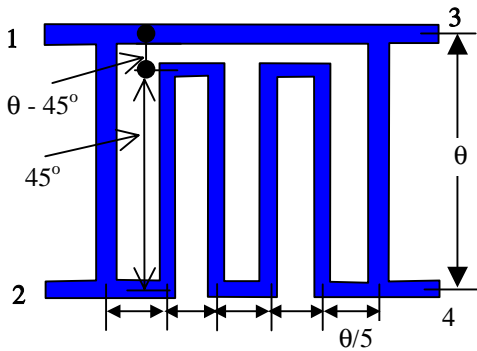


Fig. 5 Layout of square shape coupler.

III. Design Procedure and performance Trade-off

The couplers proposed herein are based on the implementation of the 180° phase inverter by half-wavelength line using special arrangement as shown in Figs. 3-5. So, the expected performance of all configurations will be approximately the same. The difference may be occurring only due to the unwanted coupling between the lines that are too close to each other. This can be eliminated by optimizing the structure to keep lines as far as possible. The coupler design can start by plotting the bandwidth and the area used, with respect to the area of the conventional type (Fig.1), against the arm electrical length θ as shown in Fig. 6. The relative bandwidth (BW) is calculated for ideal transmission line elements under the following limits:

- Port matching < -10 dB
- Coupling -2.5 to -4 dB
- Isolation < -15 dB
- Output phase balance when fed at E-port = $180^\circ \pm 12^\circ$
- Output phase balance when fed at H-port = $0^\circ \pm 10^\circ$

Fig. 6 shows that the relative bandwidth increases as θ increases. The maximum bandwidth is obtained for the conventional type, i.e when $\theta = 90^\circ$. It is also noted that the area used decreases as θ decreases. As shown in this figure, the most compact structure is that of circular shape of Fig. 4. The used area can be reduced to 13.7 % of the conventional type when $\theta = 50^\circ$. In this case, the corresponding percentage BW is 17.7%. Fig. 7 shows the characteristic impedance (Z_c) of the coupler arms calculated from (1). The characteristic impedance decreases as θ decreases. For high compactness, this will add some constraints on the selection of the substrate material since the line width increases as Z_c decreases. The increase of line width may cause the lines to be very close causing a strong coupling. Fig. 6 is used to determine the arm electrical length for a given bandwidth, and the corresponding characteristic impedance can be calculated from Fig.7.

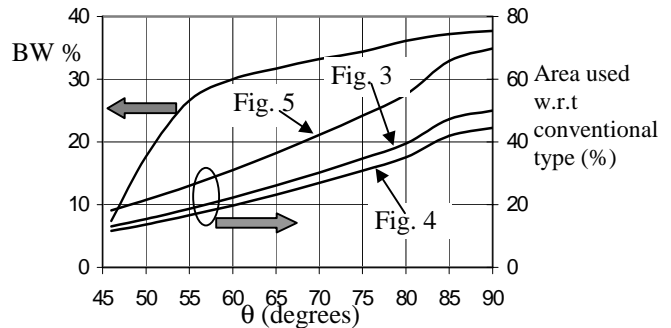


Fig. 6 Relative bandwidth and percentage area used with respect to the conventional coupler of Figs. 3-5.

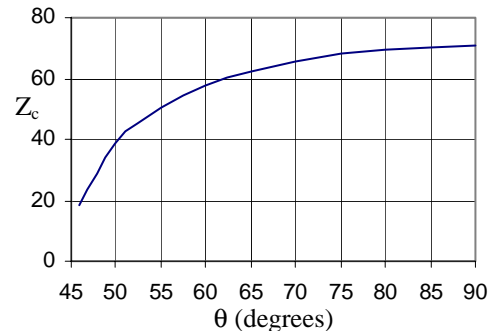


Fig. 7 Arms characteristic impedance Z_c against arms electrical length θ .

IV. Design Cases and Experimental Results

We introduce here different design cases in order to validate the proposed configurations. Duroid dielectric substrate RT/5880 with $\epsilon_r = 2.2$ and $h = 0.51$ mm is used.

For high compactness and acceptable line width, the arms electrical length are selected to be 55° . The design is carried out at 1 GHz. The resultant characteristic impedance of the coupler arms is $50\ \Omega$ (Fig. 7). Therefore the arms width and length are 1.6 and 33.3 mm, respectively. The simulation results performed by Puff software and based on ideal transmission lines are shown in Fig. 8. Within the band 0.95 to 1.1 GHz, $S_{11} < -10.5$ dB, $S_{21} = -3.25 \pm 0.35$ dB, $S_{31} = -3.5 \pm 0.6$ dB and S_{41} (isolation) < -22 dB. For this design, the ratio of the circuit layout area relative to that of the conventional ring coupler is 18.5%, 16.6%, and 26 % for circuits in Fig. 3, Fig.4 and the square shape in Fig. 5, respectively. However, wide band couplers can be designed based on (2). In this case the arms length will be 90° at 1 GHz and the characteristic impedance is $64\ \Omega$ for 20 dB return loss at the center frequency. The expected ratio of the circuit layout area with respect to that of the conventional ring coupler will be, 50%, 44%, and 70 % for circuits in Fig. 3, Fig.4 and Fig. 5., respectively.

As an example, the layout of the coupler shown in Fig. 4 is implemented. The arms length is 33.3 mm ($\theta = 55^\circ$) and $\theta_1 = 6.6^\circ$, which is 4 mm. The inner and outer radii are 17.4, and 21.2 mm, respectively. The simulation results performed by the IE3D are shown in Fig. 9. Between 0.88 and 1.15 GHz, $S_{11} < -10$ dB, $S_{21} = -3.15 \pm 0.35$ dB, $S_{31} = -3.5 \pm 0.3$ dB and $S_{41} < -14$ dB. At this case the area of coupler is approximately 17% of that of the conventional ring one, as expected from Fig. 6. The experimental results of this coupler are shown in Fig. 10. It is seen that the measured results agree well with the simulation in Fig. 9.

Conclusion

New small size configurations acting as a 3 dB $0^\circ/180^\circ$ ring coupler have been proposed. The coupler can be designed for narrow or wide band operations with significant size reduction in both cases although the size reduction is less in the wide band case. The coupler in square shape has been designed, simulated and measured. Good performance with 27% bandwidth centered at 1.015 GHz has been obtained. The coupler area is 17% of that of the conventional ring coupler. The proposed configurations allow good flexibility for MICs and MMICs applications.

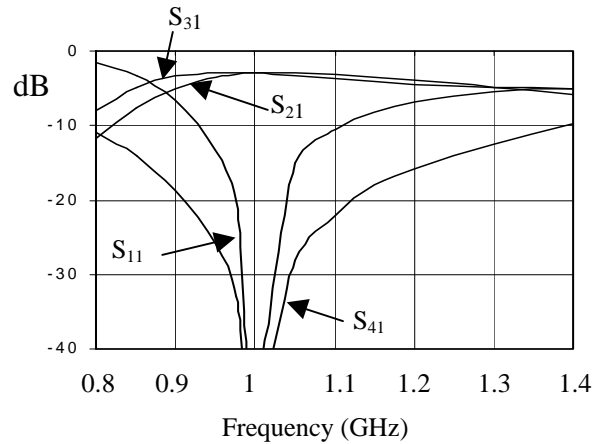


Fig. 8 Simulation results based on ideal transmission line performed using Puff software for narrow band case.

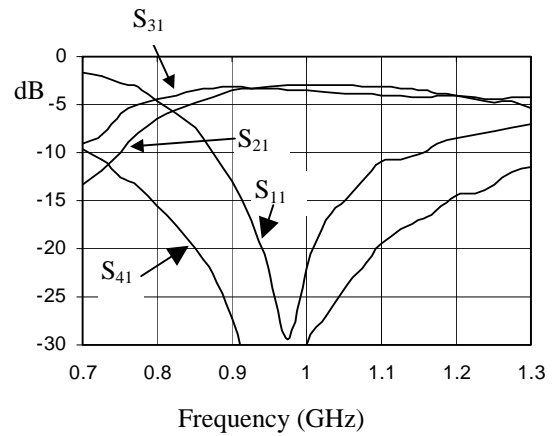


Fig. 9 Simulation results, performed by IE3D, of the layout of the circuit in Fig. 4.

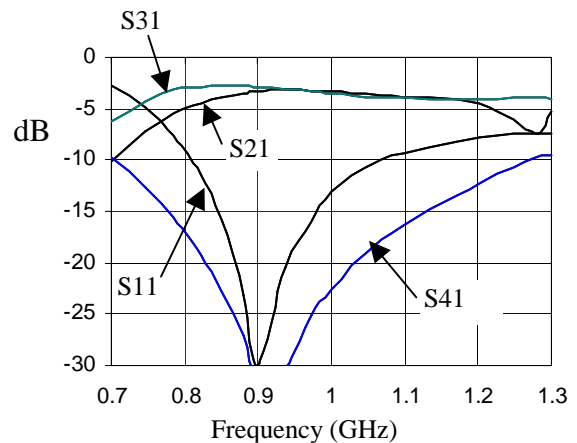


Fig.10 Experimental results of the coupler layout shown in Fig. 4.

References

- [1] A. F. Sheta, A. Mohra, S. F. Mahmoud, "A new class of miniature quadrature couplers for MIC and MMICs applications," *Microwave Opt. Technol. Lett.*, vol. 43, no. 3, pp. 215-219, August 2002.
- [2] S. Mar, "A wide band stripline hybrid ring," *IEEE Trans. Microwave Theory Tech.*, vol. MTT-16, p. 361, June, 1968.
- [3] D. I. Kim and G. S. Yang, "Design of new hybrid-ring directional coupler using $\lambda_g/8$ or $\lambda_g/6$ sections," *IEEE Trans. Microwave Theory Tech.*, vol. 39, pp. 1779-1783, Oct. 1991.
- [4] M. H. Murgulescu, E. Moisan, P. Legaud, E. Penard, and I. Zaquine, "New wideband $0.67\lambda_g$ circumference 180° hybrid ring coupler," *Electron. Lett.*, vol. 30, pp. 299-300, Feb. 1994.
- [5] T. Wang and Ke Wu, "Size reduction and band broadening design technique of uniplanar hybrid ring coupler using phase inverter for M(H)MIC's," *IEEE Trans. Microwave Theory Tech.*, vol. MTT-47, no. 2, pp. 198-206, Feb. 1999.
- [6] A. Mohra, A. F. Sheta, S. F. Mahmoud, "A small size 3 dB $0\circ/180\circ$ microstrip ring couplers," *J. of Electromagn. Waves and Appl.*, vol. 17, no. 5, 707-718, 2003.

Biography

Ashraf Shouki Seliem was born in Egypt in 1963. He received the B.Sc degree in Electronics and communications from Shoubra Faculty of Engineering in 1986. He received the M.Sc. and Ph.D. degrees in Electronics and communications from Ain Shams University, Cairo, Egypt, in 1994 and 2000, respectively. He is currently working with the Electronics Research Institutes. His current research interests include microstrip antennas, computer aided design of planar and uniplanar of MICs and MMICs.



Abdel Fattah Sheta received B.Sc. degree in Communications and Electro-physics from Alexandria University, Egypt in 1985 and the M.Sc. degree in EE, Cairo University in 1991. In 1996, he received the Ph.D. degree in microwave circuits analysis and design from ENST, Universite de Bretagne Occidentale, France. Between 1996-1998, he was based at NTI, Cairo, Egypt. In 1998 he joined Electric Engineering Department, Fayoum Branch, Cairo University. Currently he is an associate professor in Electrical Engineering at King Saud University, Saudi Arabia. His current research interests include microstrip antennas, planar and uniplanar MICs and MMICs.



Samir F. Mahmoud graduated from the Electronic Engineering Dept., Cairo University, Egypt in 1964. He received the M.Sc. and Ph.D. degrees in the Electrical Engineering Department, Queen's University, Kingston, Ontario, Canada in 1970 and 1973. During the academic year 1973-1974, he was a visiting research fellow at the Cooperative Institute for Research in Environmental Sciences (CIRES), Boulder, CO, doing research on Communication in Tunnels. He spent two sabbatical years, 1980-1982, between Queen Mary College, London and the British Aerospace, Stevenage, where he was involved in design of antennas for satellite communication. Currently Dr. Mahmoud is a full professor at the EE Department, Kuwait University. Recently, he has visited several places including Interuniversity Micro-Electronics Centre (IMEC), Leuven, Belgium and spent a sabbatical leave at Queen's University and the royal Military College, Kingston, Ontario, Canada in 2001-2002. His research activities have been in the areas of antennas, geophysics, tunnel communication, EM wave interaction with composite materials and microwave integrated circuits. Dr. Mahmoud is a Fellow of IEE and one of the recipients of the best IEEE/MTT paper for 2003.



ADVANCES IN FIELD THEORETICAL INVESTIGATIONS ON DIELECTRIC IMAGE LINE ISOLATORS IN I-LINE TECHNIQUE

Dietmar Koether¹, Peter Waldow², Member IEEE, Birgit Neuhaus², Student Member IEEE
Dominique Schreurs³, Senior Member IEEE and Adalbert Beyer¹, Fellow IEEE

¹ IMST GmbH, Carl-Friedrich-Gauss-Str. 2, 47475 Kamp-Lintfort, Germany

² Duisburg-Essen University, Bismarckstrasse 81, D-47048 Duisburg, Germany, email: a.beyer@uni-duisburg.de

³ Katholieke Universiteit Leuven, Div. ESAT-TELEMIC, Kasteelpark Arenberg 10, B-3001 Heverlee, Belgium

Abstract – Non-Radiative Dielectric Image Lines (NDGs) are waveguide structures in which a dielectric material serves to guide the electromagnetic waves. Among others, they could be accomplished as an I-guide or its modifications. This paper addresses various problems regarding to the design of a field displacement isolator in this technique. First, the electromagnetic field distribution in NDGs is shortly discussed. Subsequently, by the help of the Mode Matching (MM) technique, the calculation of isolator structures in I-line technique is performed. Thereafter, theoretical and experimental results, which show the capability of this device are introduced and intensively discussed.

Index Terms – Fields in NDG-structures, I-Line Technique, Mode Matching Method, Dielectric Image Line Isolator, Magnetic Field Distribution, Scattering Parameters in Forward- and in Reverse Direction

I. INTRODUCTION

Isolators are probably the most well-known nonreciprocal elements in the micro- and millimeter wave technology. In the ideal case, they have the characteristic to let through an undamped electromagnetic wave in the forward direction, and to close completely in the reverse direction. Thereby, no reflections of incident waves should raise in both directions. Isolators are used to match wave sources independently of the loading impedance and to protect the generator against reflected power. Also, it can be prevented, by their use in larger measurement setups, that standing waves are formed, overlaying with that signal, what can be measured and making an accurate

determination of the scattering parameters of the device under test impossible.

Such a behaviour can be obtained by several isolator-principles, which are all caused by gyrotropic materials, usually dc magnetized ferrites. Among others, the Faraday effect or phase shifters with feed back can be used, in order to develop isolators. But these possibilities have the disadvantages that either cylindrical lines are required or the operating band is too small [1]. Furthermore, there are resonance- and field displacement isolators. In reality, a clear distinction of these two types is not always possible, because the maximum field displacement arises close to the gyromagnetic resonance. Anyway, this symptom leads to direction-controlled losses, if the waveguide structure is asymmetric. Therefore, also isolators show a transmission behavior, which corresponds to a resonance characteristic according to the principle of the field displacement.

As a starting point, a brief discussion of the electromagnetic field in NDG-structures will be explained.

II. FIELDS IN NON-RADIATIVE DIELECTRIC GUIDE STRUCTURES

The dielectric image lines are suggested for applications since 1952. Usually, they are three-lateral open structures having a semicircular or a rectangular cross section. One common form of the dielectric image lines is the H-guide, which is concisely brought in between two, as ideal assumed, metallic plates (Fig. 1). Thus, it concerns of bilateral open dielectric image lines, in which different electromagnetic wave modes can propagate. This type of waveguides is well-understood

and its calculation is described in numerous papers, e.g. in [2, 3]. In the following, some results will be presented, which depict the field distribution in H- as well as in I-guides. Those findings were obtained by using the MM technique [4], see subsection III.

Fig. 1 shows the distribution of the electromagnetic field of an H-guide for the LSE₁₁ mode. Those image lines using a quasi TEM wave form (LSE₁₀) are called as I-guides. In Fig. 2 the typical field distribution is represented.

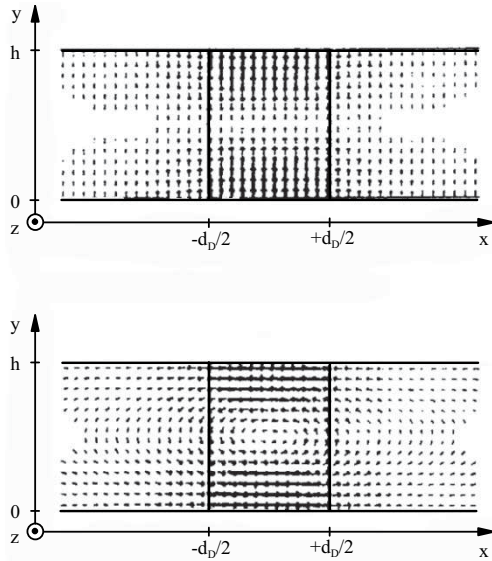


Fig. 1: Field distribution of the LSE₁₁ mode in a H-guide at a transversal plane ($f = 33$ GHz, $d_D = 4.0$ mm, $h = 5.0$ mm, $\varepsilon_r = 2.22$, $\tan \delta_\varepsilon = 2 \cdot 10^{-4}$, $\kappa = 62.5 \cdot 10^6 \frac{1}{\Omega\text{m}}$); Top: Electric Field; Bottom: Magnetic Field

As it is well-known, the transport of the electromagnetic wave in those guides takes mainly place in the dielectric material. The fields decrease in the outside space exponentially with the distance, thus this behavior describes also the concentration of the energy in the waveguide. For isotropic and gyrotropic materials the energy is directly proportional to the effective dielectric constant, which is given by the following relation-

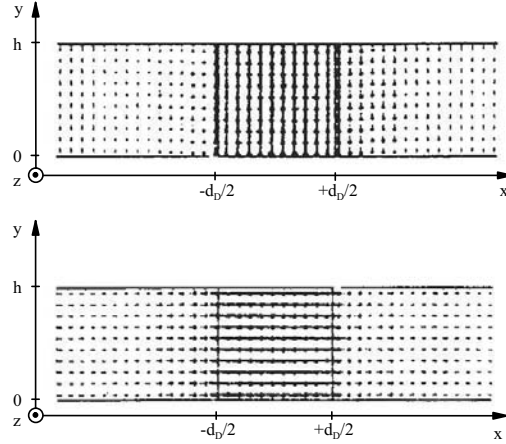


Fig. 2: Field distribution of the LSE₁₀ mode in an I-guide at a transversal plane ($f = 33$ GHz, $d_D = 3.5$ mm, $h = 3.5$ mm, $\varepsilon_r = 2.22$, $\tan \delta_\varepsilon = 2 \cdot 10^{-4}$, $\kappa = 62.5 \cdot 10^6 \frac{1}{\Omega\text{m}}$); Top: Electric Field; Bottom: Magnetic Field

ship:

$$\varepsilon_{\text{eff}} = \left(\frac{\beta}{k_0}\right)^2 \quad (1)$$

with β the phase constant and $k_0 = \omega\sqrt{\varepsilon_0\mu_0}$ the wave number of vacuum.

If the effective dielectric constant is sufficiently large, usually much larger than unity, also the electromagnetic field will vanish in the outside space. For example, in an I-guide, operating in the Ka-band and having a width of 3 mm, for a distance of 5 mm, the field values are already decreased on approximately 10% against their original values. This behavior increases with rising frequency. Thus, also high integration densities with dielectric image lines can be attained.

A hindrance is, however that at discontinuities radiations arise, which lead to unwanted coupling within the circuit. Therefore, the NRD guides are frequently used. The problem can be solved for other, that is to say radiative image kinds of waveguides, however, by the employment of absorber materials in the appropriate places and by applying smooth transitions. If in the dielectric image line structure the dielectric road is replaced by a piece ferrite, so - in case of the

I-guide - the calculation of the field distribution can be performed by means of LSE modes, see Fig. 3.

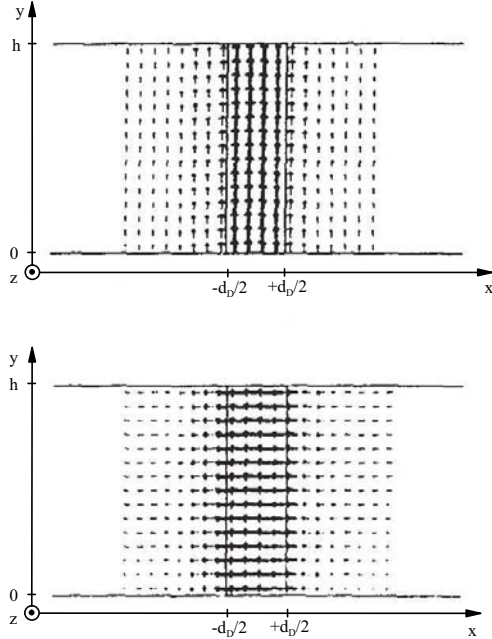


Fig. 3: Field distribution of the quasi LSE₁₀ mode in a I-guide using a TT2-111 ferrite piece at a transversal plane ($f = 33$ GHz, $H_0^i = 2,000 \frac{\text{kA}}{\text{m}}$, $h = 3.556$ mm, $d_F = 1$ mm, $\epsilon_r = 12.5$, $\tan \delta_\epsilon = 2 \cdot 10^{-4}$, $M_s = 397.9 \frac{\text{kA}}{\text{m}}$, $g = 2.11$, $\tilde{\alpha} = 0.011$)
Top: E-Field; Bottom: M-Field

It can be recognized that at such high values of the dc magnetization, the ferrite piece becomes isotropic. Thus, the field distribution is entirely analogue with that of an I-guide filled by an isotropic dielectric strip. The MM technique - which is widely used in analyzing waveguide structures with partly homogeneous material subregions - also allows the calculation of losses within this waveguide, see Fig. 4.

The computation of the dielectric losses α_d on the I-guide is relatively simple: only the dielectric constant is needed to be set complex. Following, also the phase constant β yields as a complex value. The determination of metallic losses caused through the skin effect is performed via a perturbation calculation, which takes the surface

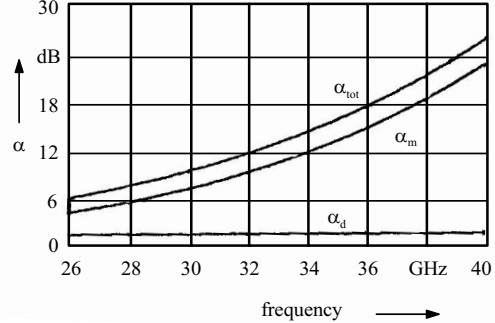


Fig. 4: Attenuation characteristic of an I-guide filled by ferrite for the LSE₁₀ mode; α_d : dielectric attenuation, α_m : gyromagnetic attenuation, α_{ges} : total attenuation. (for the data, see Fig. 3)

impedance of the metallic plates into account. If one considers the gyromagnetic losses α_m of the ferrite, then the frequency response and the magnetic losses become frequency dependent, as represented in Fig 4. Here the dc magnetic field strength H_0^i is selected in such a way that the gyromagnetic resonance can arise in a far frequency range outside the operating frequency regarded. Therefore, the magnetic losses (α_m) are partially substantially larger at low values of dc magnetic field strength.

In the following an isolator is developed in I-line technique, whose substantial mechanism is based on the field displacement by dc magnetized ferrites. The direction-controlled absorption features are caused mainly by additional absorbers.

III. FIELD THEORETICAL ANALYSIS FOR AN ISOLATOR IN I-LINE TECHNIQUE

The configuration in Fig. 5 shows an isolator, which is composed of a dielectric-, a ferrite- and an absorber material. The latter two areas are still separated from each other by a resistive foil with negligible thickness.

This structure is to be treated using the MM method [4], which is - as already mentioned - a

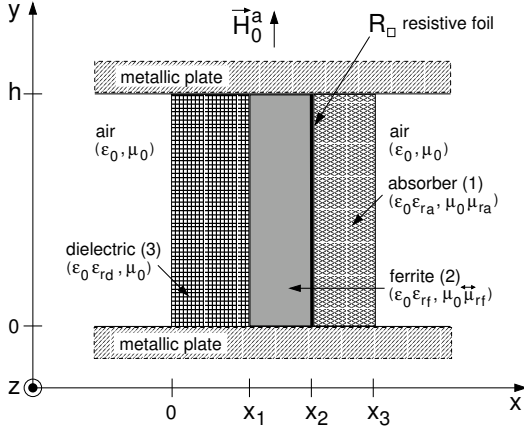


Fig. 5: Cross-section of an isolator in dielectric image line technique

very general-valid and a rigorous full-wave approach suitable for the processing of complex electromagnetic problems with partial homogeneous material subregions.

The necessary equations for matching the electromagnetic fields in the interfaces between two adjacent sub-regions (absorber (1) and ferrite (2)) [5] must also take into account the surface current, which flows in the resistance foil and is caused by the electromagnetic field.

It yields for the continuity of the electric field strength component E_y :

$$E_{y2} - E_{y1} = 0 \quad (2)$$

and for the effect of the surface current:

$$H_{z2} - H_{z1} = -S_{Fy} = -\frac{E_{y1}}{R_F} \quad (3)$$

with R_F the surface resistance of the resistive foil and S_F the surface current. Now, consider the right open region of the isolator in Fig. 5 which is filled with air and which is extended to $x \rightarrow \infty$. Thus, the following expression for LSE -waves in the electromagnetic field may be found:

$$E_y = A \exp(-k_x(x - x_a)) \exp(-\gamma z) \quad (4)$$

$$H_x = \frac{-\gamma}{j\omega\mu_0} A \exp(-k_x(x - x_a)) \exp(-\gamma z) \quad (5)$$

$$H_z = \frac{+k_x}{j\omega\mu_0} A \exp(-k_x(x - x_a)) \exp(-\gamma z) \quad (6)$$

with the propagation constant γ , the co-ordinate x_a of the interface between the layers absorber/air and the wave number k_x in x -direction. The wave number k_x is given by:

$$k_x^2 = -k_0^2 - \gamma^2. \quad (7)$$

with k_0 the wave number of vacuum given by: $k_0 = \omega\sqrt{\mu_0\epsilon_0}$.

The electromagnetic field within the left region of the isolator, which is also filled with air, can be represented similarly. Herein, the quantity $+k_x$ must be used instead of $-k_x$.

The ferrite filled region in Fig. 5 is described under the assumption, that - in case of the I-guide - no y -co-ordinate dependency of the field component exists. Furthermore, only the E_y -component of the magnetic field strength occurs. Hence, the following solutions of the Maxwell's equations can be obtained:

$$E_y = [A \sin(k_x(x - x_a)) + B \sin(k_x(x - x_b))] \cdot \exp(-\gamma z) \quad (8)$$

$$H_x = \left[A \left(\frac{+j\gamma}{\omega\mu_0\mu_{1\text{eff}}} \sin(k_x(x - x_a)) + \frac{+k_x}{\omega\mu_0\mu_{2\text{eff}}} \cos(k_x(x - x_a)) \right) + B \left(\frac{+j\gamma}{\omega\mu_0\mu_{1\text{eff}}} \sin(k_x(x - x_b)) + \frac{+k_x}{\omega\mu_0\mu_{2\text{eff}}} \cos(k_x(x - x_b)) \right) \right] \exp(-\gamma z) \quad (9)$$

$$H_z = \left[A \left(\frac{-k_x}{j\omega\mu_0\mu_{1\text{eff}}} \cos(k_x(x - x_a)) - \frac{j\gamma}{j\omega\mu_0\mu_{2\text{eff}}} \sin(k_x(x - x_a)) \right) + B \left(\frac{-k_x}{j\omega\mu_0\mu_{1\text{eff}}} \cos(k_x(x - x_b)) - \frac{j\gamma}{j\omega\mu_0\mu_{2\text{eff}}} \sin(k_x(x - x_b)) \right) \right] \exp(-\gamma z) \quad (10)$$

with the wave number k_x in x -direction

$$k_x^2 = \epsilon_r \mu_{1\text{eff}} k_0^2 + \gamma^2 \quad (11)$$

The quantities $\mu_{1\text{eff}}$ and $\mu_{2\text{eff}}$ are defined by

$$\mu_{1\text{eff}} = \frac{\mu_1^2 - \mu_2^2}{\mu_1} \quad \mu_{2\text{eff}} = \frac{\mu_1^2 - \mu_2^2}{\mu_2} \quad (12)$$

and they are elements of the permeability tensor $\overleftrightarrow{\mu}_r$:

$$\overleftrightarrow{\mu}_r = \begin{bmatrix} \mu_1 & 0 & +j\mu_2 \\ 0 & 1 & 0 \\ -j\mu_2 & 0 & \mu_1 \end{bmatrix} \quad (13)$$

The field expressions for a subarea filled by an isotropic dielectric or an absorber material (see Fig. 5) are analogous to those (see Eqs. (8) - (11)) used for the ferrite region. Only the respective material constants ε_r , $\mu_{1\text{eff}} = \mu_r$ and $\mu_{2\text{eff}} \rightarrow \infty$ have to be applied. Since the permittivity and the permeability of these materials can be complex values, the wave number k_x in x -direction, linked with these complex material characteristics, is a complex quantity, too. It should be mentioned that these conditions were used for calculating the results discussed in subsection II.

By using these field solutions, see Eqs. (4) - (13), for the different homogenous areas the unknown amplitude coefficient can be eliminated satisfying the continuity conditions of the field components given by the Eqs. (2) and (3). Subsequently, a system of homogeneous algebraic equations for the propagation constant γ may be obtained. The solutions of this system are complex values caused by the electric parameters of the materials used.

IV. RESULTS AND DISCUSSION

In order to qualify the operation of an isolator, its properties in transmission and isolation direction should be determined. This is done via the computation of the propagation constant γ for wave propagation in $+z$ (and $-z$) direction [6, 7]. The relationship of the attenuation constants α in forward and reverse direction is equal to the figure of merit. This statement is correct only if no power is transported by higher order wave modes. Otherwise, their excitation must be considered with the determination of the propagation properties of the device.

These higher order wave modes are bound more

weakly to the line and therefore also less absorbed. That affects particularly the isolation behavior. Hence, the isolators are to be dimensioned in such a way that at the discontinuities only a small amount of higher order wave modes become excited. It is important to mention that it is not possible to guarantee the propagation of the fundamental mode only because of the high values of the permittivity of ferrite materials.

The isolator structure in Fig. 6 is a combined I-guide according to the longitudinal cross-section shown in Fig. 5, which uses the field displacement effect.

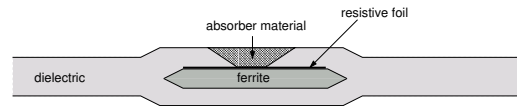


Fig. 6: Arrangement of an isolator. Dimensions of the ferrite: 6 cm x 1 mm x 3.55 mm. Type of the ferrite: TT2-111

For the isolator in Fig. 6 the computed magnitudes of the attenuation scattering parameters S_{21} and S_{12} are depicted in Fig. 7, whereas in Fig. 8 the magnetic field distribution in the x - z -plane is shown. It is visible in Fig. 8 that in the reverse direction near the resistive foil the electromagnetic field is strongly displaced.

A view of the experimental results represented in Fig. 9 shows an attenuation in forward direction of better than -3.5 dB and an attenuation in the reverse direction of better than -17.5 dB with a operating frequency band of 2 GHz and a center frequency of 29 GHz. It results in a relationship of 14 dB figure of merit and a relative operating frequency band of nearly 7%. The theoretically predicted result given in Fig. 7 is strongly overlaid from disturbances, but nevertheless, the tendency of the curves is agreeing. The disturbances result themselves on the one hand from the transition, which is still too abrupt, of the dielectric image line to the line with ferrite (jump of the dielectric constant of $\varepsilon_{r,D} = 2.22$ on $\varepsilon_{r,F} = 12.5$), and on the other hand, with the computation of the transmission characteristics of the isolator higher order wave modes are not yet considered. But they are excited at the transitions

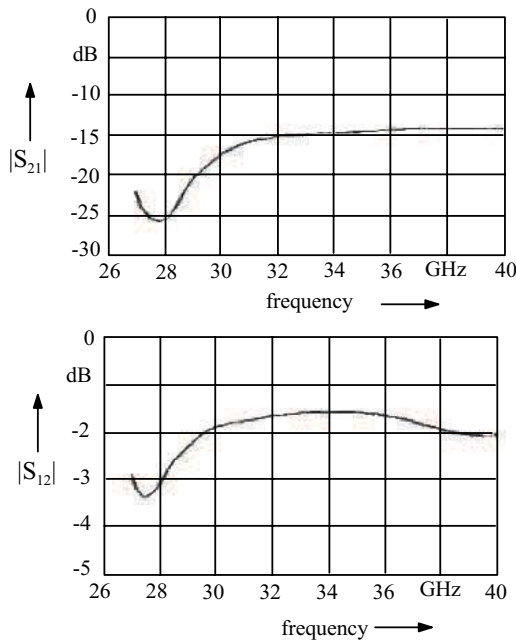


Fig. 7: Calculated magnitudes of the attenuation scattering parameters S_{21} and S_{12} of the isolator. Top: reverse attenuation Bottom: forward attenuation

and, however, as already mentioned, more weakly bound to the line. Most remarkable are the strong oscillations of the transmission curves. Since the two transitions of dielectric image line to dielectric image line with ferrite (see Fig. 6) exhibit in each case quite high reflections, they form together a resonant line system. Because the I-line with ferrite possesses a highly effective dielectric constant, the phase constant grows thus fast with the frequency and the frequency spacing between the individual resonances becomes small.

V. CONCLUSION

In the framework of this paper the dielectric image lines in I-guide technique were examined concerning their characteristics and usefulness for the fabrication of non-reciprocal devices. The I-guide is very suitable, because its technique permits both a good adjustment of the ferrite material and a simple production for the metallic plates.

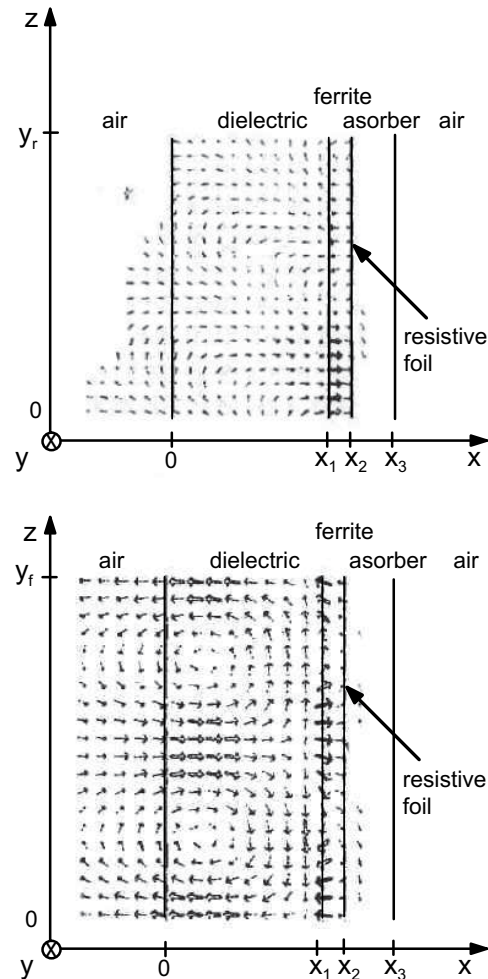


Fig. 8: Longitudinal distribution of the magnetic field strength in the x-z-plane over one wavelength. Top: reverse direction Bottom: forward direction

With the help of the "Mode Matching" approach the possibility of realizing an isolator as a non-reciprocal device was investigated. Using the numerical results obtained, a strong field displacement effect could be observed. Hence, a field displacement isolator in I-guide technique was numerically calculated, subsequently, fabricated and investigated experimentally. The results of these investigations show the applicabil-

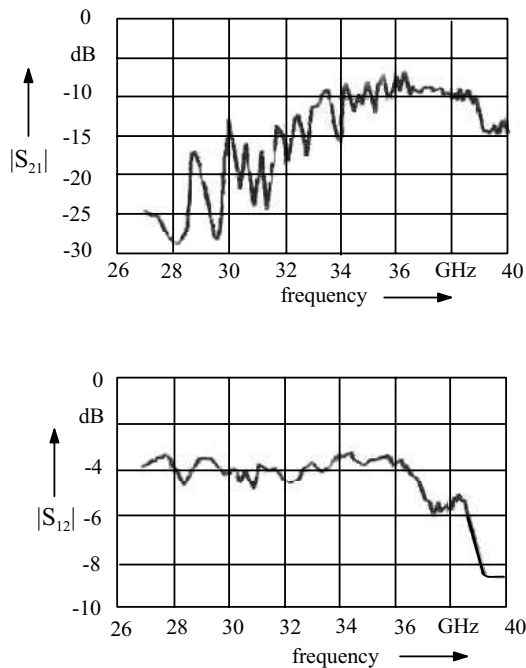


Fig. 9: Experimental determined magnitudes of the attenuation scattering parameters S_{21} and S_{12} of the isolator. Top: reverse attenuation
Bottom: forward attenuation

ity of the method proposed.

In a next work, it should be examined, how the effects of the higher order wave modes are to be reduced. It is aimed at that the ferrite material without dielectric support can be inserted. With this measure, discontinuities can be avoided, and thus, a better field displacement can be achieved. With a fewer number of discontinuities also fewer reflections will arise, and this will render possible to improve the attenuation properties and the operation frequency bandwidth, as well.

References

- [1] M. Muraguchi, K. Araki and Y. Naito, "A New Type of Isolator for Millimeter-Wave Integrated Circuits Using a Nonreciprocal Traveling-Wave Resonator", *IEEE Transactions on Microwave Theory and Techniques*, Vol.-MTT-30, No. 11, 1982, pp. 1867 - 1873.
- [2] A.A. Oliner, "Leakage from a gap in NRD guide.", *1985 IEEE MTT-S International Microwave Symposium Digest*, June 1985, pp. 619 - 622.
- [3] S.A. Tretyakov, I.S. Nefedov, P.A. Belov and A. J. Viitanen, "Recent Developments in Exotic Materials: Negative Permittivity and Permeability, Non-Reciprocal Composites", *14th International Conference on Microwaves, Radar and Wireless Communications, MIKON 2002*, Vol. 1, 2002, pp. 136 - 144.
- [4] T. Itoh (Editor), "Numerical Techniques for Microwave and Millimeter-Wave Passive Structures (Chpt. 9)", John Wiley and Sons, New York, USA, 1989.
- [5] D. Koether, "Reziproke und nichtreziproke Bildleistungsbauelemente unter Verwendung von vormagnetisierten Ferriten", *Ph.D Dissertation*, University Duisburg, Germany, 1989. (in German)
- [6] S.W. Yun and T. Itoh, "A Distributed Millimeter-Wave Isolator Using Nonreciprocal Coupling Structure", *International Journal of Infrared and Millimeter Waves*, Vol. 5, No. 6, 1984, pp. 775 - 792.
- [7] M. Tsutsumi, K. Tanaka and N. Kumagai, "Dielectric Slab Waveguide Isolator in the Millimeter Wave Frequency", *IEEE Transactions on Magnetics*, Vol. MAG-23, 1987, pp. 3739 - 3741.



Dr.-Ing. Dietmar Köther Born in 1958 in Duisburg, Germany. He received the electrical engineering degree (MSc) from the University - GH - Duisburg in 1984. From 1984 to 1988 he worked at the Department of Electrical Engineering at the University-

GH-Duisburg on the DFG project "Reciprocal and nonreciprocal image guide elements utilizing pre-magnetized ferrites". In 1989 he received the PhD degree.

From 1989 to 1992 he worked for ArguMens, responsible for the development of a CAD package and measurement programs. In 1991 the design study "40 / 80 GHz electronical MMIC circulators" started. Some activities were within the frame of Esprit II, Esprit III and BMBF DFE.

Since 1993 he is at the IMST where he was involved in the implementation of CPW elements into a CAD program. Further, non-standard measurement software for nonlinear characterization and active load pull has been developed. Since the beginning of 1995 he is head of the section „Simulation and Measurement Software“ at the IMST. From 1996 till now, he is head of the section "RF Test Centre", which operates an ISO/IEC 17025 certified lab.



Dr.-Ing. Peter Waldow (IEEE member since 1984) received the Dipl.-Ing. degree in electrical engineering from the Gerhard-Mercator-University, Duisburg in 1982 and the Dr.-Ing. degree in 1986.

Since 1987 he was working on electromagnetic field theory in various industrial

projects. He was co-founder in 1992 and is member of the Board of Directors of the Institute of Mobile and Satellite Telecommunications – IMST, Kamp-Lintfort, Germany.

Between 1999 and 2002 he was substitute of a Full Professor in the Engineering Faculty at the Gerhard-Mercator-University, Duisburg.

Currently, Dr. Waldow is adjunct Professor at the Department of Engineering Sciences, Institute of

Communications Engineering, ATE at the University Duisburg-Essen, Location Duisburg.



Dipl.-Ing. Birgit Neuhaus was born in Oberhausen, Germany, in 1969. She received her diploma in Electrical Engineering from the Gerhard - Mercator-University of Duisburg, Germany, in 1998. She is currently working toward the Ph.D. degree at the Department of Electrical Engineering Sciences, at the University

Duisburg-Essen, Location Duisburg. Her research interests are in modeling and simulation of microwave and optoelectronic devices. She is author and co-author of several papers, associate guest editor of scientific journals and workshop organizer. Mrs. Neuhaus is a member of the Association of German Engineers VDE and a Student Member of the IEEE.



Dr. Ir. Dominique M. M.-P. Schreurs (S'90-M'97-SM'02) received the M.Sc. degree in electronic engineering and the Ph.D. degree from the Katholieke Universiteit (K.U.) Leuven, Belgium, in 1992 and 1997, respectively.

She is currently a post-doctoral fellow of the fund for scientific

research-Flanders and a visiting assistant professor at K.U.Leuven. She has been a visiting scientist at Agilent Technologies, ETHZ, and NIST. Her main research interest is the use of vectorial large-signal measurements for the characterization and modeling of non-linear microwave devices.



Prof. Dr.-Ing. Adalbert Beyer received his diploma in 1964 and the Dr.-Ing. (Ph.D.) degree in 1969, both in Electrical Engineering. After occupying several industrial and academic positions, he joined the Duisburg University as Professor of Electrical Engineering and Milli-

meter-Wave Techniques. He is also foundation member of the "Sonder-forschungsbereich 254". His areas of research interest are in the field theory, microwave- and millimeter-wave techniques and in the remote sensing. In 1987 he was a visiting professor at the University of Ottawa/ Canada. In 1990 he spent a time as visiting professor at the University of Texas at Austin/TX/USA. In 1996 he was visiting professor at the Technical University of Warsaw/ Poland. He is author and co-author of several books, patents and more than 300 technical articles. Professor Beyer is a Fellow of IEEE and a member of the IEEE MTT Symposia Technical Program Committes: MTT-S Education Committee, MTT-S Technical Committees MTT-13 and MTT-15. He is an Associate Editor of the *International Journal of RF and Microwave Computer-Aided Engineering* and a member of the editorial board of several scientific journals.

A LU Decomposition Useful for Antenna Optimization

K. Jamil and E. H. Newman

Ohio State University ElectroScience Lab

Abstract - This paper describes a LU decomposition technique useful when solving a series of matrix equations in which only a small fraction of the original matrix changes from run to run. On the first run, the entire matrix must be computed and LU decomposed. However, on the second or subsequent runs, only those rows and columns of the matrix which have changed need be recomputed and re-LU decomposed. If only a small fraction of the matrix has changed, this results in a substantial saving in CPU time both in the computation of the original matrix and in its LU decomposition.

I. Description of Procedure

Many computational techniques in electromagnetics and other branches of engineering are based upon the solution of a matrix equation. For example, a Method of Moments (MM) solution with N unknowns requires setting up and solving an order N matrix equation of the form $[Z]I = V$. In this case, order N^2 CPU time is required to set up the $[Z]$ matrix, and order N^3 CPU time to solve the matrix equation by direct methods [1]. For a multidimensional optimization procedure, requiring thousands of runs, the total CPU time can become prohibitive. Assuming that the change in the geometry only impacts the lower numbered unknowns of the problem, this paper presents a LU decomposition procedure which saves CPU time since only the rows and columns of the $[Z]$ matrix which have changed need be re-LU decomposed. The technique has been implemented in the

author's *Electromagnetic Surface Patch Code: Version V (ESP5)* for the MM analysis of the electromagnetic radiation and scattering from geometries which can be modeled as an interconnection of thin wires, polygonal plates, and polygonal dielectric volumes [2,3].

An ideal application of the method would be the design of an antenna on a large body of fixed geometry. Figure 1 shows a MM $[Z]$ matrix with N_A modes on the antenna and N_B modes on the fixed geometry body. On the first run, the entire order $N = N_A + N_B$ MM $[Z]$ matrix would need to be computed and LU decomposed. However, on the second and subsequent runs only the first N_A rows and columns of the $[Z]$ matrix would need to be recomputed and re-LU decomposed, resulting in a substantial saving in CPU time if $N_A \ll N_B$.

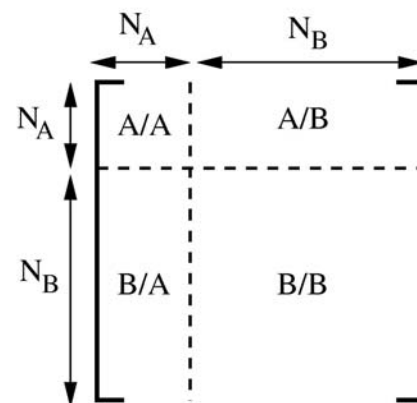


Fig. 1. The MM impedance matrix for an antenna on a large body.

II. Description of the Method

The appendix describes an LU technique that begins at the lower right hand corner of the matrix, and proceeds to the upper left corner. Figure 2 shows a snapshot of the $[Z]$ matrix part of the way through the LU process. At this point, the $N_2 \times N_2$ block in the lower right corner has been LU decomposed, but the first N_1 rows and columns have not. The important point is that as the method continues to LU decompose the first N_1 rows and columns, the elements in the $N_2 \times N_2$ block in the lower right corner do not change. Thus, if one is performing a series of MM computations in which the last N_2 expansion functions do not change, then the $N_2 \times N_2$ block in the lower right hand corner of both the $[Z]$ and LU of $[Z]$ matrices will not change. Only the first N_1 rows and columns of the $[Z]$ matrix need to be recomputed and re-LU decomposed. This reduces the number of elements that must be computed in the $[Z]$ matrix from N^2 to $2N_1N$. More importantly, only the first N_1 rows and columns need to be re-LU decomposed, thus reducing the solve time from $O(N^3)$ to $O(N_1N^2)$. If $N_1 \ll N$, this will result in a significant saving in CPU time. Note that the method works if N_1 changes, and thus one is free to change the number of expansion functions used to model the antenna.

III. The ESP5 Implementation

In the ESP5 implementation of the method, on the first run a LUD (LU to Disk) command causes the code to write two files to disk containing (1) the LU of the $[Z]$ matrix and (2) the detailed MM expansion function geometry. On the second or subsequent runs a DLU (Disk to LU) command causes the code to read the expansion function geometry from the disk

file and to compare it to that for the present run in order to identify N_1 and N_2 . Assuming $N_1 < N$, the code then reads the LU of the $[Z]$ matrix from the disk, and recomputes and re-LU decomposes only the first N_1 rows and columns.

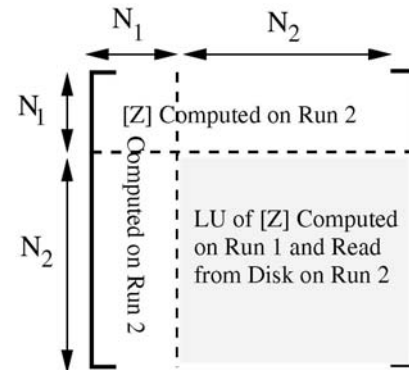


Fig. 2. The MM $[Z]$ matrix part of the way through the LU procedure.

Table 1 shows CPU times for a problem involving $N = 4804$ wire expansion modes. On run 1, 6015 sec. were required to fill the $[Z]$ matrix, and 7289 sec. were required to do a full LU decomposition. Writing the LU of the $[Z]$ matrix to the disk required 166 sec., and a far zone pattern at 360 angles took 26 sec. On run 2, only the first mode changed, and thus $N_1 = 1$ and $N_2 = 4803$. In this case, 50 sec. were required to read the LU of the $[Z]$ from the disk, 2 sec. were required to re-compute and 13 sec. to re-LU decompose the 1st row and column of the $[Z]$ matrix. If $N_1 \ll N$ modes had changed, then these times would be approximately multiplied by N_1 . For example, if the first $N_1 = 10$ modes had changed, then approximately 20 sec. would be required to recompute, and 130 sec. to re-LU decompose the $[Z]$ matrix.

Table 1. CPU times in sec. for runs 1 and 2 with $N = 4804$ wire modes, and with only the first mode changing on run 2.

Run	Comp. [Z]	LU [Z]	Write [Z]	Read [Z]	Comp. Pattern
1	6015	7289	166	N/A	26
2	2.0	13.0	N/A	50	26

Appendix

This appendix will describe a matrix LU procedure that begins at the lower right hand corner and proceeds to the upper left hand corner¹. Referring to Figure 2, it has the advantage that if the $N_2 \times N_2$ block in the lower right hand corner of the original matrix does not change, then this block in the LU matrix also will not change, and one needs only re-LU decompose the first $N_1 = N - N_2$ rows and columns of the matrix. This reduces the total operation count and CPU time from order N^3 to $N_1 N^2$.

Assuming the order N [Z] matrix is in the form of Figure 2, the following procedure will re-LU decompose into $[Z] = [L][U]$.

for $i = N_1 : 1 : -1$

for $row = i : 1 : -1$

$$L_{row,i} = Z_{row,i} - \sum_{j=i+1}^N L_{row,j} U_{j,i}$$

end

for $col = i - 1 : 1 : -1$

$$U_{i,col} = (Z_{i,col} - \sum_{j=i+1}^N L_{i,j} U_{j,col}) / Z_{i,i}$$

end

end

¹ The LU procedure described below may or may not be new. It was introduced to the author by Mr. Brian Lynch when he was a graduate student at The Ohio State University, Department of Electrical Engineering, ElectroScience Lab in 1989.

On run 1, set $N_1 = N$ to LU decompose the full [Z] matrix.

The backward substitution to solve $[L]Y = V$ for Y proceeds as follows.

for $row = N : 1 : -1$

$$Y_{row} = (V_{row} - \sum_{j=row+1}^N L_{row,j} Y_j) / L_{row,row}$$

end

The forward substitution to solve $[U]I = Y$ for the solution vector I is

for $row = 1 : N$

$$I_{row} = Y_{row} - \sum_{j=1}^{row-1} U_{row,j} I_j$$

end

References

- [1] G.H. Golub and C.F. Van Loan, *Matrix Computations*, 3rd Ed., Johns Hopkins Univ. Press, 1996.
- [2] K. Jamil, "Enhancements to The Electromagnetic Surface Patch Code for Printed Antennas and Optimization," MSc. thesis, Ohio State Univ., Dept. of Elec. Engr. 2002.
- [3] E.H. Newman, "A User's Manual for the Electromagnetic Surface Patch Code: Version V," Ohio State University, ElectroScience Lab, Unpublished Report, 2003.

Khalid Jamil was born in Lahore, Pakistan, on Feb 7, 1973. He received B.S.E.E. degree from University of Engineering and Technology, Lahore, Pakistan in 1996 and M.S. degree from The Ohio State University in 2002. Presently, he is pursuing his Ph.D. degree as a Graduate Research



Associate at the ElectroScience Lab, The Ohio State University. He worked as a Research Engineer at Advanced Engineering Research Organization, Pakistan, from 1996 to 2000. His research interests include computational electromagnetic techniques, scattering from random media and antennas.

Edward H. Newman was born in Cleveland Ohio on July 9, 1946.



He received the BSEE, MS, and PhD degrees in electrical engineering from The Ohio State University in 1969, 1970, and

1974, respectively.

Since 1974 he has been a member of the Ohio State University, Department of Electrical Engineering, ElectroScience Laboratory, where he is currently a Professor. His primary research interest is in the development of method of moments techniques for the analysis of general antenna or scattering problems, and he is the primary author of the ``Electromagnetic Surface Patch Code" (ESP). Other research interests include electromagnetic shielding and antennas on automobiles, aircraft and similar platforms. He has published over 50 journal articles in these areas, and is a coauthor of the IEEE Press book "Computational Electromagnetics (Frequency Domain Method of Moments)."

Dr. Newman is a Fellow of the IEEE, and is a member of Commission B of URSI and the Electromagnetics Institute. He is a recipient of the 1986 and 1992 College of Engineering Research Award, and is a past chairman of the Columbus sections of the IEEE Antennas and Propagation and Microwave Theory and Techniques Societies.

ACES COPYRIGHT FORM

This form is intended for original, previously unpublished manuscripts submitted to ACES periodicals and conference publications. The signed form, appropriately completed, MUST ACCOMPANY any paper in order to be published by ACES. PLEASE READ REVERSE SIDE OF THIS FORM FOR FURTHER DETAILS.

TITLE OF PAPER:

RETURN FORM TO:

Dr. Atef Z. Elsherbeni
University of Mississippi
Dept. of Electrical Engineering
Anderson Hall Box 13
University, MS 38677 USA

AUTHORS(S)

PUBLICATION TITLE/DATE:

PART A - COPYRIGHT TRANSFER FORM

(NOTE: Company or other forms may not be substituted for this form. U.S. Government employees whose work is not subject to copyright may so certify by signing Part B below. Authors whose work is subject to Crown Copyright may sign Part C overleaf).

The undersigned, desiring to publish the above paper in a publication of ACES, hereby transfer their copyrights in the above paper to The Applied Computational Electromagnetics Society (ACES). The undersigned hereby represents and warrants that the paper is original and that he/she is the author of the paper or otherwise has the power and authority to make and execute this assignment.

Returned Rights: In return for these rights, ACES hereby grants to the above authors, and the employers for whom the work was performed, royalty-free permission to:

1. Retain all proprietary rights other than copyright, such as patent rights.

2. Reuse all or portions of the above paper in other works.

3. Reproduce, or have reproduced, the above paper for the author's personal use or for internal company use provided that (a) the source and ACES copyright are indicated, (b) the copies are not used in a way that implies ACES endorsement of a product or service of an employer, and (c) the copies per se are not offered for sale.

4. Make limited distribution of all or portions of the above paper prior to publication.

5. In the case of work performed under U.S. Government contract, ACES grants the U.S. Government royalty-free permission to reproduce all or portions of the above paper, and to authorize others to do so, for U.S. Government purposes only.

ACES Obligations: In exercising its rights under copyright, ACES will make all reasonable efforts to act in the interests of the authors and employers as well as in its own interest. In particular, ACES REQUIRES that:

1. The consent of the first-named author be sought as a condition in granting re-publication permission to others.

2. The consent of the undersigned employer be obtained as a condition in granting permission to others to reuse all or portions of the paper for promotion or marketing purposes.

In the event the above paper is not accepted and published by ACES or is withdrawn by the author(s) before acceptance by ACES, this agreement becomes null and void.

AUTHORIZED SIGNATURE

TITLE (IF NOT AUTHOR)

EMPLOYER FOR WHOM WORK WAS PERFORMED

DATE FORM SIGNED

Part B - U.S. GOVERNMENT EMPLOYEE CERTIFICATION

(NOTE: if your work was performed under Government contract but you are not a Government employee, sign transfer form above and see item 5 under Returned Rights).

This certifies that all authors of the above paper are employees of the U.S. Government and performed this work as part of their employment and that the paper is therefor not subject to U.S. copyright protection.

AUTHORIZED SIGNATURE

TITLE (IF NOT AUTHOR)

NAME OF GOVERNMENT ORGANIZATION

DATE FORM SIGNED

PART C - CROWN COPYRIGHT

(NOTE: ACES recognizes and will honor Crown Copyright as it does U.S. Copyright. It is understood that, in asserting Crown Copyright, ACES in no way diminishes its rights as publisher. Sign only if ALL authors are subject to Crown Copyright).

This certifies that all authors of the above Paper are subject to Crown Copyright. (Appropriate documentation and instructions regarding form of Crown Copyright notice may be attached).

AUTHORIZED SIGNATURE

TITLE OF SIGNEE

NAME OF GOVERNMENT BRANCH

DATE FORM SIGNED

Information to Authors

ACES POLICY

ACES distributes its technical publications throughout the world, and it may be necessary to translate and abstract its publications, and articles contained therein, for inclusion in various compendiums and similar publications, etc. When an article is submitted for publication by ACES, acceptance of the article implies that ACES has the rights to do all of the things it normally does with such an article.

In connection with its publishing activities, it is the policy of ACES to own the copyrights in its technical publications, and to the contributions contained therein, in order to protect the interests of ACES, its authors and their employers, and at the same time to facilitate the appropriate re-use of this material by others.

The new United States copyright law requires that the transfer of copyrights in each contribution from the author to ACES be confirmed in writing. It is therefore necessary that you execute either Part A-Copyright Transfer Form or Part B-U.S. Government Employee Certification or Part C-Crown Copyright on this sheet and return it to the Managing Editor (or person who supplied this sheet) as promptly as possible.

CLEARANCE OF PAPERS

ACES must of necessity assume that materials presented at its meetings or submitted to its publications is properly available for general dissemination to the audiences these activities are organized to serve. It is the responsibility of the authors, not ACES, to determine whether disclosure of their material requires the prior consent of other parties and if so, to obtain it. Furthermore, ACES must assume that, if an author uses within his/her article previously published and/or copyrighted material that permission has been obtained for such use and that any required credit lines, copyright notices, etc. are duly noted.

AUTHOR/COMPANY RIGHTS

If you are employed and you prepared your paper as a part of your job, the rights to your paper initially rest with your employer. In that case, when you sign the copyright form, we assume you are authorized to do so by your employer and that your employer has consented to all of the terms and conditions of this form. If not, it should be signed by someone so authorized.

NOTE RE RETURNED RIGHTS: Just as ACES now requires a signed copyright transfer form in order to do "business as usual", it is the intent of this form to return rights to the author and employer so that they too may do "business as usual". If further clarification is required, please contact: The Managing Editor, R. W. Adler, Naval Postgraduate School, Code EC/AB, Monterey, CA, 93943, USA (408)656-2352.

Please note that, although authors are permitted to re-use all or portions of their ACES copyrighted material in other works, this does not include granting third party requests for reprinting, republishing, or other types of re-use.

JOINT AUTHORSHIP

For jointly authored papers, only one signature is required, but we assume all authors have been advised and have consented to the terms of this form.

U.S. GOVERNMENT EMPLOYEES

Authors who are U.S. Government employees are not required to sign the Copyright Transfer Form (Part A), but any co-authors outside the Government are.

Part B of the form is to be used instead of Part A only if all authors are U.S. Government employees and prepared the paper as part of their job.

NOTE RE GOVERNMENT CONTRACT WORK: Authors whose work was performed under a U.S. Government contract but who are not Government employees are required so sign Part A-Copyright Transfer Form. However, item 5 of the form returns reproduction rights to the U. S. Government when required, even though ACES copyright policy is in effect with respect to the reuse of material by the general public.

January 2002

INFORMATION FOR AUTHORS

PUBLICATION CRITERIA

Each paper is required to manifest some relation to applied computational electromagnetics. **Papers may address general issues in applied computational electromagnetics, or they may focus on specific applications, techniques, codes, or computational issues.** While the following list is not exhaustive, each paper will generally relate to at least one of these areas:

- 1. Code validation.** This is done using internal checks or experimental, analytical or other computational data. Measured data of potential utility to code validation efforts will also be considered for publication.
- 2. Code performance analysis.** This usually involves identification of numerical accuracy or other limitations, solution convergence, numerical and physical modeling error, and parameter tradeoffs. However, it is also permissible to address issues such as ease-of-use, set-up time, run time, special outputs, or other special features.
- 3. Computational studies of basic physics.** This involves using a code, algorithm, or computational technique to simulate reality in such a way that better, or new physical insight or understanding, is achieved.
- 4. New computational techniques,** or new applications for existing computational techniques or codes.
- 5. “Tricks of the trade”** in selecting and applying codes and techniques.
- 6. New codes, algorithms, code enhancement, and code fixes.** This category is self-explanatory, but includes significant changes to existing codes, such as applicability extensions, algorithm optimization, problem correction, limitation removal, or other performance improvement. **Note: Code (or algorithm) capability descriptions are not acceptable, unless they contain sufficient technical material to justify consideration.**
- 7. Code input/output issues.** This normally involves innovations in input (such as input geometry standardization, automatic mesh generation, or computer-aided design) or in output (whether it be tabular, graphical, statistical, Fourier-transformed, or otherwise signal-processed). Material dealing with input/output database management, output interpretation, or other input/output issues will also be considered for publication.
- 8. Computer hardware issues.** This is the category for analysis of hardware capabilities and limitations of various types of electromagnetics computational requirements. Vector and parallel computational techniques and implementation are of particular interest.

Applications of interest include, but are not limited to, antennas (and their electromagnetic environments), networks, static fields, radar cross section, shielding, radiation hazards, biological effects, electromagnetic pulse (EMP), electromagnetic interference (EMI), electromagnetic compatibility (EMC), power transmission, charge transport, dielectric, magnetic and nonlinear materials, microwave components, MEMS technology, MMIC technology, remote sensing and geometrical and physical optics, radar and communications systems, fiber optics, plasmas, particle accelerators, generators and motors, electromagnetic wave propagation, non-destructive evaluation, eddy currents, and inverse scattering.

Techniques of interest include frequency-domain and time-domain techniques, integral equation and differential equation techniques, diffraction theories, physical optics, moment methods, finite differences and finite element techniques, modal expansions, perturbation methods, and hybrid methods. This list is not exhaustive.

A unique feature of the Journal is the publication of unsuccessful efforts in applied computational electromagnetics. Publication of such material provides a means to discuss problem areas in electromagnetic modeling. Material representing an unsuccessful application or negative results in computational electromagnetics will be considered for publication only if a reasonable expectation of success (and a reasonable effort) are reflected. Moreover, such material must represent a problem area of potential interest to the ACES membership.

Where possible and appropriate, authors are required to provide statements of quantitative accuracy for measured and/or computed data. This issue is discussed in “Accuracy & Publication: Requiring, quantitative accuracy statements to accompany data,” by E. K. Miller, *ACES Newsletter*, Vol. 9, No. 3, pp. 23-29, 1994, ISBN 1056-9170.

EDITORIAL REVIEW

In order to ensure an appropriate level of quality control, papers are peer reviewed. They are reviewed both for technical correctness and for adherence to the listed guidelines regarding information content.

JOURNAL CAMERA-READY SUBMISSION DATES

March issue	deadline 8 January
July issue	deadline 20 May
November issue	deadline 20 September

Uploading an acceptable camera-ready article after the deadlines will result in a delay in publishing this article.

STYLE FOR CAMERA-READY COPY

The ACES Journal is flexible, within reason, in regard to style. However, certain requirements are in effect:

1. The paper title should NOT be placed on a separate page. The title, author(s), abstract, and (space permitting) beginning of the paper itself should all be on the first page. The title, author(s), and author affiliations should be centered (center-justified) on the first page.
2. An abstract is REQUIRED. The abstract should be a brief summary of the work described in the paper. It should state the computer codes, computational techniques, and applications discussed in the paper (as applicable) and should otherwise be usable by technical abstracting and indexing services.
3. Either British English or American English spellings may be used, provided that each word is spelled consistently throughout the paper.
4. Any commonly-accepted format for referencing is permitted, provided that internal consistency of format is maintained. As a guideline for authors who have no other preference, we recommend that references be given by author(s) name and year in the body of the paper (with alphabetical listing of all references at the end of the paper). Titles of Journals, monographs, and similar publications should be in italic font or should be underlined. Titles of papers or articles should be in quotation marks.
5. Internal consistency shall also be maintained for other elements of style, such as equation numbering. As a guideline for authors who have no other preference, we suggest that equation numbers be placed in parentheses at the right column margin.
6. The intent and meaning of all text must be clear. For authors who are NOT masters of the English language, the ACES Editorial Staff will provide assistance with grammar (subject to clarity of intent and meaning).
7. Unused space should be minimized. Sections and subsections should not normally begin on a new page.

PAPER FORMAT

The preferred format for initial submission and camera-ready manuscripts is 12 point Times Roman font, single line spacing and double column format, similar to that used here, with top, bottom, left, and right 1 inch margins. Manuscripts should be prepared on standard 8.5x11 inch paper.

Only camera-ready electronic files are accepted for publication. The term **“camera-ready”** means that the material is neat, legible, and reproducible. Full details can be found on ACES site, Journal section.

ACES reserves the right to edit any uploaded material, however, this is not generally done. It is the author(s)

responsibility to provide acceptable camera-ready pdf files. Incompatible or incomplete pdf files will not be processed, and authors will be requested to re-upload a revised acceptable version.

SUBMITTAL PROCEDURE

All submissions should be uploaded to ACES server through ACES web site (<http://aces.ee.olemiss.edu>) by using the upload button, journal section. Only pdf files are accepted for submission. The file size should not be larger than 5MB, otherwise permission from the Editor-in-Chief should be obtained first. The Editor-in-Chief will acknowledge the electronic submission after the upload process is successfully completed.

COPYRIGHTS AND RELEASES

Each primary author must sign a copyright form and obtain a release from his/her organization vesting the copyright with ACES. Copyright forms are available at ACES, web site (<http://aces.ee.olemiss.edu>). To shorten the review process time, the executed copyright form should be forwarded to the Editor-in-Chief immediately after the completion of the upload (electronic submission) process. Both the author and his/her organization are allowed to use the copyrighted material freely for their own private purposes.

Permission is granted to quote short passages and reproduce figures and tables from and ACES Journal issue provided the source is cited. Copies of ACES Journal articles may be made in accordance with usage permitted by Sections 107 or 108 of the U.S. Copyright Law. This consent does not extend to other kinds of copying, such as for general distribution, for advertising or promotional purposes, for creating new collective works, or for resale. The reproduction of multiple copies and the use of articles or extracts for commercial purposes require the consent of the author and specific permission from ACES. Institutional members are allowed to copy any ACES Journal issue for their internal distribution only.

PUBLICATION CHARGES

ACES members are allowed 12 printed pages per paper without charge; non-members are allowed 8 printed pages per paper without charge. Mandatory page charges of \$75 a page apply to all pages in excess of 12 for members or 8 for non-members. Voluntary page charges are requested for the free (12 or 8) pages, but are NOT mandatory or required for publication. A priority courtesy guideline, which favors members, applies to paper backlogs. Authors are entitled to 15 free reprints of their articles and must request these from the Managing Editor. Additional reprints are available to authors, and reprints available to non-authors, for a nominal fee.

ACES Journal is abstracted in INSPEC, in Engineering Index, DTIC, Science Citation Index Expanded, the Research Alert, and to Current Contents/Engineering, Computing & Technology.